The Winds of Change: The effects of katabatic winds on fjord circulation, sea-ice export and glacier stability at Sermilik Fjord and Helheim Glacier.

Iain Wheel

Scott Polar Research Institute

University of Cambridge

This dissertation was submitted for the degree of

Master of Philosophy

Hughes Hall June 2019

Declaration:

I declare that the contents of this dissertation are original and have not been submitted previously to the university or any other institute, except where specific reference is made to the work of others. I declare that this work in its entirety is mine except for specific reference to others within the text and as stated in the Acknowledgements. I confirm this dissertation contains fewer than 20,000 not including the figure captions and references.

Iain Wheel, June 2019

Acknowledgements:

Firstly, I would like to thank my supervisor Poul Christoffersen for his support and guidance throughout the masters. I thank Sebastian Mernild for the provision of the Station Coast meteorological data. Thanks must also go to Toby Benham for his help and advice on using MODIS imagery and AMSR-E, and for almost instantaneously solving any of my GIS issues. SPRI has been a fantastic place to work at for a year with a great community atmosphere making the whole MPhil far more rewarding. I would like to thank Amelia and Adam for their company all year, along with the rest of MPhil cohort and the PhD students for their encouragement throughout the year. I grateful to SPRI and the Debenham family for the provision of the scholarship that has enabled me to undertake this masters. Finally, thanks to my family and friends for their support throughout the year.

Abstract:

Katabatic winds or downslope wind events, across the southeast of Greenland, can lead to large scale changes in fjord circulation, sea-ice export and glacier terminus stability, but despite this few studies have investigated their wider implications. In period of rapidly retreating tidewater glaciers, katabatic winds are known to aid retreat indirectly, through inducing warm Atlantic origin water influx into the fjord, and directly via the removal of the ice melange in front of the glacier terminus. Using ERA5 reanalysis data, verified by two local weather stations, katabatic winds across Sermilik Fjord are shown to occur predominately in non-summer months with no clear long-term trend. Hydrographic data, from 2009-2013, positioned across the fjord and adjacent shelf waters, showed the expected warm water influxes are lower in scale in comparison to intermediary circulation associated with barrier winds. However, submarine melt rates at the top of the fjord can increase during downslope wind events by up to 1000%. Melt rates vary according to katabatic wind strength. Thresholds of katabatic wind speeds for the removal of sea-ice from the shelf and the removal of the ice-melange of 12m/s and 20m/s, respectively, were observed. Rapid retreat of Helheim glacier occurred during strong downslope wind events which removed the ice melange, and the well documented retreat of Helheim between 2001-2005 is predicted to be in part because of strong katabatic winds. Removal of the ice-melange led to a series of calving events, driven by a lack of buttressing and weakness propagation up the glacier. Although previous research has dismissed katabatic winds as relatively unimportant due to much greater heat influxes associated with barrier winds, direct influences on Helheim Glacier terminus stability show perhaps katabatic winds play a much large role in glacier retreat in southeast Greenland than previously appreciated.

Contents

List of Figures:

Chapter 1:

Introduction:

Rationale:

Mass loss from the Greenland Ice Sheet has tripled over the last twenty years (Shepherd *et al.* 2012, Enderlin *et al.* 2014, Mouginot *et al.* 2019) with the majority of mass loss resulting from calving and melt of tidewater glaciers associated with an increase in ocean temperature (Holland *et al.* 2008, Cowton *et al.* 2018). Fjords control the access of heat to the glacier, along with corresponding export of freshwater to the shelf (Inall *et al.* 2014, Jackson and Straneo 2016, Straneo *et al.* 2016). As such, changes in fjord circulation can have wide ranging impacts, both to the Greenland Ice Sheet and global circulation (Bamber *et al.* 2012, Straneo *et al.* 2016).

Atmospheric and ocean warming are ultimately responsible for the rapid mass loss of the Greenland Ice Sheet (Holland *et al.* 2008, Van Den Broeke *et al.* 2009, Ettema *et al.* 2010, Motyka *et al.* 2011, Shepherd *et al.* 2012, Straneo and Heimbach 2013). However, the interaction and relative importance of these two components is poorly understood, especially when considering how other sources of forcing, such as katabatic winds, modify their interaction with the glacier and its sensitivity to temperature-induced retreat (Christoffersen *et al.* 2012). The increase in glacial meltwater, caused by the retreat of Greenland tidewater glaciers, creates greater freshwater export out of the fjord into shelf waters and can have possible consequences for the Atlantic Meridional Overturning Current (AMOC) and global thermohaline circulation (Bamber *et al.* 2012, Gillard *et al.* 2016).

Fjord circulation is increasingly understood to be the key control on warm water access to the glacier front, and thereby affecting submarine melting (Sciascia *et al.* 2013, Jackson *et al.* 2014). Fjord circulation has, however, been shown to be highly variable with coastal wind events leading to fjord scale changes in temperature and current profiles (Straneo *et al.* 2010a, Harden *et al.* 2011, Jackson *et al.* 2018). Therefore, despite the clear importance of fjord circulation in glacier retreat, its impact is poorly understood (Straneo and Cenedese 2015). There is limited data availability on fjord circulation and water column properties, especially towards the upper fjord and during non-summer months, with data collection often restricted to summer months only and at limited locations at the fjord mouth or on shelf waters (Johnson *et al.* 2011, Mortensen *et al.* 2011, Christoffersen *et al.* 2012, Straneo *et al.* 2012, Inall *et al.* 2014).

Another significant gap in the current research concerns the effects of katabatic winds, both directly on the glacier and on the circulation within the fjord, especially when considering the monopolising effect of katabatic flow on the local area during a Downslope Wind Event (DWE). There is limited research looking at both katabatic winds (Oltmanns *et al.* 2014) and their effect on fjord circulation (Spall *et al.* 2017). The limited studies performed indicate that katabatic winds form an important component of the fjord-shelf interaction, fjord warm water renewal and the export of freshwater into the Irminger Sea (Spall *et al.* 2017, Spall and Pedlosky 2018). Previous studies have also suggested that strong katabatic winds can directly trigger glacier retreat through open water formation at the terminus (Christoffersen *et al.* 2012).

Aim and Objectives:

The study focusses on Sermilik Fjord in East Greenland, with the dual aims of A) characterising katabatic wind effects across the glacier-fjord system as a whole, and B) assessing the direct and indirect links between katabatic winds and retreat of Helheim Glacier. To achieve this, four objectives were defined.

Identify katabatic winds (objective 1)

To create a reliable historical catalogue of down-fjord wind events at Sermilik Fjord based on multiple weather station and reanalysis data. Parameters were drawn to identify winds as katabatic separately for each dataset whilst providing a good comparison between the datasets. This allowed other factors, such as fjord circulation and sea-ice export to be analysed for each event within the timeseries.

Assess the change in fjord circulation and associated heat flux within the fjord (objective 2).

Using the limited temperature and current profiles from stationary buoys taken in Sermilik Fjord, changes in the water column were observed during each DWE identified during the period of the hydrograph series. These observations focused mainly on current velocities and temperature fluctuations across the fjord from shelf to the glacier terminus. The importance of the magnitude of katabatic winds and how their influence across the fjord changes were assessed. The study also investigated whether, prior to DWEs, the water column conditions play a role in altering wind induced processes.

Assess scale of ice-melange break-up and sea-ice export from the fjord and continental shelf and their importance both locally and to larger scale processes (objective 3).

Satellite and passive microwave imaging were used to determine the direct role katabatic winds have on ice-melange break-up, and thus on terminus stability, along with sea-ice export out the fjord. Sea ice in the fjord can act as a protective barrier preventing wind stress from influencing fjord circulation. Its removal or presence may change the influence of katabatic winds on heat influx into the fjord. On a wider scale, DWEs may have implications on global circulation through sea-ice export into the Irminger Sea so quantification of the magnitude of DWE induced sea-ice export was determined.

Determine whether katabatic winds affect Helheim Glacier terminus stability (objective 4).

Using the above objectives, determination of whether katabatic winds have a direct effect (through break-up of the ice-melange) or an indirect effect (through increased heat influx into the fjord) on the stability of Helheim Glacier. Pinpointing the most important katabatic wind influences on the glacier-fjord system was therefore possible. Finally, the overall importance of katabatic winds, in a changing climate, on the retreat of the Greenland Ice Sheet became clearer.

Background:

Tidewater glaciers:

Retreat of tidewater glaciers in Greenland accounts for 75% of the mass loss from the Greenland Ice Sheet (Moon *et al.* 2012, Beaird *et al.* 2018). The tidewater glaciers connect ocean warming to the ice sheet, but are also affected by surface melt and runoff (Rignot and Kanagaratnam 2006, Hanna *et al.* 2009). As a result, internal glacier dynamics play an important role in transferring increasing ocean heat content (Benn *et al.* 2007, Bassis and Jacobs 2013). Ice-ocean systems are notoriously complicated systems with ocean warming, fjord dynamics, glacier meltwater, sea-ice, wind forcing and geometry all playing important interlinking roles, each of which can alter internal glacier dynamics and retreat (Amundson *et al.* 2010, Christoffersen *et al.* 2012, Harden, Pickart, *et al.* 2014, Straneo and Cenedese 2015, Benn *et al.* 2017, Cowton *et al.* 2018, Schild *et al.* 2018). Given the associated nature of many of the drivers of tidewater glacier retreat, understanding each individual component of the system and its relationship to others is a clear desideratum.

The melting of the Greenland Ice Sheet has contributed to 16% of global sea level rise over the last two decades (Khan *et al.* 2014). Along with sea level rise, increased freshwater input from the melting of marine terminating glaciers can lead to changes in coastal and global circulatory systems (Bamber *et al.* 2012, Gillard *et al.* 2016). It is therefore crucial to understand the drivers and feedback loops associated with tidewater glacier retreat, especially within understudied areas such as katabatic wind driven changes. Increased understanding in such areas will allow a more complete picture of glacier retreat, aiding the development and accuracy of future prediction or models.

Terminus stability:

The retreat of tidewater glaciers in Greenland is heavily linked to shifts in the calving dynamics at the front of glaciers, since calving dominates terminal ablation in fast flowing glaciers (Bartholomaus *et al.* 2013, Luckman *et al.* 2015). Calving style is controlled by internal glacier dynamics (Benn *et al.* 2007, Bassis and Jacobs 2013), but environmental factors play an important role in the manifestation of individual events and therefore calving rate (Schild *et al.* 2018), although the geometry of the fjord and glacier also has an impact (Enderlin and Howat 2013, Schild and Hamilton 2013).

Terminus stability, and so calving rate, is dependent on the level of buttressing provided by the ice melange (Amundson *et al.* 2010, Vieli and Nick 2011, Christoffersen *et al.* 2012), although factors such as fjord bathymetry (Nick *et al.* 2013, Rignot *et al.* 2016) and water circulation and temperature can also influence calving (Holland *et al.* 2008, Straneo and Heimbach 2013, Luckman *et al.* 2015). Processes such as crack propagation, which is facilitated by ice-ocean interactions, highlight the link between internal tidewater glacier mechanics and external forcing from the fjord water at the terminus (Benn *et al.* 2007, 2017).

The retreat of Helheim Glacier between 2000-2005 has been shown to have resulted from changing calving dynamics at the terminus (Nick *et al.* 2009), but the driver behind the increased calving has remained unclear. Currently the focus of research has been understanding the relationship between submarine melting, and so ocean heat content, and calving dynamics. However, limited research has looked at the relationship between the ice melange and submarine melting and the indirect effect of submarine melting on terminus stability (Amundson *et al.* 2010).

Importance of ice melange:

Ice melange suppresses calving rate (Reeh *et al.* 2001) aiding the readvancement of tidewater glaciers in winter (Amundson *et al.* 2010). Presence of ice melange has been shown to be responsible for the seasonal retreat and advance of Store Glacier (Todd and Christoffersen 2014). Winter re-advance at other tidewater glaciers, such as Jakobshavn Isbrae, has been associated with a deceleration in glacier velocity because of changes in geometry and additional friction provided at the front (Joughin, Howat, Fahnestock, *et al.* 2008, Amundson *et al.* 2010).

At Helheim Glacier, the ice-melange has been shown to move consistently with the glacier terminus at a speed of 19-25±1.1m/d (Enderlin and Howat 2013, Foga *et al.* 2014). Here, there is a noticeable stepped movement of the ice-melange and attached icebergs which has been attributed to katabatic winds (Sutherland, Roth, *et al.* 2014). Once free of the ice-melange, the iceberg movement was no longer characterised by a stepped movement. This suggests currents become more important in iceberg movement when no longer constrained by the ice-melange, with wind forcing the main

driver of movement when in the melange. Compression of ice-melange close to the glacier front has been suggested by a negative velocity gradient of icebergs, trapped within the melange, against distance from the terminus (Sutherland, Roth, *et al.* 2014). This highlights the buttressing stress put upon the melange from the terminus.

It has been hypothesised that katabatic winds, along with increased air temperature, were the driving force behind the retreat of Kangerdlussuaq Glacier in 2004-2005 through the removal of ice melange (Christoffersen *et al.* 2012). As previously highlighted, removal of melange can lead to increased calving and glacier retreat (Amundson *et al.* 2010). Similarities can be drawn between katabatic wind exposure, fjord circulation and glacier retreat at Kangerdlussuaq Fjord and Sermilik fjord raising the possibility that katabatic winds can effect Helheim Glacier terminus retreat (Joughin, Howat, Alley, *et al.* 2008, Jackson *et al.* 2014, Oltmanns *et al.* 2014, Sutherland, Straneo, *et al.* 2014).

Ice melange presence and size are not purely controlled by wind stress (Christoffersen *et al.* 2012), but are also a function of submarine melt rate (Amundson *et al.* 2010, Enderlin and Howat 2013) and air temperature (Christoffersen *et al.* 2012). Increased basal and submarine melting from increased water temperature could lead to an earlier seasonal break or iceberg release from melange (Joughin *et al.* 2012). Melting of the ice melange can therefore act as an indirect link between submarine melt rate and calving rate increase inducing higher terminus velocities.

Submarine melting:

Increased submarine melting often facilitates calving through undercutting (O'Leary and Christoffersen 2013, Benn *et al.* 2017, Slater *et al.* 2017) and has been shown to be responsible for the small scale calving in Svalbard (How *et al.* 2017). However, melt rates are rarely quantified (Schild *et al.* 2018). This is often because of the difficulty in obtaining *in situ* measurements - especially close to the ice melange (Amundson *et al.* 2010). The effects of submarine melt rates is widely debated, with conclusions ranging from promoting calving to reducing it, dependant on the glacier and model used (Ma and Bassis 2019).

Submarine melt induced calving can occur with or without amplification. Calving without amplification develops over a region of undercutting at the glacier terminus, where mass is lost only from the area above the undercutting (Benn *et al.* 2017). No further changes are made to the terminus or therefore to the internal dynamics of the glacier, apart from effect of the mass loss. Amplification occurs when ice is lost further into the glacier than the undercutting, resulting in crack or weakness propagation up the glacier (O'Leary and Christoffersen 2013, Benn *et al.* 2017). There is limited understanding of what processes control calving amplification, although it has been suggested that the magnitude of submarine melting prior to calving plays an important role (Schild

et al. 2018). Submarine melt rate can also vary with terminus velocity, creating a positive feedback loop once calving has occurred and so glacier speed increases (Jenkins 2011).

Three generic types of submarine melting have been identified (Fig. 1.1). The first type, free convection, is the process where water meets the ice, melting it and releasing freshwater into the system (El-Tahan *et al.* 1987, Chauché *et al.* 2014, Magorrian and Wells 2016). Density driven circulations develops as the buoyant freshwater moves to the surface along the ice-ocean boundary. Free convection can drive weak buoyancy driven fjord circulation (Magorrian and Wells 2016). The second type of submarine melting, horizontal fjord circulation, is caused by the forcing of water horizontally across the glacier terminus (Cowton *et al.* 2015). However this method of melting is poorly understood and has not been observed in the field (Schild *et al.* 2018). Nonetheless this methods has been suggested to have the potential to cause more melting than free convection (Schild *et al.* 2018). The final submarine melt process, meltwater discharge, results from the entrainment of warm water by buoyant plumes rising from the base of the glacier terminus (Christoffersen *et al.* 2012, Cenedese and Linden 2014, Chauché *et al.* 2014, Carroll *et al.* 2016, Slater *et al.* 2017). The discharged plume and entrained warm water rise, melting the terminus during its ascent, until the discharged plume reaches the surface or acquires the density of the *in situ* water.

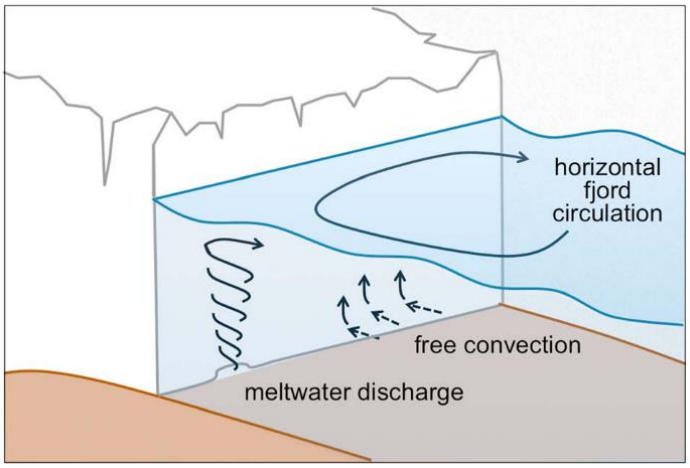

Figure 1.1: Schematic of submarine melt processes with the arrows showing the theoretical movement of water. Adapted from Schild *et al*., (2018).

Multiple sites can develop across the glacier front producing large scale melting over the terminus (Fried *et al.* 2015, Slater *et al.* 2015). Discharge plume formation drives fjord-scale buoyancy circulation (Xu *et al.* 2012, Carroll *et al.* 2015, Cowton *et al.* 2015). Of these three types of submarine melting, meltwater discharge is the dominant cause of submarine melting linked to glacier retreat (Schild *et al.* 2018). This suggests that, when discharge decreases in non-summer months, submarine melt rate reduces, making understanding summer melt dynamics more important (Sciascia *et al.*

2013, Cowton *et al.* 2016). However winter months control the sensitivity of the terminus to increased melt rates from summer discharge, through positive feedbacks from winter readvancement and ice melange protection (Reeh *et al.* 2001, Joughin, Howat, Fahnestock, *et al.* 2008, Amundson *et al.* 2010, Christoffersen *et al.* 2012, Todd and Christoffersen 2014).

Ultimately submarine melt rate through any of these processes is controlled by *in situ* water temperature at the glacier front (Jenkins 2011) and therefore understanding the transfer of warm water from the ocean shelf through the fjord system is essential (Straneo and Cenedese 2015). As submarine melting plays an important role in calving rate, it is no surprise that the calving rate has been shown to correlate with ocean heat content (Luckman *et al.* 2015).

Fjord circulation:

Terminal retreat of tidewater glaciers has been associated with ocean temperature rise (Luckman *et al.* 2015), with mass loss across Greenland corresponding linearly to the increased heat availability from the ocean (Cowton *et al.* 2018). Although ocean temperatures can be linked to glacier melt, the transfer of heat across the fjord is complicated by various circulation processes (Straneo and Cenedese 2015). Fjords mediate the submarine melting at the glacier front sourced from the ocean through their circulation. Circulatory patterns are highly variable despite the quasi-linear response of terminus retreat to ocean temperature (Jackson *et al.* 2014, Cowton *et al.* 2018) which suggests that fjords circulation is fairly consistent on yearly timescales. However, this neglects the importance of strong infrequent sources of fjord renewal.

Fjords in east Greenland are characterised by having deep sills, depths of at least 600m, and two main waters masses (Straneo *et al.* 2010a, Sutherland, Straneo, *et al.* 2014). The water on the shelf can be shallower than that in the fjord (Sutherland, Roth, *et al.* 2014) so that the sill interaction with fjord-shelf exchange only becomes important when its maximum height is greater than the boundary layer of the two dominant water masses (Spall *et al.* 2017). By comparison fjords in west Greenland, which have shallower sills, show lower variability and interaction with shelf waters (Bendtsen *et al.* 2014, Gladish, Holland, Lee, *et al.* 2015). Polar origin water, which is glacially modified, forms the top 200m, while below the pycnocline the bottom layer is comprised of relatively warm, saline Atlantic origin water (Straneo *et al.* 2012, Jackson *et al.* 2014).

Circulation of water within the fjord is a result of many circulatory processes (Fig. 1.2). Base circulation from the fjord is driven by buoyancy circulation from glacial input (Mortensen *et al.* 2011) often from plume dynamics at the glacier terminus (Jenkins 2011, Sciascia *et al.* 2013, Mankoff *et al.* 2016). Further processes are caused by wind forcing (Moffat 2014, Oltmanns *et al.* 2014), intermediary circulation or exchange with the shelf (Klinck *et al.* 1981, Straneo *et al.* 2010a), or deep

water renewal (Cottier *et al.* 2010). Surface runoff can also drive classical estuarine circulation (Geyer and MacCready 2014).

Non-summer circulation is driven by shelf forcing (Jackson *et al.* 2014), while summer circulation is dominated by increased buoyancy circulation from increased freshwater input, reducing the impact of intermediary circulation (Jackson and Straneo 2016). Strong down-fjord winds have been shown to aid buoyancy circulation (Moffat 2014).

Shelf forced flow is primarily driven by barrier wind events down the east Greenland Coast (Harden, Pickart, *et al.* 2014). Intermediary circulation creates two flows, one above 150m out the fjord and an opposite in-fjord flow from 150-450m. This secondary in-fjord flow is made up out of Atlantic origin water which is relatively warm and saline, maintaining the stability of the water column (Jackson *et al.* 2014). Intermediary circulation can alter the density structure within the fjord and so change the position at which freshwater plumes from the glacier terminus enter the water column (Mortensen *et al.* 2011, Inall *et al.* 2014).

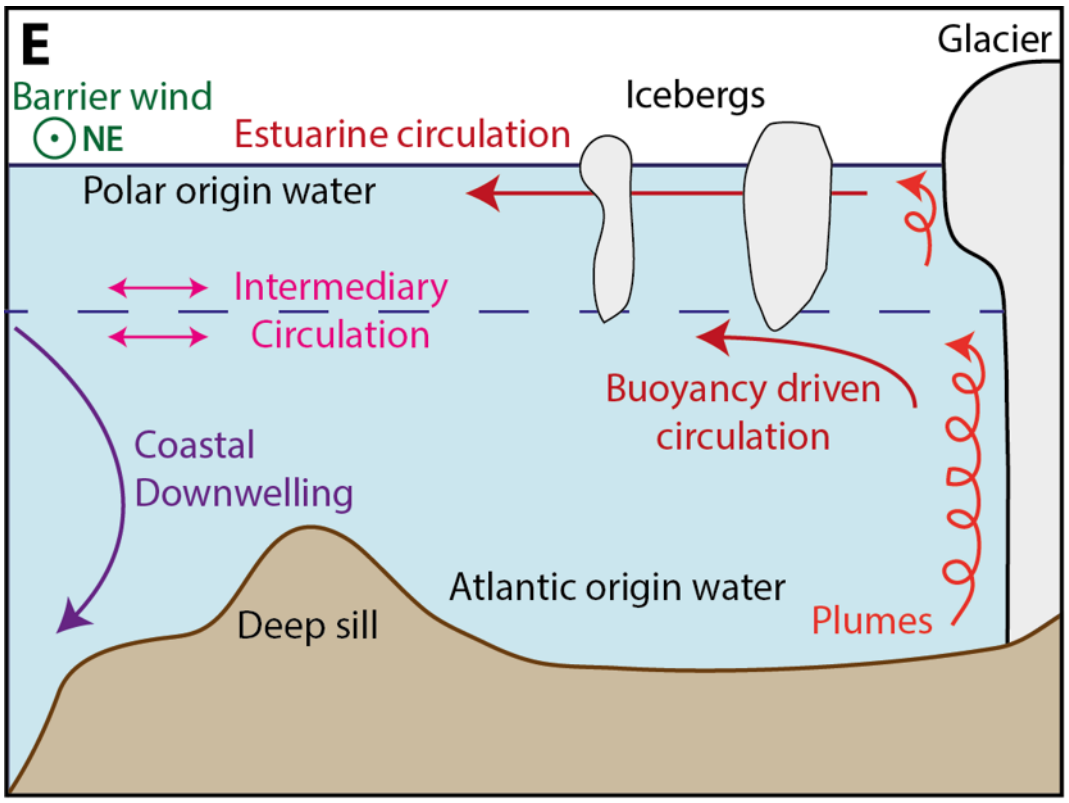

Figure 1.2: Schematic of fjord circulatory processes in a typical eastern Greenland fjord. Dotted line represents the thermocline. Author's own.

Previous work has suggested that across-fjord gradients and variations in currents are weak (Sutherland, Straneo, *et al.* 2014). However, iceberg outflow has been shown to be strongest towards the western side of the fjord mouth (Sutherland, Roth, *et al.* 2014). Other studies have concluded that 2D models of fjords are insufficient since such models cannot emulate the necessary across-fjord dynamics (Jackson *et al.* 2018).

High iceberg velocities across Sermilik Fjord mouth have been used to support the notion that the East Greenland Coastal Current (EGCC) passes right by the fjord and possibly dipping into the fjord itself (Sutherland, Roth, *et al.* 2014). This is unlikely to alter deep water renewal but could aid high sea-ice concentrations on the shelf and in the fjord.

Warm water influxes from wind events:

Barrier wind events down the east coast of Greenland (Moore *et al.* 2005, Harden *et al.* 2011) can indirectly drive fjord-shelf exchange through intermediary circulation (Straneo *et al.* 2010a, Harden, Straneo, *et al.* 2014, Jackson *et al.* 2014, Sutherland, Straneo, *et al.* 2014). These wind jets result from cyclonic systems meeting the steep east Greenland topography, causing strong southward flows (Moore *et al.* 2005, Harden *et al.* 2011). Through Ekman transport this wind stress leads to coastal downwelling, creating a strong baroclinic exchange and coastal wind set up (Fig. 1.3). A reverse flow is then triggered once the pycnocline relaxes, bringing warm saline water into the fjord (Fig. 1.3). Interest in the barrier winds was sparked after the resultant intermediary circulation was shown to cause large scale warm water renewal at the base of the fjord (Straneo *et al.* 2010a). Despite numerous studies since, it remains unclear whether warm water renewal reaches the top of fjord and the glacier terminus, via this process (Fraser and Inall 2018). Intermediary circulation is the primary driver of warm water influx into the fjord during non-summer months (Jackson *et al.* 2018), and therefore of submarine melting. However, this compares poorly to summer heat fluxes which are an order of magnitude higher (Inall *et al.* 2014, Sutherland, Straneo, *et al.* 2014) or models (Cowton *et al.* 2016). Although renewal is rapid, with 25% of fjord waters renewed within 10 days whereas buoyancy circulation only renews 10% over the same time period (Cowton *et al.* 2016), over longer time periods the uniformity of buoyancy driven circulation means it plays a more dominate role in summer (Cowton *et al.* 2016).

Barrier wind events can last for several days (Harden *et al.* 2011) but their effect on the fjord system is sustained for more than 10 days (Jackson *et al.* 2014, Cowton *et al.* 2016). Around 16 barrier wind

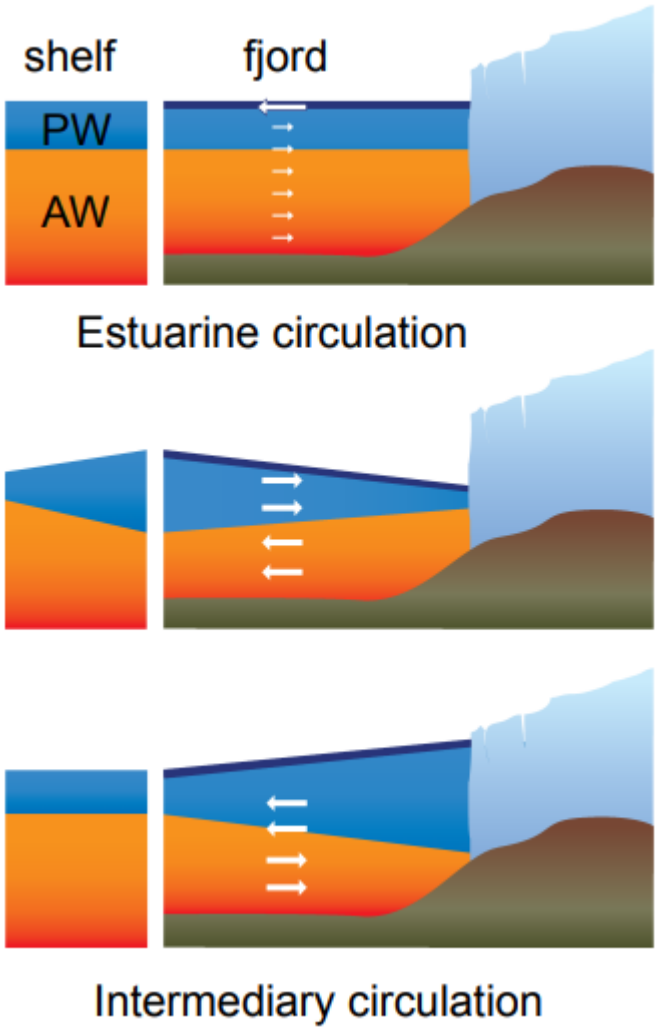

Figure 1.3: Schematic of estuarine circulation and barrier wind set up leading to intermediary circulation. Figure from Ben Harden.

events that lead to intermediary circulation occur each year (Jackson *et al.* 2014). It is primarily these events which drive the high variability in temperature profiles in Sermilik and Kangerdlussuaq Fjords even if these events are not the main cause of submarine melting (Jackson *et al.* 2014, Fraser and Inall 2018). Fjord renewal and warm water inflow into the fjord system is poorly understood, especially regarding how the shelf forced flow penetrates up the fjord (Straneo and Cenedese 2015). Shelf forced flow is strongest at the mid-fjord and wanes towards the top of the fjord (Jackson *et al.* 2014). These observations from moored buoys have also been confirmed by iceberg tracking which show maximum movement towards the centre of the fjord (Sutherland, Roth, *et al.* 2014). Intermediary circulation has also been shown to be more efficient at transferring energy to the front of the glacier, with heat availability at the terminus modelled to be similar to that of buoyancy driven circulation - despite the lower heat influx into the fjord (Fraser and Inall 2018). However, this model neglects glacier discharge - which as the main driver of buoyancy driven circulation could alter the heat influx across the fjord (Cowton *et al.* 2016, Jackson and Straneo 2016).

Although it is unclear how significant a role shelf forced exchange, driven by barrier winds, plays in glacier retreat, it has been established that the barrier winds are key to fjord variability and renewal (Jackson *et al.* 2014, Sutherland, Straneo, *et al.* 2014, Straneo and Cenedese 2015). Through the study of barrier wind driven fjord renewal, it has been accepted that strong infrequent wind events can play an important role in fjord circulation and so impact submarine melting at the glacier front

(Straneo *et al.* 2010a), with melt rates no longer assumed to purely be a function of season, glacier dynamics and ocean temperature (Inall *et al.* 2004, 2014). It therefore odd that few studies have attempted to understand the more intense but less frequent katabatic wind events prevalent in the same locations (Oltmanns *et al.* 2014).

Katabatic winds:

Katabatic winds, or Downslope Wind Events (DWEs), can reach a magnitude equivalent to a hurricane on the Saffir-Simpson damage-potential scale, reaching wind speeds up to 90m/s (Born and Böcher 2001, Mernild *et al.* 2008). Due to their cold air mass nature, they can reduce *in situ* temperatures by -20°C (Born and Böcher 2001). Sermilik and Kangerdlussuaq fjords are characterised by such air flows (Bromwich *et al.* 1996, Oltmanns *et al.* 2014). Here, katabatic winds are less frequent than barrier winds but the katabatic winds are more intense (Spall *et al.* 2017). Between 4-8 downslope wind events happen per year, with the majority of such events centred around non-summer months (Oltmanns *et al.* 2014).

Katabatic winds originate from radiational cooling above the Greenland Ice Sheet, forming a dense air mass which then accelerates down the steep topography (Fig. 1.4, Parish and Bromwich 1987, Heinemann 1999, Parish *et al.* 2001). Katabatic winds are stronger in winter due to increased surface cooling and lower solar radiation (van Angelen *et al.* 2011). The potential for strong downslope wind flow in Sermilik Fjord is magnified by the extreme gradient of the coastal topography in Ammassalik (Bromwich *et al.* 1996, 2002, Klein *et al.* 2001). Despite the simple origin of katabatic winds, other

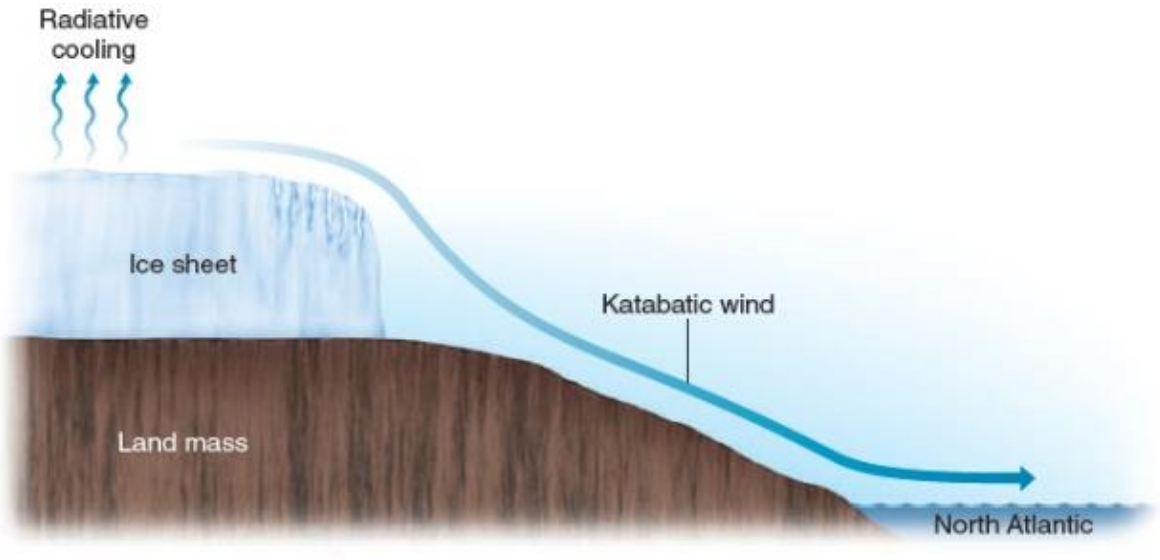

Figure 1.4: Schematic of katabatic wind formation and downslope flow. Adapted from Brandi, (2016).

factors such as mountain wave breaking and mesoscale cyclones have been suggested to aid or alter their magnitude (Klein and Heinemann 2002, Doyle *et al.* 2005). Cyclones aid katabatic flow where the geostrophic flow direction is the same as the downward topography (Bromwich *et al.* 2002, Heinemann and Klein 2002, Klein and Heinemann 2002). Tip jets precede 31% of DWEs (Våge *et al.* 2009, Oltmanns *et al.* 2014).

Despite the effort put into resolving the origin and causes of katabatic winds, relatively little has been done to characterise them and their possible impacts (Oltmanns *et al.* 2014). Research has instead focused on other wind events such as tip jets (Moore *et al.* 2005, Renfrew *et al.* 2009, Våge *et al.* 2009, Moore and Moore 2014) and barrier winds (Moore *et al.* 2005, 2013, Harden *et al.* 2011). DWEs could lead to large heat flux over the Irminger Sea (Oltmanns *et al.* 2014) and therefore affect ocean convection (Pickart *et al.* 2003), AMOC (Jungclaus *et al.* 2005, Stouffer *et al.* 2006), northern European climate (Cohen *et al.* 2014, Overland *et al.* 2015), and deep ocean carbon sequestration (Sabine Christopher *et al.* 2004). Buoyancy losses could also occur over the Irminger Sea as cold, dry air is advected offshore, and DWEs have been calculated to account for one fifth of wintertime losses (Oltmanns *et al.* 2014).

DWEs over Tasiilaq, analysed using ERA-Interim dataset, form broad jets with a width of 300km, height of 2500m and have a maximum speed of 25m/s (Oltmanns *et al.* 2014). As the wind increases there is a corresponding drop in temperature and pressure, with minimum pressure reached just before maximum wind speeds are reached, and the minimum temperature occurring just after that timepoint (Oltmanns *et al.* 2014). Models with a topographical and model resolution of 60km or greater, such as ERA-Interim, underestimate maximum wind speed by up 20m/s compared to an equivalent finer, 1.67km, resolution model (Oltmanns *et al.* 2015). Despite surface wind speeds in DWEs being sensitive to both topographical and model resolution, the large extent of the downslope morphology of the Sermilik Fjord region allows ERA-Interim to successfully show katabatic flow (Oltmanns *et al.* 2014). Higher model resolution would allow the simulation of wave dynamics, while higher topographical resolution would give a better representation of the wave dynamics (Oltmanns *et al.* 2015).

Katabatic wind effects on fjord circulation:

Katabatic winds have been suggested to have an influence on fjord circulation (Sutherland, Roth, *et al.* 2014). The upper layer of water in the fjord moves out towards the shelf, matching the wind (Moffat 2014, Spall *et al.* 2017). This movement results in a return flow of deeper waters from the shelf into the fjord - similar to the later stage of shelf forced intermediary circulation (Fig. 1.3, Jackson *et al.* 2014, Sutherland, Straneo, *et al.* 2014). However, unlike intermediary circulation,

previous stages of cold-water pumping into the upper layer of the fjord are not expected to occur. This could ultimately mean greater submarine melting as the cold water pumping stages lead to a reduction of melting at the glacier front, although compensatory warm inflows then increase melt rates (Straneo *et al.* 2010a, Jackson *et al.* 2014, Sutherland, Straneo, *et al.* 2014).

The one study looking at the fjord circulation effects of DWEs based off the MITgcm model estimated that 10% of the surface waters are exported during each event (Spall *et al.* 2017). Upper layer movement in the model was in phase with wind forcing, with bottom waters out of phase and exhibiting lower velocity (Spall *et al.* 2017). There are large uncertainties in the conversion of wind velocity to wind stress, as icebergs and sea ice can have a dampening effect. There is also uncertainty in the volume exchange because of poor ADCP coverage. The study concluded that barrier wind driven shelf forced exchange has a stronger and more frequent effect on fjord circulation (Spall *et al.* 2017). Analysis based on Wedderburn number calculations, ratio of wind driven set up to the mixed layer depth, suggest down-fjord winds are significant in winter but have limited influence in summer (Sutherland, Straneo, *et al.* 2014, Inall *et al.* 2015).

The expected down-fjord flow from the downslope wind event could also increase across-fjord variation through Ekman transport at lower levels. This is also likely to be aided by favourable sea-ice and iceberg removal from the right-hand side of the fjord (Sutherland, Roth, *et al.* 2014). As a result, wind stress will be higher down this side of the fjord, increasing the across-fjord gradients during katabatic wind events.

Sea-ice and freshwater shelf export:

Sea-ice removal from the fjord and shelf regions on the East Coast of Greenland is well known to occur but has been rarely quantified or the possible consequences considered (Oltmanns *et al.* 2014). Sea-ice forms a barrier preventing the direct transfer of wind forcing onto the surface water, although thin ice can increase the transmission due to increased air-ice and ice-ocean drag coefficients (Spall and Pedlosky 2018). It is therefore important to account for these factors when performing any analysis of wind driven fjord circulation. Reduced sea-ice concentration within the fjord system is linked to glacier retreat, as it aids the stability of the terminus through buttressing and the reduction in open water (Howat *et al.* 2010, Walter *et al.* 2012). The sea ice in the upper fjord also aids with the formation and persistence of the ice melange in the front of the calving front (Christoffersen *et al.* 2012).

Once advected from the shelf and the Irminger Sea, the sea ice will melt quickly given the warm *in situ* water leading to a local freshening (Sutherland *et al.* 2013). Considering the prevalence of katabatic winds down the East Coast of Greenland and the ready supply of sea ice exported from the

Fram Strait (Doyle *et al.* 2005), sea-ice export into the Irminger Sea could be on a large scale. Freshwater fluxes from the southeast Greenland coast have also been associated with the freshening of the Labrador Sea (Close *et al.* 2018).

Total offshore flux has been modelled to be around 20-40km^3/yr from katabatic winds (Spall and Pedlosky 2018) which compares to freshwater flux of 1500km^3/yr from EGC and 500km^3/yr from glacier meltwater (Holfort *et al.* 2008). However, there are large uncertainties in these estimations, but they do hint that wind forcing does form an important component of freshwater budget of the Greenland Shelf. The study also ignores *in situ* current effects which can alter resultant flow and sea-ice movement (Spall and Pedlosky 2018). Glacial meltwater water export can have large scale effects on AMOC (Bamber *et al.* 2012, Weijer *et al.* 2012) and alter coastal waters (Bacon *et al.* 2014). A decrease in the salinity of the EGC also has the potential to disrupt global thermohaline circulation (Spall and Pedlosky 2018). This could have potential long-term feedback mechanisms on the Greenland Ice Sheet and fjord circulation.

Analysis of 32 DWEs showed mean removal of 29% of the of sea-ice within the fjord and 26% on the shelf (Oltmanns *et al.* 2014). However, it is unclear how these change with the strength of the DWE and seasonally. Quantification of sea-ice removal from the shelf would allow more accurate predictions of the importance of katabatic winds in the Irminger Sea freshwater budget. Within the fjord system, association of sea-ice removal with wind speed could be accounted for when considering fjord circulation. Sea-ice may dampen katabatic wind induced circulation below a certain threshold, when the wind is strong enough to remove the sea ice. The duration of DWE may also play an important role is sea-ice removal, with longer events capable of removing the sea ice before driving fjord circulation.

Chapter 2:

Study site:

Helheim Glacier:

Helheim Glacier is the 5th largest outflow from the Greenland Ice Sheet (Enderlin *et al.* 2014) and so has been extensively studied (Howat *et al.* 2005, Joughin *et al.* 2005, Luckman *et al.* 2006, Nick *et al.*

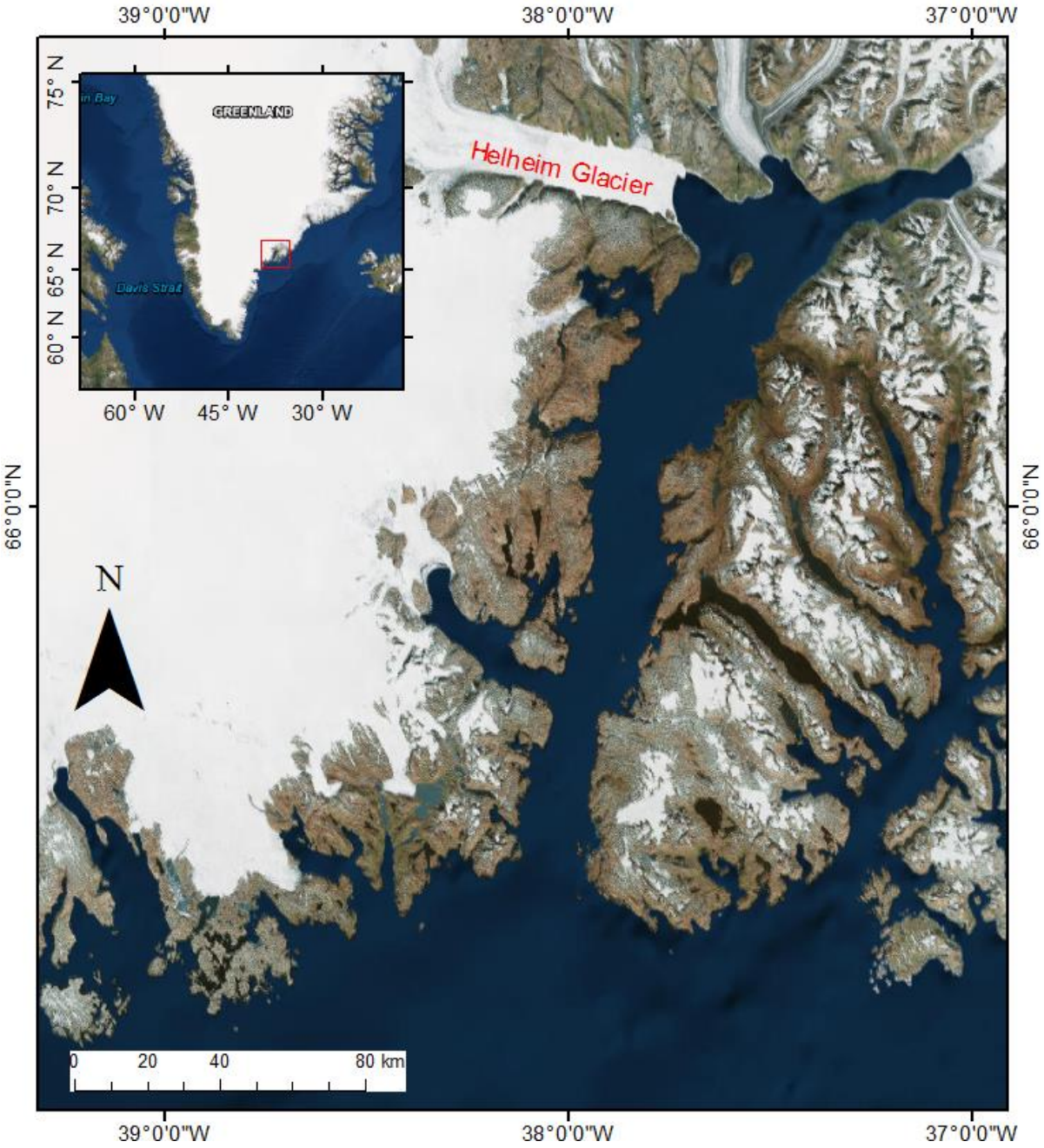

Figure 2.1: Location of Sermilik Fjord and Helheim Glacier in south east Greenland. Base map produced Esri world imagery.

2009). It is a tidewater glacier in south eastern Greenland, extending into Sermilik Fjord where it is grounded at a depth of around 600m (Fig. 2.2, Straneo *et al.* 2012)). Between 2003-2006 mass losses at Helheim were estimated to be 51±8 km^3/yr after losses increased rapidly in 2003 (Stearns and Hamilton 2007). Large scale acceleration of the glacier was observed during the same period in correspondence with the increased mass loss (Joughin *et al.* 2005). Over smaller time scales the glacier's velocity has been shown to vary in accordance to calving events, where periodic accelerations occur post calving (Nettles *et al.* 2008).

Mass loss at Helheim Glacier is a combination of melt and calving (Rignot *et al.* 2011, Enderlin *et al.* 2014), heavily linked to increased submarine melting from increased ocean temperatures transferred through Sermilik Fjord (Holland *et al.* 2008). Changes in ocean temperature have been shown to explain 76% of terminus position, while fluctuations in glacier discharge can explain 75% (Cowton *et al.* 2018).

Helheim Glacier terminus flows between 8-11km/yr (Moon *et al.* 2012). An ice-melange usually extends 10km from the glacier terminus, varying seasonally (Sutherland, Roth, *et al.* 2014), and has been speculated to play an important role buttressing the glacier in non-summer months. As well as Helheim, two smaller glaciers, Fenris and Midgard, flow into the north and northeast of Sermilik Fjord (Jackson and Straneo 2016).

Sermilik Fjord:

Sermilik Fjord is the most extensively studied fjord on the east Greenland Coast (Straneo *et al.* 2010a, Jackson *et al.* 2014, Sutherland, Roth, *et al.* 2014, Sutherland, Straneo, *et al.* 2014, Jackson and Straneo 2016). It is around 100km in length and has an average width of about 7km (Sutherland, Straneo, *et al.* 2014, Fig. 2.1). The shallowest sill lies at around 550m depth, well below any potential pycnocline across the fjord mouth (Fig. 2.2, Sutherland, Straneo, *et al.* 2014). Deeper parts of the fjord reside at around 900m making parts of the shelf shallower (Fig. 2.2, Jackson *et al.* 2014, Sutherland, Roth, *et al.* 2014). Two water masses form the water column; polar origin water above ~200m depth and warm saline Atlantic origin water from the shelf below (Straneo *et al.* 2011). Glacial modified waters reside in the upper layer (Straneo *et al.* 2011, Sutherland, Straneo, *et al.* 2014). The upper layer is less stratified in non-summer months due to the lower freshwater input. Circulatory patterns are typical of an eastern Greenlandic fjord, with high variability and periodic shelf forced inflows (Fig. 1.2, Straneo and Cenedese 2015). Attempts have been made to link non-summer shelf forced flows to terminus retreat but given the complexity of fjord and glacier dynamics no conclusive result has been achieved. Melt rates have been shown to increase on short

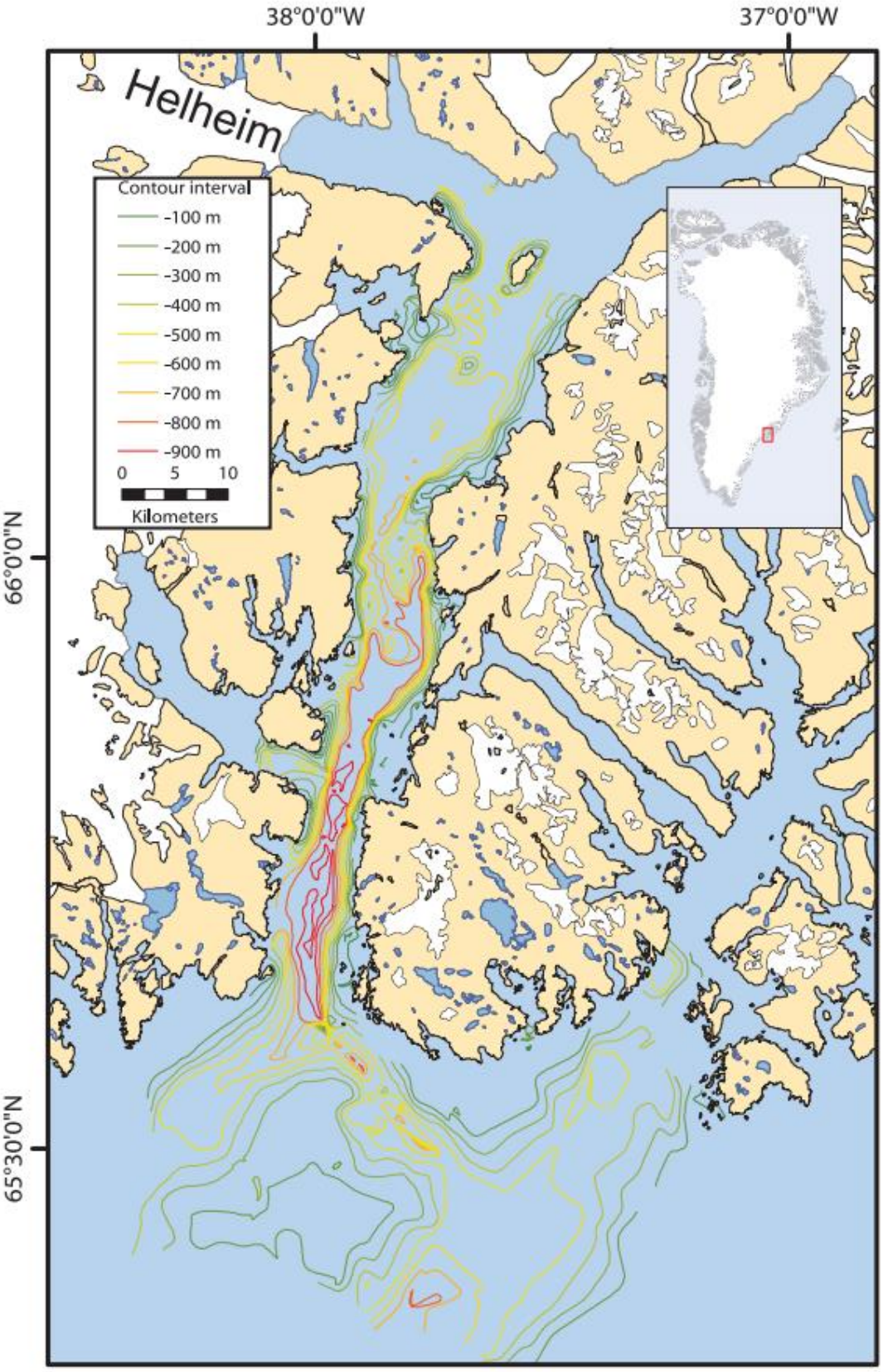

Figure 2.2: Bathymetry of Sermilik Fjord and immediate shelf showing depths of up to 900m at the fjord mouth. The fjord becomes shallower towards the Helheim Glacier, but it remains at a depth of at least 500m. Compared to the fjord mouth, the depths of the shelf are much shallower. Adapted from Schjøth *et al*., (2012).

term scales because of intermediary circulation, but summer discharge driven melt still accounts for 60% of yearly melt on the most optimistic models (Jackson *et al.* 2014, Straneo *et al.* 2016).

Helheim Glacier freshwater input into Sermilik Fjord between 1998-2008 was 33.9 km^3/yr from ice discharge and 6.5 km^3/yr from surface melt and runoff (Mernild *et al.* 2010). However, this quantification lacks any input from melt of the icebergs which flow from the terminus down the fjord. The vast majority of freshwater input occurs in summer months and creates meltwater plumes and buoyancy driven circulation (Jackson *et al.* 2014). It is this freshwater discharge which drives the summer peak of submarine melting, suggesting a partial dominance over other causes of terminus melt (Straneo *et al.* 2016). When meltwaters subside in non-summer months, shelf forced intermediary circulation is the main source of fjord renewal and submarine melt (Straneo *et al.* 2011, Sutherland, Straneo, *et al.* 2014).

Tidal movement in Sermilik Fjord is suggested to be around 0.02m/s from both moored time series (Sutherland, Straneo, *et al.* 2014) and iceberg tracking (Sutherland, Roth, *et al.* 2014). This is far below non-tidal movements of between 0.3-0.4m/s from moored data (Sutherland and Straneo 2012, Jackson *et al.* 2014) and from iceberg tracking (Sutherland, Roth, *et al.* 2014).

Oceanographic setting:

The close proximity of two major ocean currents, the Irminger Current and the East Greenland Current (EGC), dictate the water masses found in Sermilik Fjord, making them incredibly important for understanding changes at Helheim Glacier (Fig. 2.3, Straneo *et al.* 2010). The polar origin water, which forms the upper layer of the water column, is sourced by a combination of the EGC and glacier meltwater (Straneo *et al.* 2011). Bottom waters are brought in from the warm saline Irminger Current, which is key to the retreat of the glacier (Straneo *et al.* 2010a). A clear geographic boundary within east Greenland of glacier stability lies at around 69°N, below which glaciers, such as Helheim, are undergoing rapid retreat (Seale *et al.* 2011). Coincidently this also marks the uppermost boundary of the Irminger Current suggesting the importance of regional ocean temperature variability in glacier retreat (Seale *et al.* 2011, Walsh *et al.* 2012).

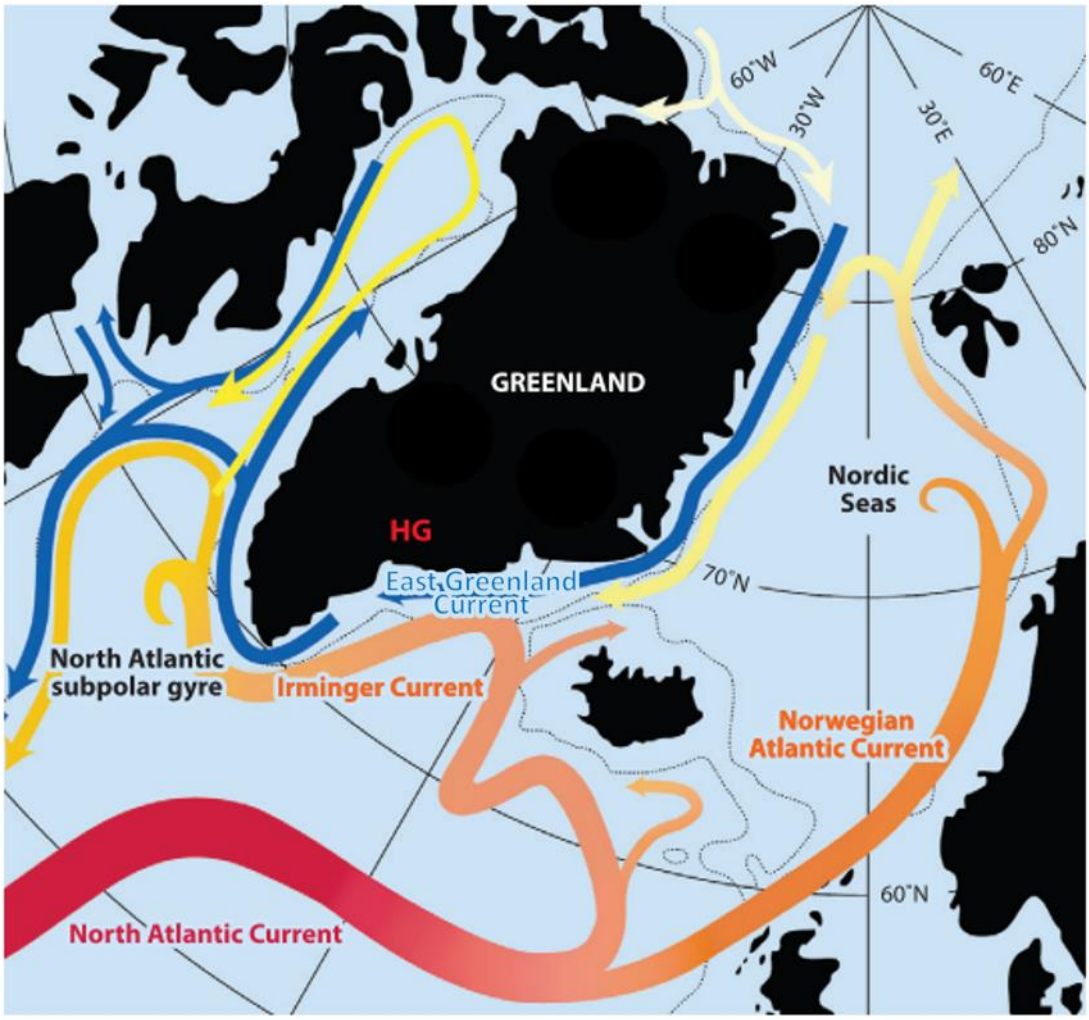

Figure 2.3: Oceanographic setting around Greenland, Nordic Sea and North Atlantic. Warm currents are presented in red with blue representing cold currents. The location of Helheim Glacier is marked with a red "HG". Note the cold East Greenland Current heading south west and the warm Irminger Current flowing in the opposite direction nearby. Adapted from Straneo and Cenedese (2015).

The East Greenland Coastal Current (EGCC), the inner branch of the EGC, is found at the mouth of Sermilik Fjord (Bacon *et al.* 2014). Once out of the fjord, iceberg flow is parallel to the shelf following the pattern of the EGCC with speeds up to 1m/s (Sutherland and Pickart 2008, Bacon *et al.* 2014, Sutherland, Roth, *et al.* 2014). This is also supported by higher iceberg velocities at the fjord mouth vicinity (Sutherland, Roth, *et al.* 2014).

Meteorological setting:

As well as strong coastal currents, strong wind events are frequently observed in East Greenland (Harden *et al.* 2011, Oltmanns *et al.* 2014). The high topographical gradient in the Ammassalik valley around Sermilik fjord is the main cause of such extreme wind events. When low pressure cyclones come into contact with the steep topography, barrier winds are produced which flow north westerly

down the coast (Harden *et al.* 2011). These winds can reach speeds of at least 20m/s and last for several days driving intermediary circulation into Sermilik Fjord (Harden *et al.* 2011, Jackson *et al.* 2014, Sutherland, Straneo, *et al.* 2014). Around 16 shelf driven flows resulting from barrier winds occur annually at Sermilik Fjord (Jackson *et al.* 2014). Dense air formation above the Greenland Ice Sheet flows down the steep Ammassalik topography as katabatic winds (Oltmanns *et al.* 2014). Although less frequent than barrier winds, averaging only around 6 ocurrences per year, katabatic winds can reach higher speeds and have been observed at speed of up to 90m/s (Born and Böcher 2001, Oltmanns *et al.* 2014). Both barrier and katabatic wind events predominate in winter with only occasional summer occurrences (Harden *et al.* 2011, Oltmanns *et al.* 2014).

Sea-ice coverage:

Seasonal sea-ice coverage is common both in Sermilik Fjord and across the nearby shelf. However, the fjord is rarely completely covered indicating the variability of its circulation (Andres *et al.* 2015). Sea-ice concentrations are considerably higher and are more consistent on the shelf, where a constant flow of sea ice comes down on the EGC, ultimately exported from the Arctic Ocean via the Fram Strait. Upon contact with the Irminger Current or Sea, the sea-ice rapidly melts creating localised areas of freshwater (Sutherland *et al.* 2013).

Chapter 3

Data and Methods:

Data:

Two weather stations were used to provide meteorological data for Sermilik Fjord (Fig. 3.1). The first was the Danish Meteorological Institute station in Tasiilaq which provided data spanning from 1958-2018 (Cappelen 2019). The second was the University of Copenhagen's research station on the banks of Sermilik Fjord (Mernild *et al.* 2008), which provided a timeseries from 1998 until 2014. To supplement the data from the weather stations, The European Centre for Medium-Range Weather Forecasts' ERA5 reanalysis was used, providing an hourly timeseries from 1978-2018 (Olauson 2018, available at: https://cds.climate.copernicus.eu).

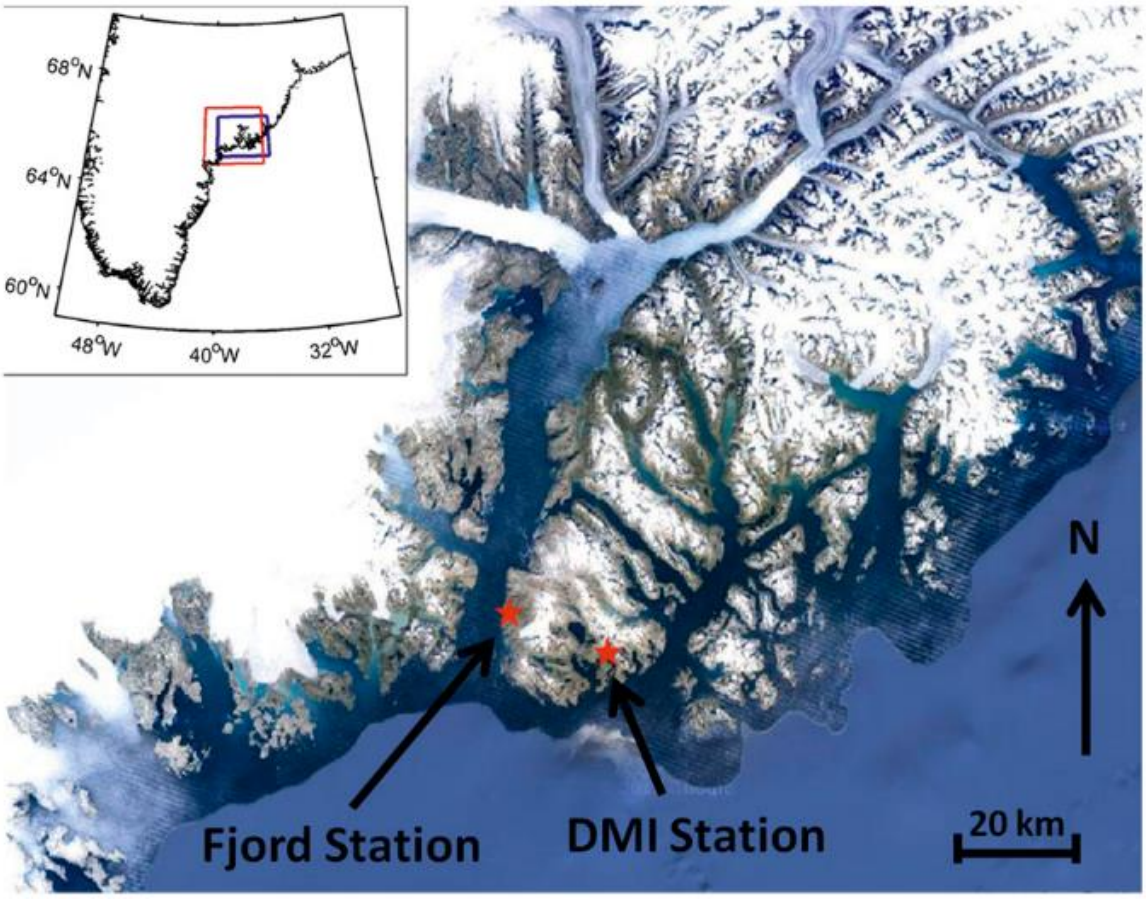

Figure 3.1: Location of Sermilik Fjord and Helheim Glacier in south east Greenland showing the location of University of Copenhagen Fjord Station and the Danish Meteorological Institute (DMI) station. Adapted from Oltmanns *et al*., (2014).

Moored buoy data was obtained for across Sermilik Fjord from the National Oceanographic Database Center (NODC). Data for the following seasons was obtained: 2009-2010 (Straneo 2015a), 2010-2011 (Straneo 2015b), 2011-2012 (Straneo, Sutherland, Harden, *et al.* 2015) and 2012-2013 (Straneo, Sutherland, and Harden 2015). The site numbers were given to each buoy based on the year it was placed and its buoy number within the accession. The location of each site used in this study has been mapped onto Sermilik Fjord (Fig. 3.2). The number of probes on each buoy varied greatly. Site 9_3 had temperature probes at 135m, 145m, 155m, 165m, 175m, 185m, 195m and

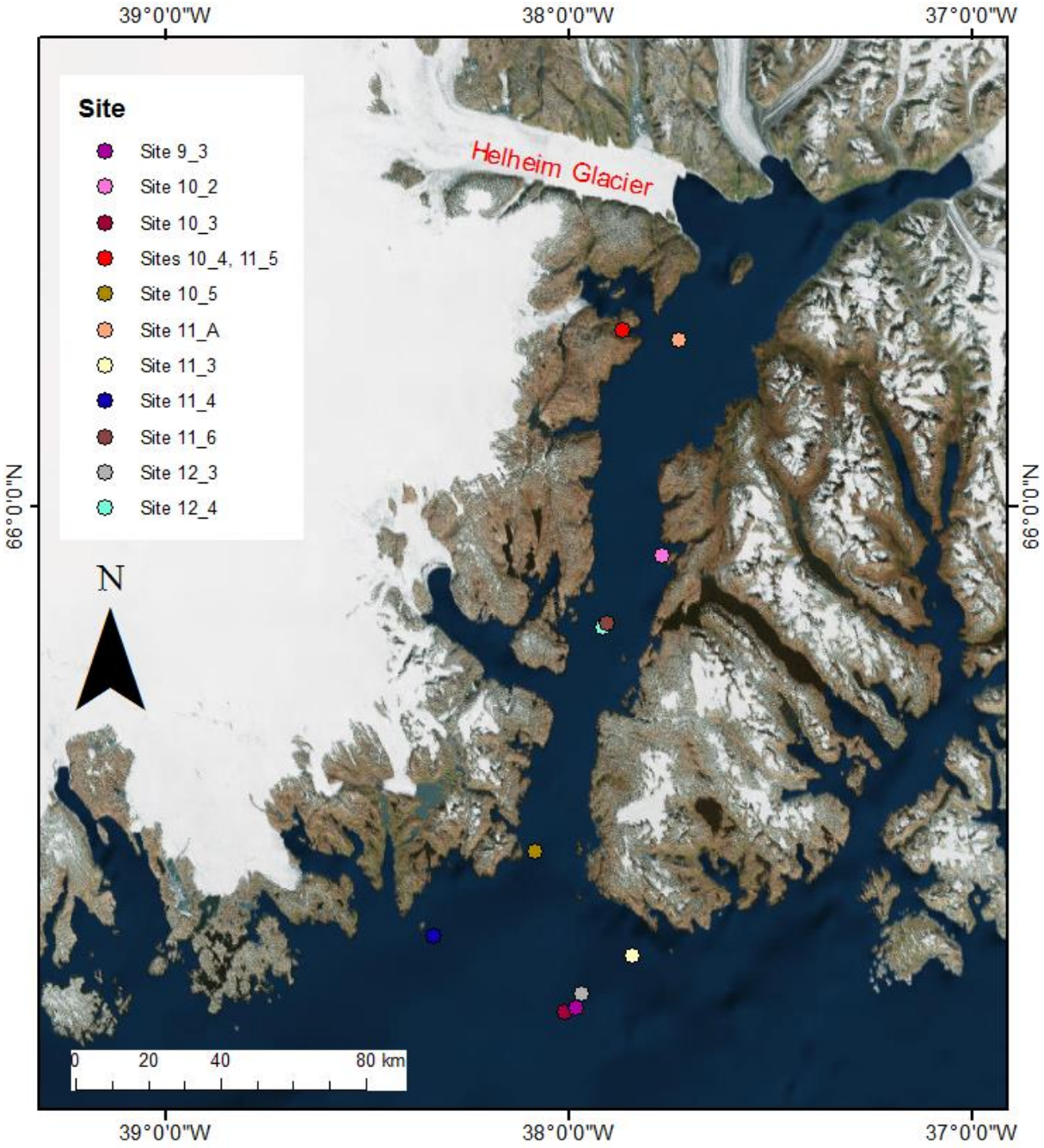

Figure 3.2: Location of Sermilik Fjord and Helheim Glacier in south east Greenland showing the location of each site used in this study. Base map produced Esri world imagery.

224m along with an ADCP at a depth of 224m. Site 10_2 had temperature probes at depths of 294m, 304m, 324m, 364m and 390m. Site 10_3 has temperature probes at depths of 155m, 165m, 175m, 185m, 195m, 215m, 235m and 262m. Sites 10_4 and 11_5 only had one temperature probe at 13m depth. Site 10_5 had temperature and salinity probes at 250m, 405m and 505m depth, along with a current profiler at 520m. Site 11_A had an upward facing ADCP at 315m which profiled the water in 8m bins up to a depth of 43m. Site 11_3 had temperature probes at depths of 220m, 240m, 260m, 280m, 300m and 305m. Site 11_4 had temperature probes at depths of 240m, 328m, 410m and 515m. Site 11_6 had temperature probes at depths of 250m, 270m, 290m, 310m, 330m, 350m, 400m, 550m and 650m, along with an upward facing ADCP at 381m which profiled the water up to 1m in 10m bins. Sites 12_3 had a current profiler at a depth of 280m. Finally, site 11_6 had temperature probes at 250m, 260m, 280m, 290m, 300m, 310m, 330m, 340m, 350m, 400m and 550m.

MODIS satellite imagery was used to observe Sermilik Fjord and Helheim Glacier as this imagery provides daily coverage between the years of 2009-2013, the timespan of the hydrographic data obtained for Sermilik Fjord (available at: https://www.ncdc.noaa.gov/gibbs/). Sea-ice concentrations for Sermilik Fjord and the nearby shelf for 2009-2013 were obtained from the University of Bremen Sea Ice Today (available at: https://seaice.uni-bremen.de/sea-ice-concentration/). These sea-ice concentrations are based on ASI algorithm from AMSR-E and AMSR2 passive microwave remote sensing (Spreen *et al.* 2008).

Methods:

Katabatic winds events were defined as down-fjord winds above at a certain wind threshold for at least three hours. Since temporary drop offs below the threshold before a resurgence taking the wind back up over the threshold was commonly observed, if the wind speed dropped to half the threshold the resurgence was classified as a separate event. If not, then the two peaks were classified as the same event. A wind direction window was also set to separate the katabatic wind from barrier wind related high wind speeds. As it is known that the estimated magnitude of downslope winds vary between the three datasets (Oltmanns *et al.* 2014) the parameters were set slightly differently for each dataset. For the Fjord Station (FS), the wind speed threshold was set at 12m/s with no direction parameter, since no non-down-fjord wind produces a wind speed above the threshold at this location (Oltmanns *et al.* 2014). The parameters set for the Danish Meteorological Station (DMI), were a wind speed of 11m/s and a direction between 280-360°. For the ERA5 dataset, the wind speed threshold was 10m/s and the wind direction window was 250-005°. The ERA5 dataset was used for most of the analysis in this study as, in contrast to the two weather stations, it provided consistent hourly wind speeds with no periods of missing data. Its predecessor, ERA-

Interim, is known to have successfully predicted katabatic wind events (Oltmanns *et al.* 2014) and accurately represented barrier winds along the Southeast Coast of Greenland (Harden *et al.* 2011). ERA5 correlated well with the two weather station datasets, especially between 2009-2014 (Fig. 4.2), making it a reliable source to show down-fjord wind speeds (Oltmanns *et al.* 2014). DWEs can also be predicted from ERA-Interim, although it fails to resolve mountain wave-breaking and maximum speeds are below measured wind speeds (Oltmanns *et al.* 2014, 2015) and a similar problem is seen in ERA5. This is not a particular problem, but any wind speed values quoted in this study will need to be converted, before it can be given as an infield value. The ERA5 pixel above Tasiilaq and over the DMI station (Fig. 3.1) correlated best with the weather stations, so this was used to represent wind speeds over Sermilik Fjord and shelf. Regression analysis was performed to show the relationship between DWE maximum wind speed and duration.

Using the discussed parameters, a catalogue of DWEs was created, using ERA5 reanalysis, for Sermilik Fjord from 1978-2018. The creation of this catalogue allowed the filtering of hydrographic, sea-ice and satellite imaging for the periods associated with katabatic winds.

Temperature profiles for each site was linearly interpolated in 10m bins to give a better resolution of the water column, similar to the steps taken by Jackson et al., (2014). The profiles from the upward facing ADCPs at sites 11_A, 11_6 and 12_4 were backwardly interpolated from the top of the profile down, since recordings from shallower depths were often missing because of icebergs (Jackson *et al.* 2014). Temperature and current velocity timeseries were created for three days either side of each DWE occurring during the buoy's lifespan, based off the ERA5 DWE catalogue. The most relevant and informative profiles have been presented in this study (Results).

Submarine melt rates (SMR) were calculated for each site with a temperature profile. Again, the ERA5 catalogue of DWEs was used to provide a time reference frame and SMRs were calculated across the duration of each DWE between 2009-2013. SMRs were derived from the quadratic method used in Jackson et al., (2014). Here, SMR is defined as:

$$SMR = \frac{\left(T - T_f\right)^2 - (\overline{T - T_f})^2}{(\overline{T - T_f})^2}$$

where SMR = submarine melt rate, T is the average water column temperature and T_f is the *in situ* freezing temperature. Calculation of T_f was performed using a modified Newton-Raphson iteration based on temperature, pressure and salinity (McDougall and Wotherspoon 2014). The saturation rate was assumed to be one. Further to this, two forms of percentage deviation of SMR were defined:

$$PDS = \frac{SMR - \overline{SMR}}{\overline{SMR}} x\ 100 \qquad PDS = \frac{SMR - SMR_{sr}}{SMR_{sr}}$$

where PDS = percentage deviation in submarine melt rate, SMR = submarine melt rate and SMR_{sr} = submarine melt rate prior to DWE. As the extent of the temperature profiles varied at every site, T, was not always calculated at the same depth. Instead a 50m section as close to 250m as possible was used as T. The following depths were used to calculate T: site 9_3 – 175m-225m, site 10_2 – 294m-344m, site 10_3 – 215m-265m, sites 10_4 and 11_5 – 13m, site 10_5 – 250m-300m, site 11_3 – 230m-280m, site 11_4 – 240m-290m, site 11_6 – 250m-300m and site 12_4 – 250m-300m. To see the variation between DWEs, PDS for the particular event, based off a starting reference point, was divided by the mean PDS over all DWEs at each site so as to remove the variability from location:

$$PDS\ variation\ at\ site\ for\ DWE = \frac{PDS_{DWE}}{\overline{PDS}}$$

$$PDS\ variation\ across\ the\ fjord\ for\ DWE = \overline{PDS\ variation\ at\ site\ for\ DWE}$$

where PDS_{DWE} = percentage deviation in SMR during a particular site during a particular DWE and $\overline{PDS}$ = the mean percentage deviation at the particular site.

From the University of Bremen sea-ice concentrations derived from AMSR-E and AMSR2 (Spreen *et al.* 2008), the change in sea-ice concentration on the shelf was calculated. The shelf area was defined (Fig. 4.18), and the percentage change within this area was measured from the day beforer the DWE to the day after the DWE. The change on sea-ice concentration was calculated for all the katabatic wind events that occurred in the 2009-2013 time-period in non-summer months when sea-ice was present. However, there is a slight gap in the data for 2011-2012 during the switch from AMSR-E to AMSR2.

Satellite imagery for each DWE between 2009-2013, based on the ERA5 DWE catalogue, was analysed. MODIS Terra and Aqua true color, thermal, Terra 367 and Aqua 721 were used, but only Aqua 721 is presented in this study as it provided the best degree of distinction between the sea-ice and the snow-covered land.

Chapter 4:

Results:

Katabatic winds and downslope wind event (DWEs) in Sermilik Fjord:

Analysing the full ERA5 dataset from 1979, DWEs in Tasiilaq ranged in duration from 3hrs, the duration minimum cut off, to 53hrs and had a mean length of 14.7hrs of which on average 13.8hrs were above the 10m/s threshold. The maximum wind speed observed was 23.6m/s, while the weakest event on the record only reached a maximum speed of 10.4m/s. Maximum speeds were considerably lower than the fjord station and DMI datasets, which had maxima of 36.2m/s and 54m/s respectably. As shown by the methods of filtering the data for katabatic wind events the fjord station showed the consistently higher wind speeds followed by the DMI station then ERA5 data. Higher wind speed was associated with a longer duration of the DWE ($p<0.01$). Change in duration explained 35% of the variation in wind speed (Fig. 4.1).

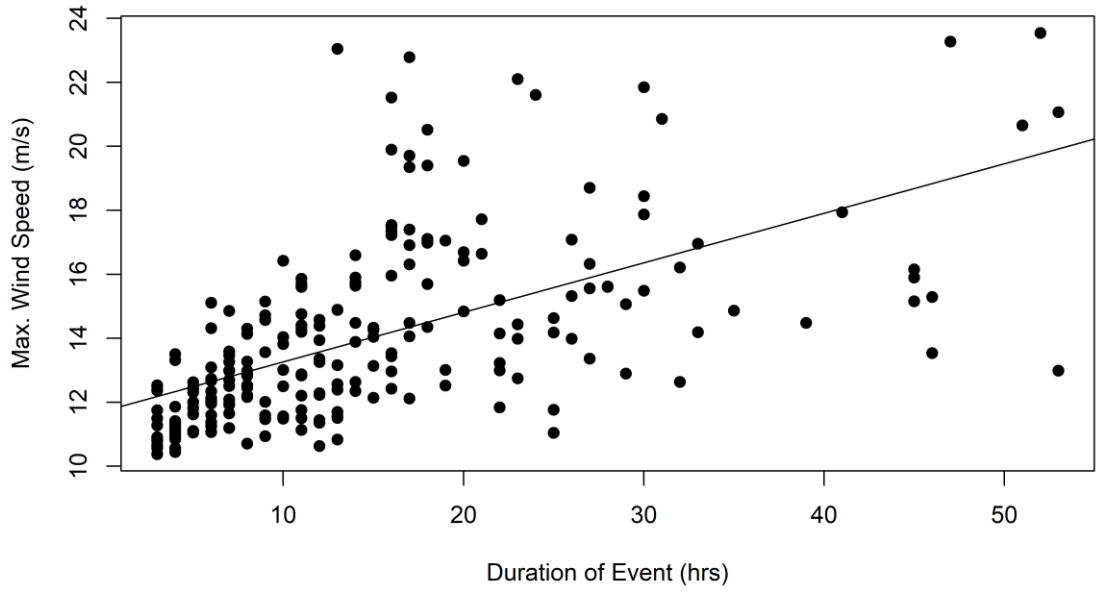

Figure 4.1: Maximum wind speed against duration of DWEs at Sermilik Fjord from 1979-2019 based off ERA5 reanalysis data. Regression line is also plotted. R-squared value of 0.3467 and $p < 0.0001$.

Event fluctuation over time:

Over the course of the ERA5 timeseries 242 downslope wind events (DWEs) were identified resulting in an average of 6.21 events per year. In comparison the DMI record showed 417 DWEs at rate of 7.3 per the year. The fjord station showed a similar occurrence to ERA5 dataset of 6.6 DWEs occurring on a yearly basis, giving a total count of 119 events. The datasets compare very well in identifying similar numbers of katabatic winds per year (Fig. 4.2). Over recent timescales, from 2001 onwards, the correlation extremely good. There is no clear pattern in the timeseries of either an increase or a decrease, although there is a large interannual variability (Fig. 4.2).

DWEs are mainly occur in non-summer months with the highest monthly means between October and March (Fig. 4.3). Again, there is good agreement between the datasets although summer event numbers are noticeably higher at Station Coast in the fjord. February numbers were considerably lower in the ERA5 data (Fig. 4.3).

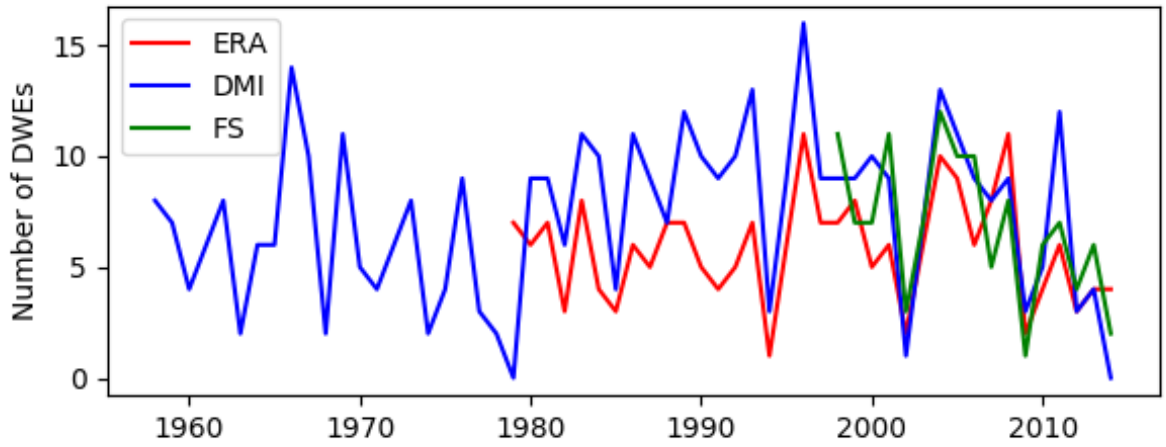

Figure 4.2: DWE events over the course of three datasets. The blue line is the DMI station in Tasiilaq spanning from 1956-2015. The red line the ERA5 reanalysis data for Tasiilaq spanning from 1979 to 2015. The green line is the data from the Coast Station on Sermilik Fjord from 1998 to 2015.

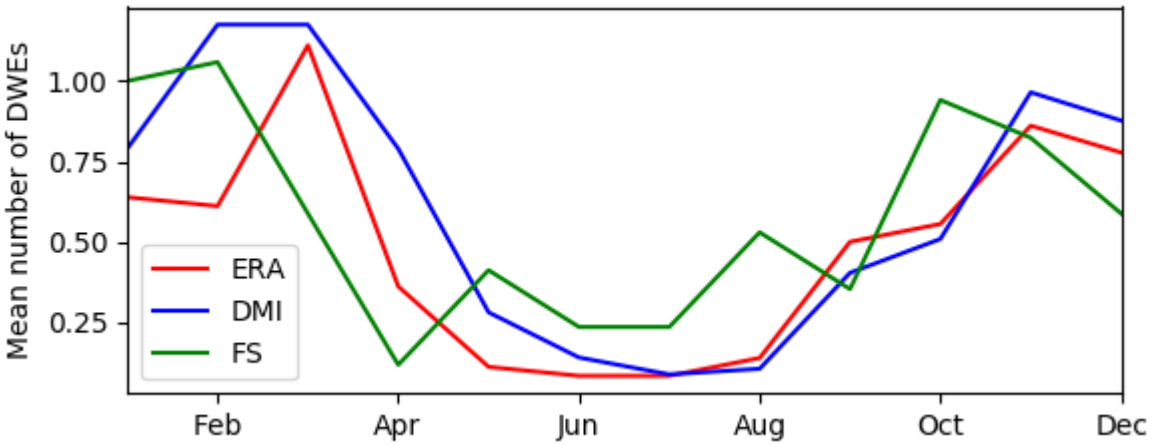

Figure 4.3: Comparison of mean number of DWEs per month throughout the year based of three datasets. The blue line is the DMI station in Tasiilaq spanning from 1956-2015. The red line the ERA5 reanalysis data for Tasiilaq spanning from 1979 to 2015. The green line is the data from the Coast Station on Sermilik Fjord from 1998 to 2015.

Fjord Circulation:

Fjord mouth:

Coastal circulation at intermediate depths is dominated by the along coast currents which oscillate between 0.2m/s west and east (Fig. 4.4). Outside the east-west movement, currents beyond the fjord mouth on the immediate shelf at 224m, were highly variable. The coastal current heading east, therefore down the Greenlandic coast, peaked during or immediately after the katabatic wind event, however, earlier peaks were also be seen in the profiles (Fig. 4.4). Post DWE, there seems to be no discernible change in the current which remained highly variable with regular peaks and troughs.

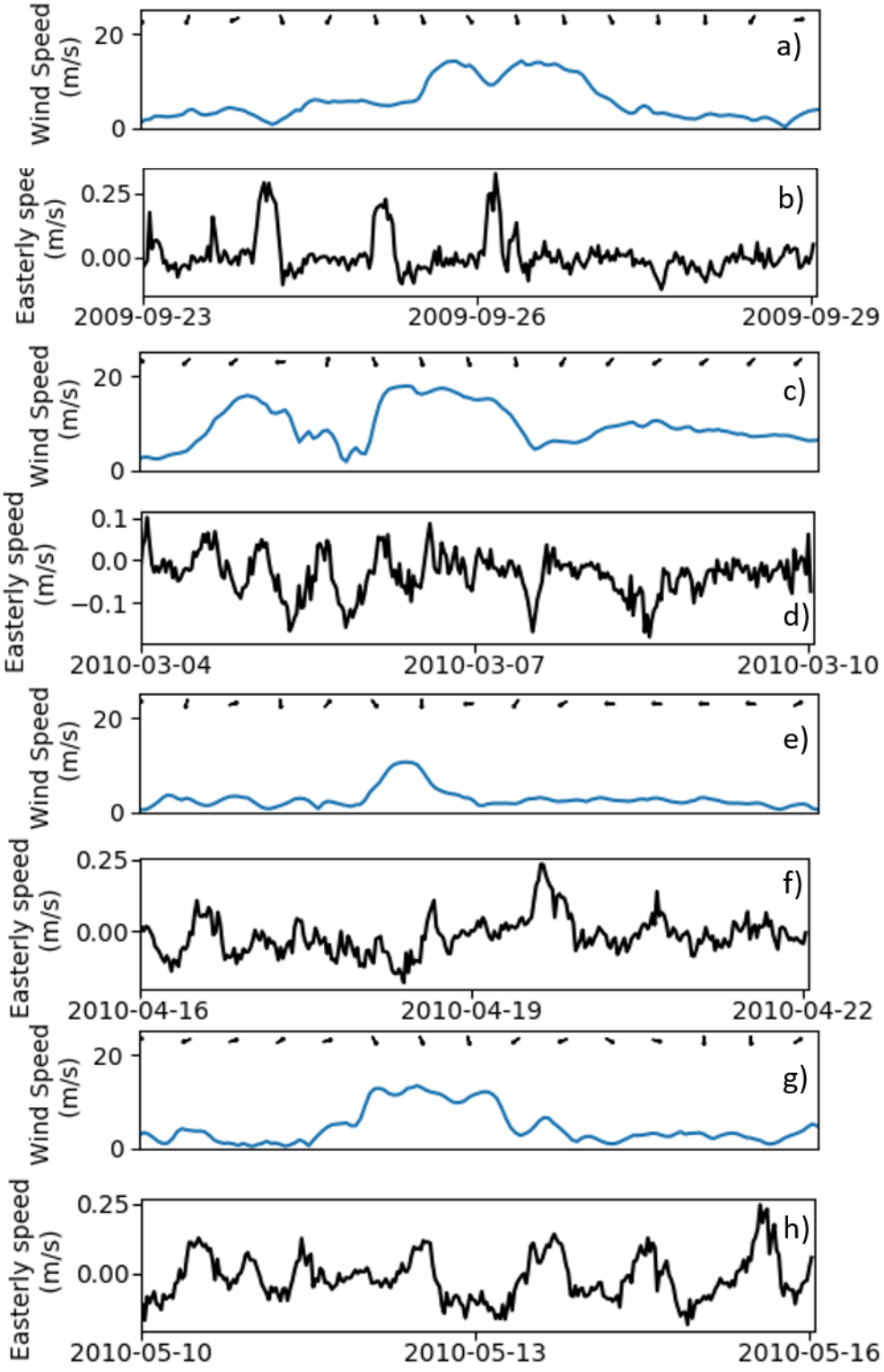

Figure 4.4: Wind speed and direction for four DWEs in 2009 at Sermilik Fjord and the corresponding shelf current velocities: a, c, e, g) wind speed and direction; b, d, f, h) current speed in the plane of the fjord direction at Site 9_3 at 224m. See Fig. 3.2 for exact location. Note the differing y scales across the panels.

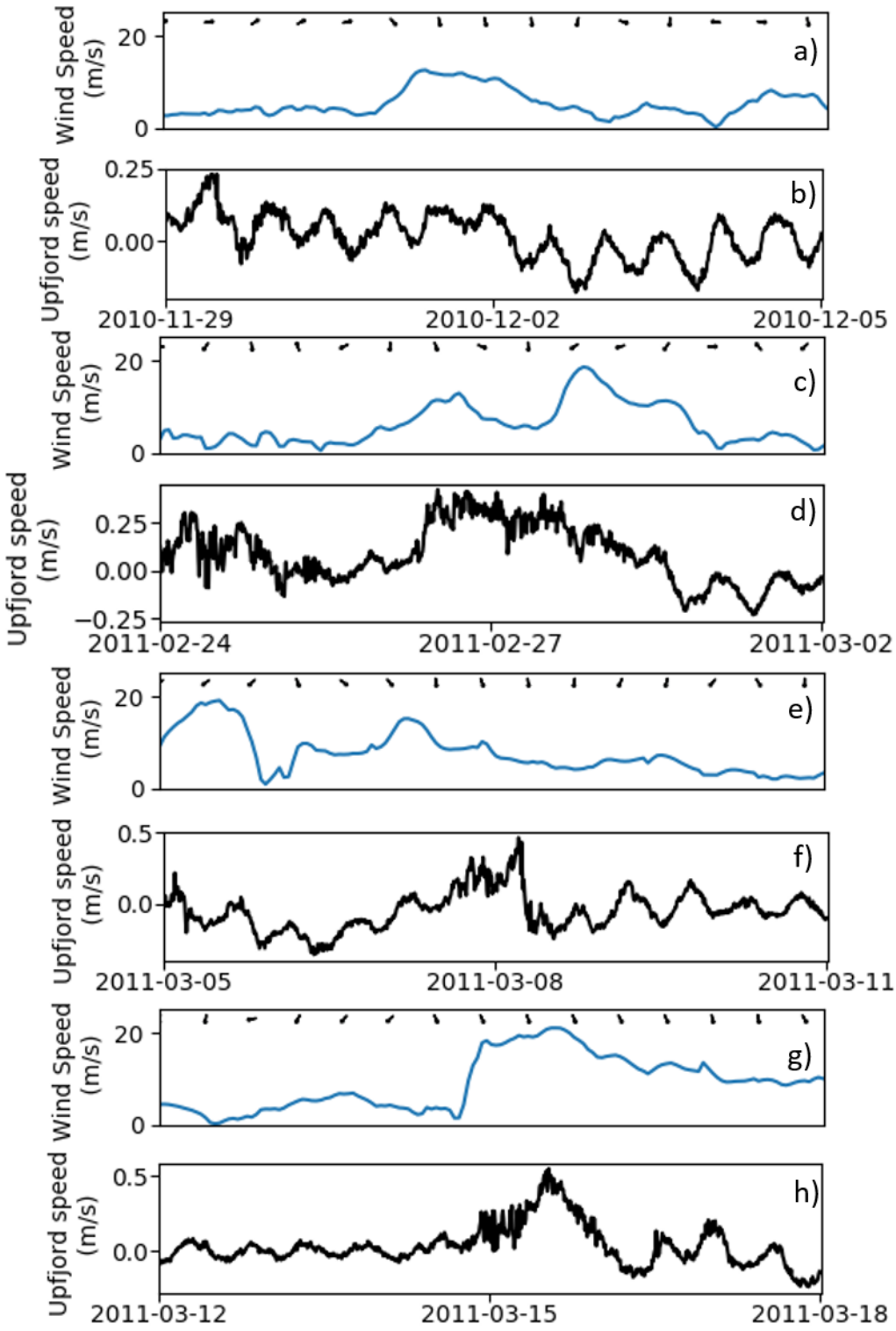

Figure 4.5: Wind speed and direction for four DWEs in 2010 at Sermilik Fjord and the corresponding current velocities at the fjord mouth: a, c, e, g) wind speed and direction; b, d, f, h) current velocity in the plane of the fjord direction at Site 10_5 at 520m. See Fig. 3.2 for exact location. Note the differing y scales across the panels.

Moving further into the fjord and in deeper waters circulation can be classified into up-fjord or down-fjord (Fig. 4.5). Again, the current at 520m depth, oscillated between these two directions but,

with a period of around 12hrs (Fig. 4.5). Some weaker DWEs appear to have limited influence on the currents as they remained alternating between up-fjord and down-fjord currents at a magnitude of around 0.1m/s with the period remaining consistent. Stronger DWEs caused an up-fjord surge of water which reached a peak flow of 0.5m/s and lasted from usually around a day but could continue for longer periods in relation to the duration of the DWE (Fig. 4.5). The oscillating alternating currents resumed after this influx to return to similar magnitudes and period as observed prior to the DWE (Fig. 4.5). There was no clear subsidiary return of this flux within the deep waters although on some occasions the resumed alternating flow oscillated around a point of down-fjord flow (Fig. 4.5).

Mid-fjord:

Circulation in the middle of the fjord was also predominated by up-fjord and down-fjord movements of water and followed the trend of increasing velocity further up the fjord (Fig. 4.6). Prior to the

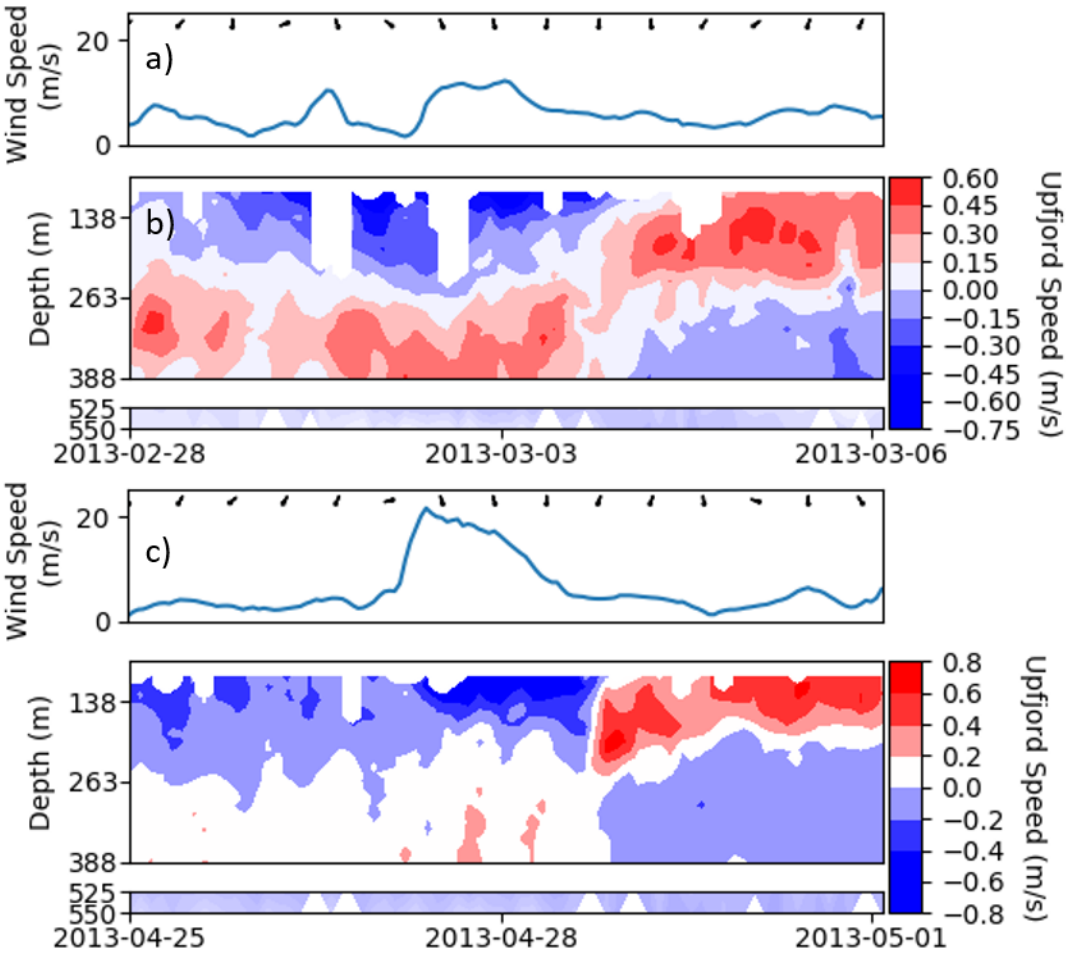

Figure 4.6: Wind speed and direction for two DWEs in 2012 at Sermilik Fjord and the corresponding current velocities at the mid-fjord: a, c) wind speed and direction; b, d) current velocity in the plane of the fjord direction at Site 12_4 between 13-550m. See Fig. 3.2 for exact location. Note the differing speed scales between the panels.

DWE, the upper layer of water, above 250m, flowed down-fjord at around 0.4m/s. This down-fjord flow intensified during the wind event reaching up to 0.8m/s. The flow rate seems to increase almost immediately with little noticeable lag between it and higher wind speeds (Fig. 4.6). The magnitude of the increased flow is relative to the strength of the DWE. Within 12hrs of the decline of the wind forcing the upper waters alternate to an opposite flow that is up-fjord. The strength and duration of this flow were roughly equal in magnitude to the previous down-fjord flow replaced. For the weaker of the two events in 2012, the change in flow was relatively gradual and seems to be the upward movement of the deep-water current (Fig. 4.6). The change in current direction was much more rapid for the stronger event of 2012, with only a couple of hours separating a strong, 0.8m/s, up-fjord flow with a similar down-fjord velocity. The origin of the up-fjord flow in the top layer seems less clear too.

The flow in the second layer, 250-388m, was consistently up-fjord throughout the DWE and as for the flow seen in the upper layer the flow strength and duration correlated to the wind speed. The up-

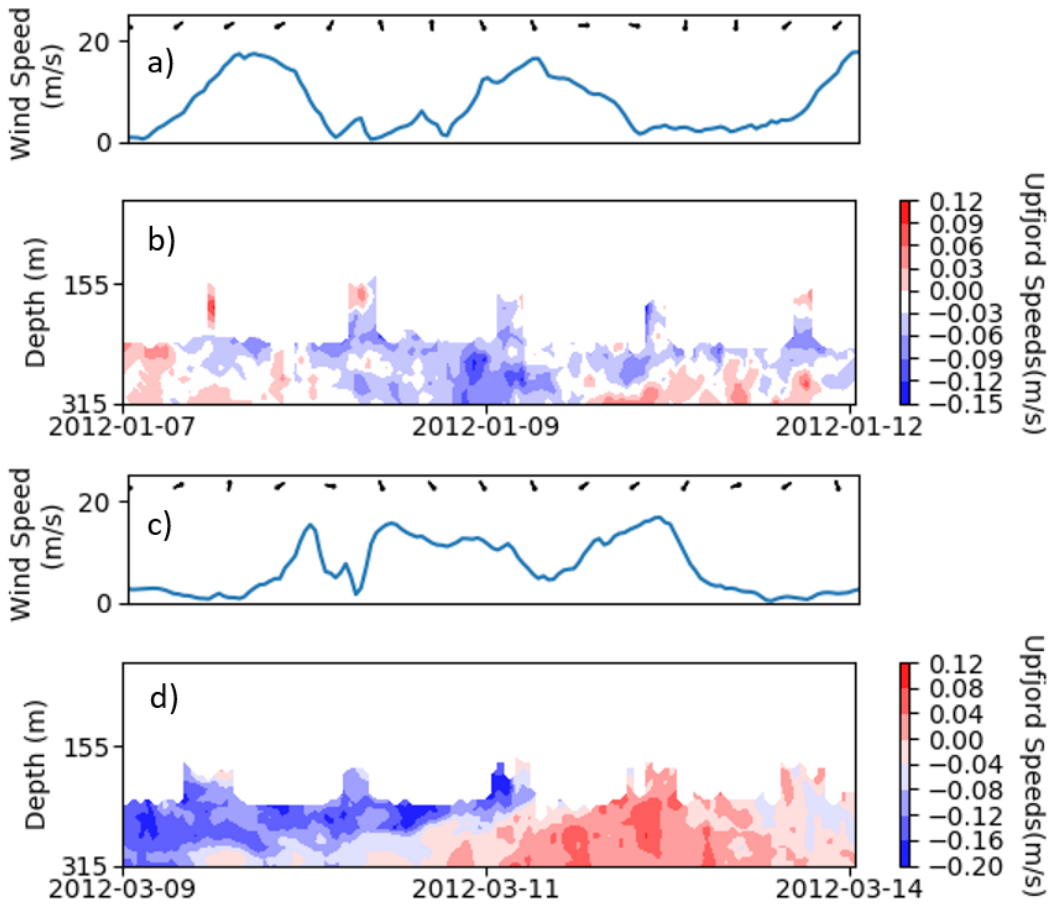

Figure 4.7: Wind speed and direction for two DWEs in 2011 at Sermilik Fjord and the corresponding current velocities in the upper fjord: a, c) wind speed and direction; b, d) current velocity in the plane of the fjord direction at Site 11_A between 43-315m. See Fig. 3.2 for exact location.

fjord flow was present prior to the first event in 2012, and this flow continued during the katabatic wind with some apparent strengthening in velocity. When the up-fjord current was not previously present a small, short-lived pulse of up-fjord flow, of around 0.3m/s, was seen for several hours during the peak of the katabatic wind. As the wind speed declined this flow subsided and secondary layer currents remain fairly neutral until the dramatic shift in the top layer. This shift in the current direction was matched by an opposite switch in the second layer. Around 12hrs after the DWE the second layer became a steady down-fjord flow of around 0.2m/s. Bottom layer, 525-550m, currents remained at a much lower magnitude with no clear alteration during or after a DWE (Fig. 4.6).

Upper Fjord:

Further up the fjord current velocities were more limited and tended to range between ±0.25m/s. Results here were also more limited given the close proximity to the ice-melange and glacier calving front. Intermediary waters changed from down-fjord to up-fjord flow during DWEs. They responded within the duration of the event and these changes lasted for days after the start of the katabatic wind (Fig. 4.7). The transition to an up-fjord flows, which takes around 12hrs, occurred first at deeper waters before then affecting shallower waters.

Changes in temperature profile:

The temperature profile of the fjord changed in relation to the katabatic wind, depending on the fjord depth and position of the profile within the fjord. Generally, the thermocline became shallower during and after a DWE although this was not always the case. The response period of the water column also varied with its location and depth.

Shelf waters:

The upper shelf waters, above 250m, responded differently to katabatic winds based on the season (Fig. 4.8). In winter the upper waters of the shelf have an influx of heat corresponding to down-fjord wind increase. Inversely in late summer there was no immediate response to the wind stress before a very warm water mass, up to 8°C, and 4°C higher than surrounding water, appears above 180m depth. This occurs around six hours after the end of the DWE, and 36hrs after it starts (Fig. 4.8). The warm influx of water lasted just over a day and spanned around 50m vertically. During non-summer months, the response shelf water responded to the DWE by the intensification of warm water from the base of the profile upwards, shoaling the thermocline (Fig. 4.8). The thermocline was displaced upwards by around 50m, to a depth of between 130-160m depending on its original depth. The water below the thermocline increased in temperature by 1.5-3°C to temperatures reaching 6°C but

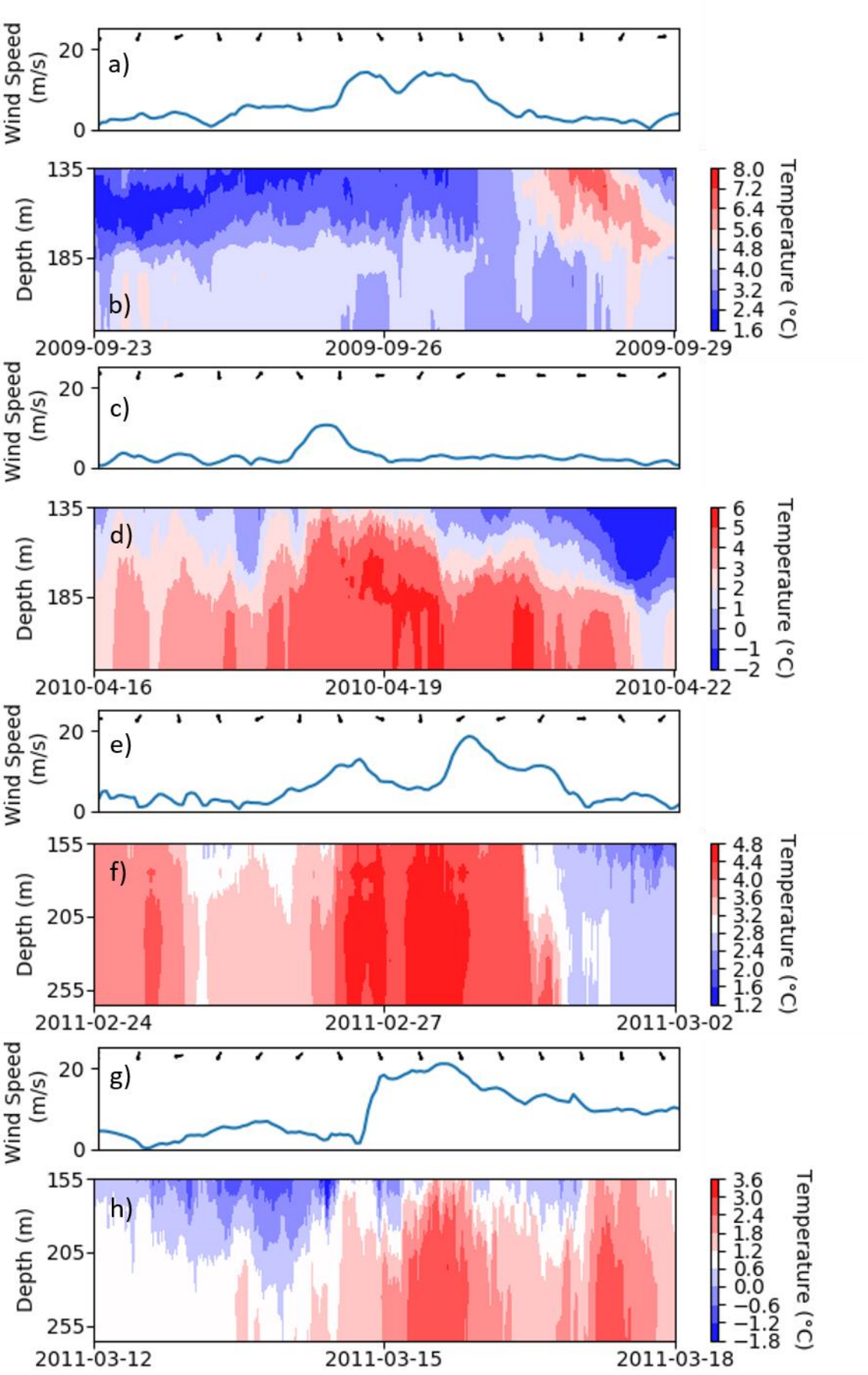

Figure 4.8: Wind speed and direction for four DWEs between 2009 and 2010 at Sermilik Fjord and the temperature profiles on the shelf outside Sermilik Fjord: a, c, e, g) wind speed and direction; b, d) temperature profiles at site 09_3; f, h) temperature profiles at site 10_3. See Fig. 3.2 for exact locations. Note the differing temperature scales between the panels.

this was dependent on the temperature prior to the DWE. The increase in temperature occurred irrespective of the original temperature profile (Fig. 4.8). The strongest DWE provided the largest increase in temperature, around 3°C, although the maximum reached was only 3.6°C. Much weaker

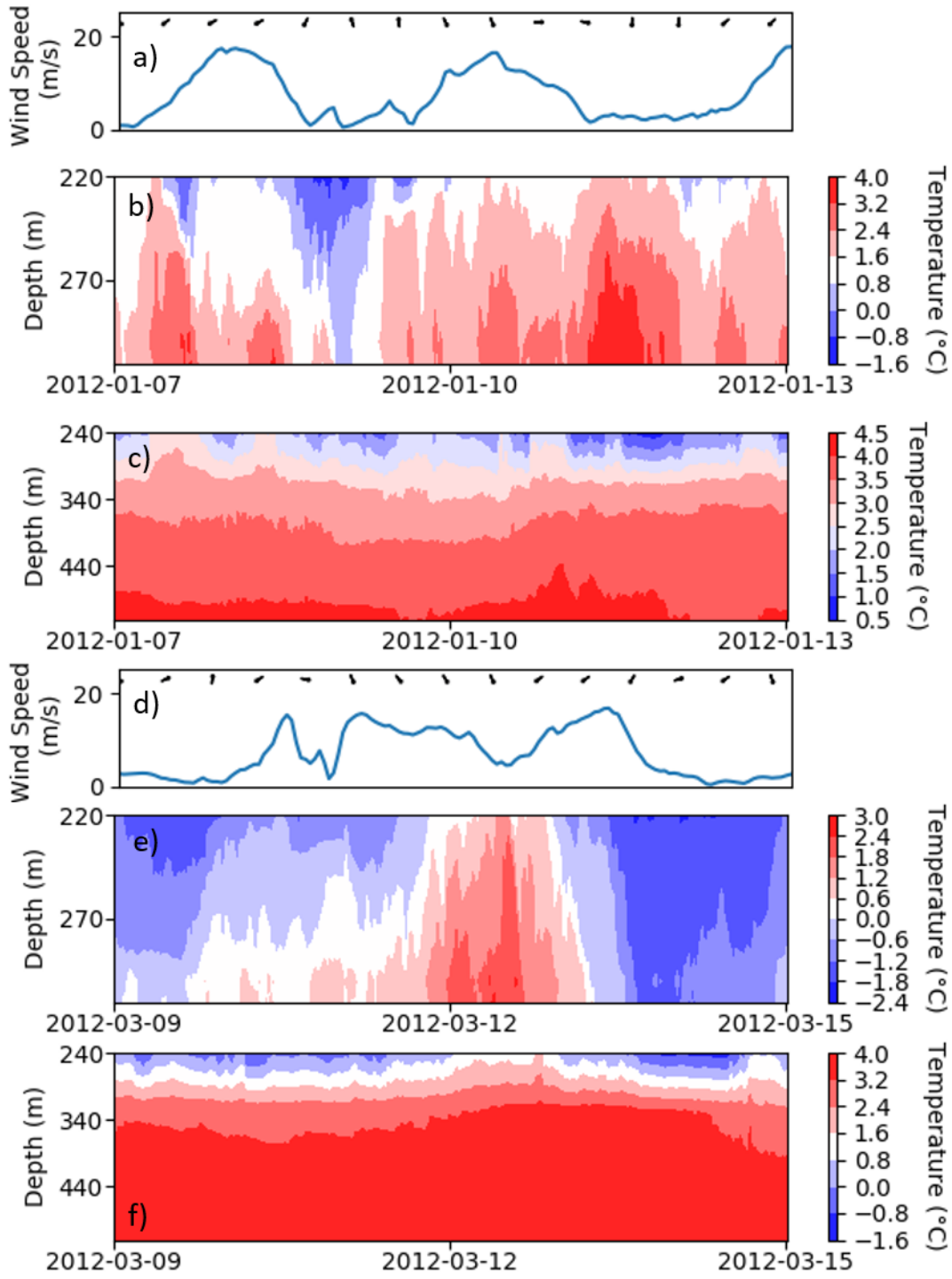

Figure 4.9: Wind speed and direction for four DWEs in 2011 at Sermilik Fjord and the corresponding temperature profiles outside the fjord mouth: a, d) wind speed and direction; b, e) temperature profiles at site 11_3 to the east of the fjord mouth; c, f) temperature profiles at site 11_4 to the west of the fjord mouth. See Fig. 3.2 for exact location. Note the differing temperature scales between the panels.

events, which reached half the wind speed, still provide a similar increase in temperature of 2.5°C. Given the limited span of the depth of the profile, it is uncertain whether the warm water is coming from depth or another location.

Post-DWE the thermocline deepened after a length of time roughly equal to the duration of the DWE wind forcing. Consequently longer, and generally stronger events, provide a longer period of thermocline shoaling (Fig. 4.8). It is unclear how far up the fjord profile the shoaling extends given the limits of the data extent. The thermocline was then noted to deepen again, far below its position prior to the DWE, as a large influx of very cold water takes position from 160m upwards. This deepening of the thermocline typically occurs 6 to 12 hrs after each shoaling.

The influence of katabatic wind events on the shelf waters varied according to the position of the temperature profile in relation to the fjord mouth. The water column to the east of the fjord mouth, and so further up the EGCC, showed a response very similar to as previously described for the area directly in front of the fjord. In contrast, to the west of the fjord mouth the water displayed limited change (Fig. 4.9). Shoaling of the thermocline and an influx of warm water appeared, corresponding to the increase in down-fjord wind speed as seen to the east, with temperatures increasing by around 3°C. However, unlike south of the fjord mouth, this trend appears true for both late summer and non-summer months. In non-summer months, the shoaling of the thermocline was short-lived, stopping shortly after the end of the DWE, before it deepened past its original position. The thermocline was pushed rapidly downward as a very cold-water mass, ~1.8°C, took position from 300m upwards and replacing the warm water influx. The replacement by a very cold-water mass in non-summer months is akin to the processes described south of the fjord mouth except with a noticeably shorter transition to a deeper thermocline. Limited shoaling of the thermocline was seen to the west of the fjord mouth, for both summer and non-summer months. However, the movement of warm water upwards was observed to a depth of 450m, although any shoaling of the thermocline was very short-lived and lasted only a couple of hours. In non-summer months, the thermocline appeared to shoal for the duration of the DWE but only between 10-20m and showed very limited variation in the rest of the profile (Fig. 4.9).

Fjord mouth:

Compared to the shelf, little variation in temperature associated with DWEs was seen in the fjord mouth between the depths of 250m-520m. The event in December 2010 showed some shoaling of the thermocline but it appears to be unrelated to the down-fjord wind speed in terms of timing (Fig. 4.10). Another event in the same year in February showed an increase in temperature of around 1°C

at 250m and associated shoaling of the thermocline (Fig. 4.10). Any increase in temperature here was far less marked than in shelf waters for the same event (Fig. 4.9). The final event presented showed a reduction temperature at 250m by around 2°C from the start of the DWE contrary to the pattern showed by the same event at shelf over the same time (Figs. 4.9, 4.10). However deeper waters, below 350m, remained consistent throughout the DWE.

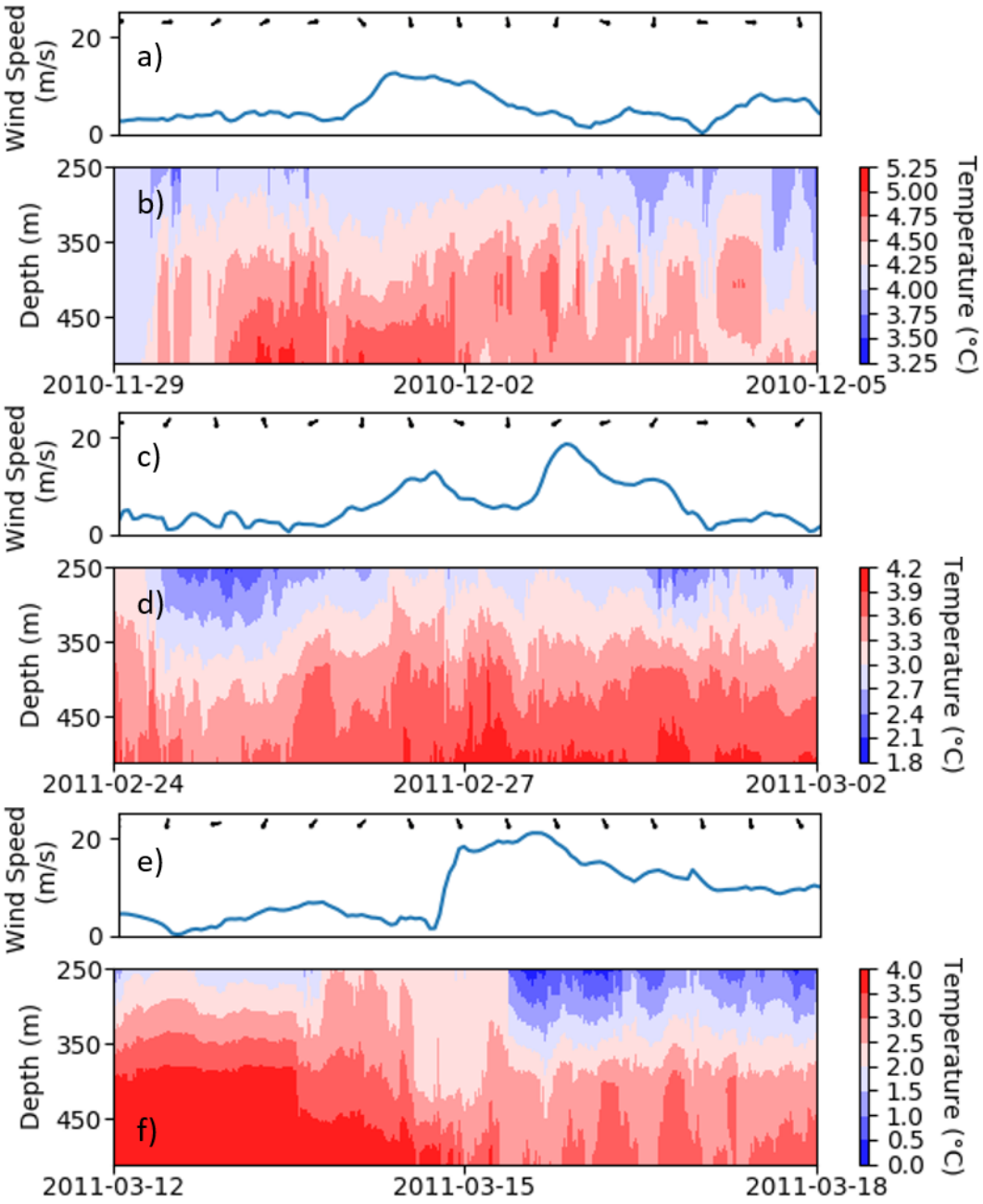

Figure 4.10: Wind speed and direction for four DWEs in 2010 at Sermilik Fjord and the corresponding temperature at the fjord mouth: a, c, e) wind speed and direction; b, d, f) temperature profiles at site 10_5 at the fjord mouth. See Fig. 3.2 exact location. Note the differing temperature scales between the panels.

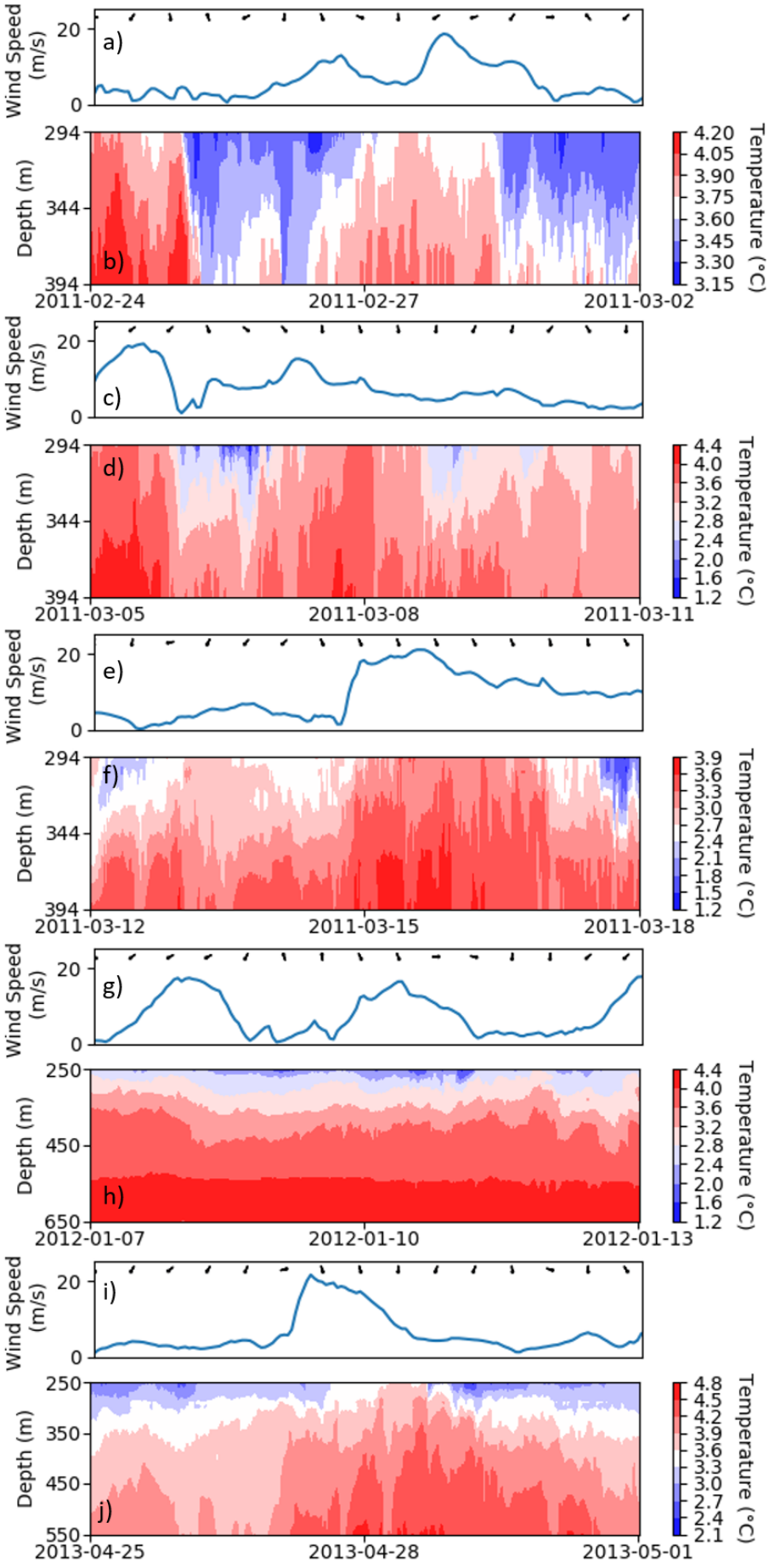

Figure 4.11: Wind speed and direction for four DWEs between 2010 and 2012 at Sermilik Fjord and the corresponding temperature profiles at the middle of the fjord: a, c, e, g, i) wind speed and direction; b. d. f) temperature profiles at site 10_2 in the east of the mid-fjord: h) temperature profile of site 11_6 at centre of the mid-fjord: j) temperature profile at site 12_4 at the centre of the mid-fjord. See Fig. 3.2 for exact locations. Note the differing temperature scales between the panels.

Mid-fjord:

Unlike the fjord mouth there was a clear increase in temperature down the depth profile during a DWE in the middle of the fjord (Fig. 4.11). The patterns displayed for the 2nd and 4th event in the 2010 timeseries are very similar to those seen on the shelf (Figs. 4.9, 4.11). The scale of the change is reduced with temperatures increasing by only by 0.8-1.2°C although it should be noted that these profiles are in deep water. Water temperatures increased during the DWEs throughout the profile, from 294-390m, and lasted for 12hrs after the end of the katabatic wind.

In the centre of the mid-fjord profiles more closely resembled those at the mouth of the fjord, during late summer, with little apparent reaction to the increased wind stress from a DWE (Fig. 4.11). Some shoaling of the thermocline can be seen slightly 6hrs after the increase in down-fjord wind speed, with waters between 250-350m warming by 0.5°C. The profile returned to its original conditions after the DWE declined. When a similarly strong DWE occurred in non-summer temperature increases of around 1°C can be seen down the whole profile (Fig. 4.11). Peak temperatures occurred around 6hrs after the maximum wind speed. The thermocline reduced in depth from around 275m to out of the profile above 250m where it remained while the wind speed stayed high. After the wind dropped off, the thermocline resumed a position around 275m, although for the 6hrs immediately after is more clearly defined with the water around it highly stratified. This pronounced stratification reduced with time (Fig. 4.11).

Upper-fjord:

The surface waters, probes at 13m, closer to the glacier terminus and at the top of the fjord show an almost immediate response to down-fjord wind forcing (Fig. 4.12). The temperature of surface waters increased by up to 0.75°C raising temperatures to -0.3°C. For all of the events analysed a sharp temperature jump occurred, usually an increase of ~0.5°C, as the DWE became established. The peak was maintained for a time period of between 4-12hrs before a sharp decline in temperature occurred even if down-fjord wind speed was maintained. Subsequence peaks of a similar magnitude were common, especially if the down-fjord wind speed has remained high (Fig. 4.12).

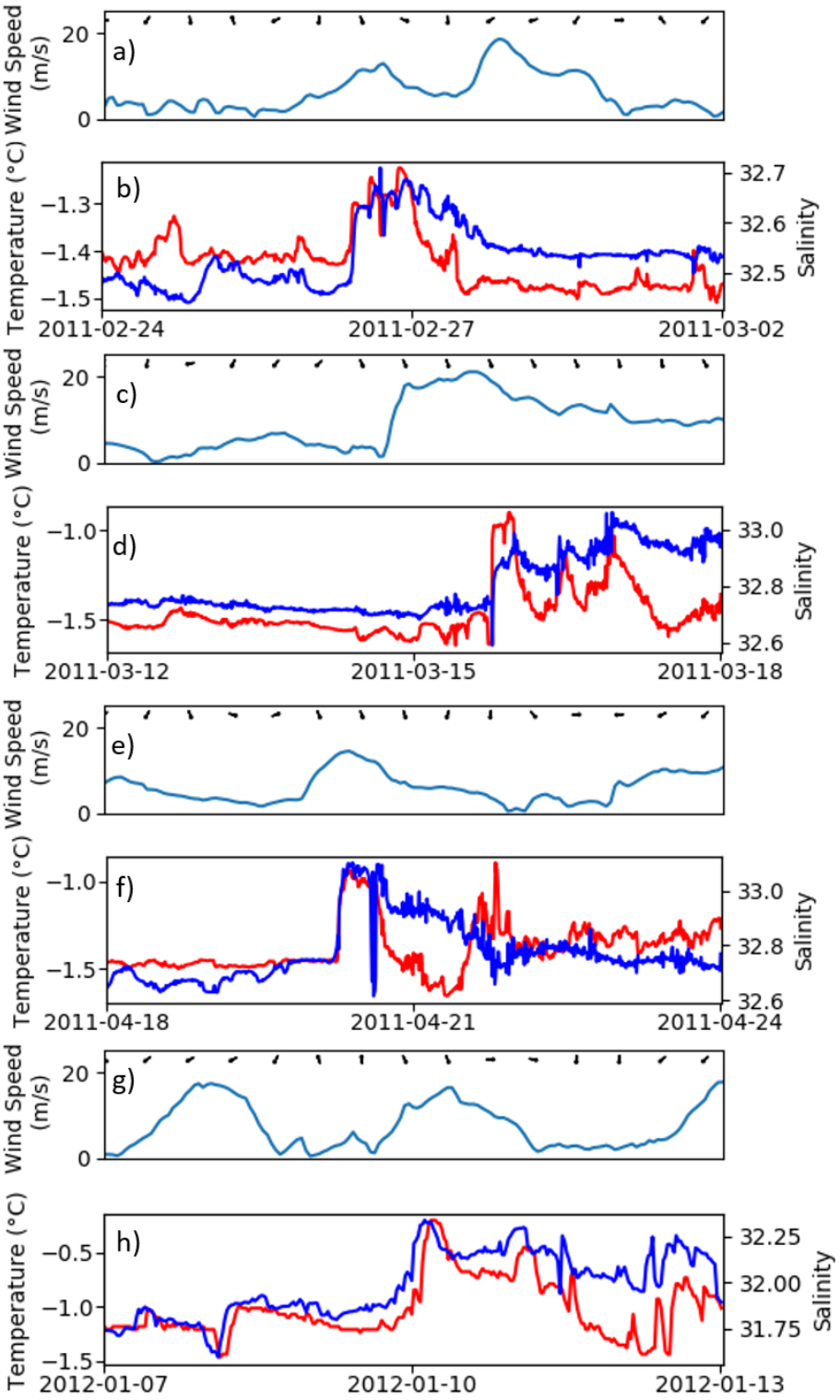

Figure 4.12: Wind speed and direction for four DWEs between 2010 and 2011 at Sermilik Fjord and the corresponding temperature and salinity at upper-fjord: a, c, e, g) wind speed and direction; b, d, f,) temperature and salinity profiles at site 10_4 at a depth of 13m: h) temperature and salinity profiles at site 11_5 at a depth of 13m. Note the differing scale between the subfigures. See Fig. 3.2 for exact location. Note the differing salinity and temperature scales between the panels.

Salinity profile:

The salinity profile across the fjord and range of depths within it varied but was closely related to the temperature profile (Fig. 4.13). An exception to this observation was near the glacier, ice melange and sea ice where high temperature peaks were followed by lower temperatures, while the salinity remained high (Fig. 4.12). Peaks of temperature in the surface waters at the top fjord are matched by similar jumps in salinity. However, the temperature decreased after 6-12hrs, before subsequent stepped increase in temperature, salinity undergoes a shallower drop off so is maintained at a higher level (Fig. 4.12). A similar pattern occurred with the subsequent sudden increases of temperature, which widen the relative gap between salinity and temperature (Fig. 4.12).

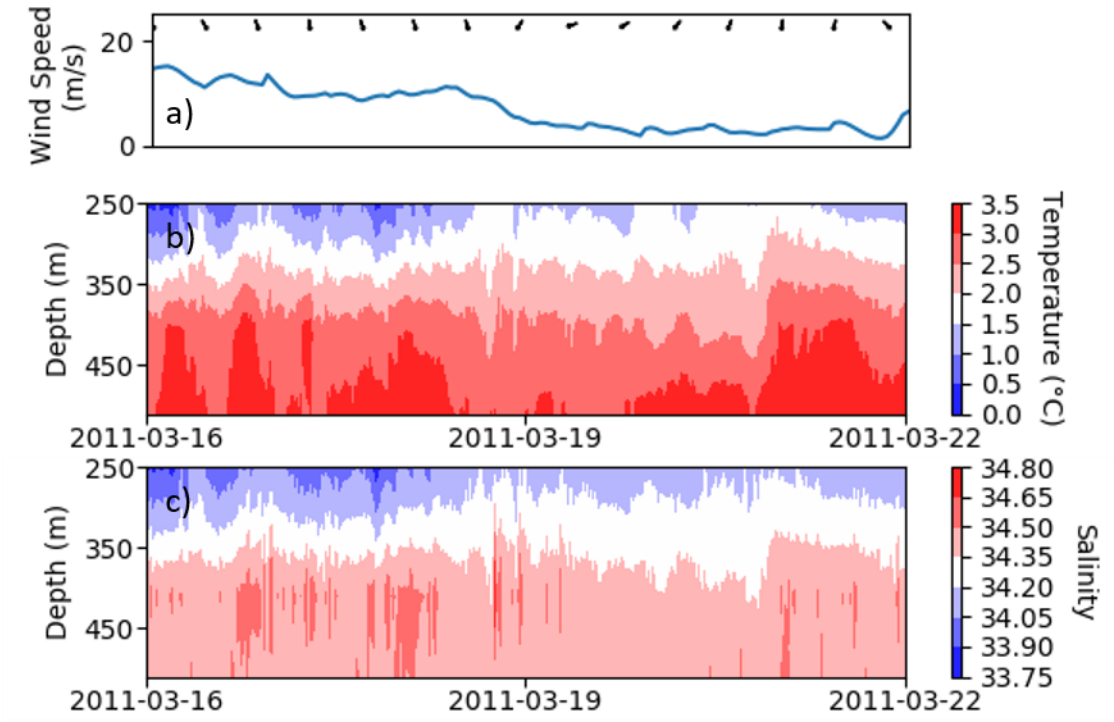

Figure 4.13: Wind speed and direction for an DWE in 2010 at Sermilik Fjord and the corresponding temperature and salinity at fjord mouth: a) wind speed and direction; b) temperature profile at site 10_5: c) salinity profile at site 10_5. See Fig. 3.2 for exact location.

Heat flux across the fjord:

Submarine melt rate varied during DWEs across the fjord compared to both mean melt rate and a starting reference point (Fig. 4.14). Sites within the fjord itself showed some negative PDS derived from yearly means. Therefore, during a DWE the maximum submarine melt at the site was lower than the mean submarine melt rate for that year. This was noticeable in the upper fjord, sites 10-4 and 11-5, where minimum PDS were -90% and -60% respectively (Fig. 4.14). However, it should be

noted that depth of SMR calculations at these sites was 13m over 150m shallower than any other site. Calculations of SMRs at sites using shallower depths tended to be more positive as can be seen by comparing the sites on the shelf (Fig. 4.14).

PDS based on a yearly mean for the east and west of the fjord mouth were very similar. However, when PDS was calculated using a starting reference the results differed greatly with the east of the mouth showing huge variation whilst the west showed a smaller magnitude over a much more confined range (Fig. 4.14).

All sites showed an increase in SMR for every DWE measured apart from site 10-5 for the event on 2011-03-07, where no change occurred. The highest SMR compared to a starting reference occurred in the upper fjord, where melt rates increased by up to 1034% during a single DWE event (Fig. 4.14). The profile at site 10-2 was noticeably deeper than others at the mid-fjord and correspondingly the PDS from the starting reference point was lower (Fig. 4.14).

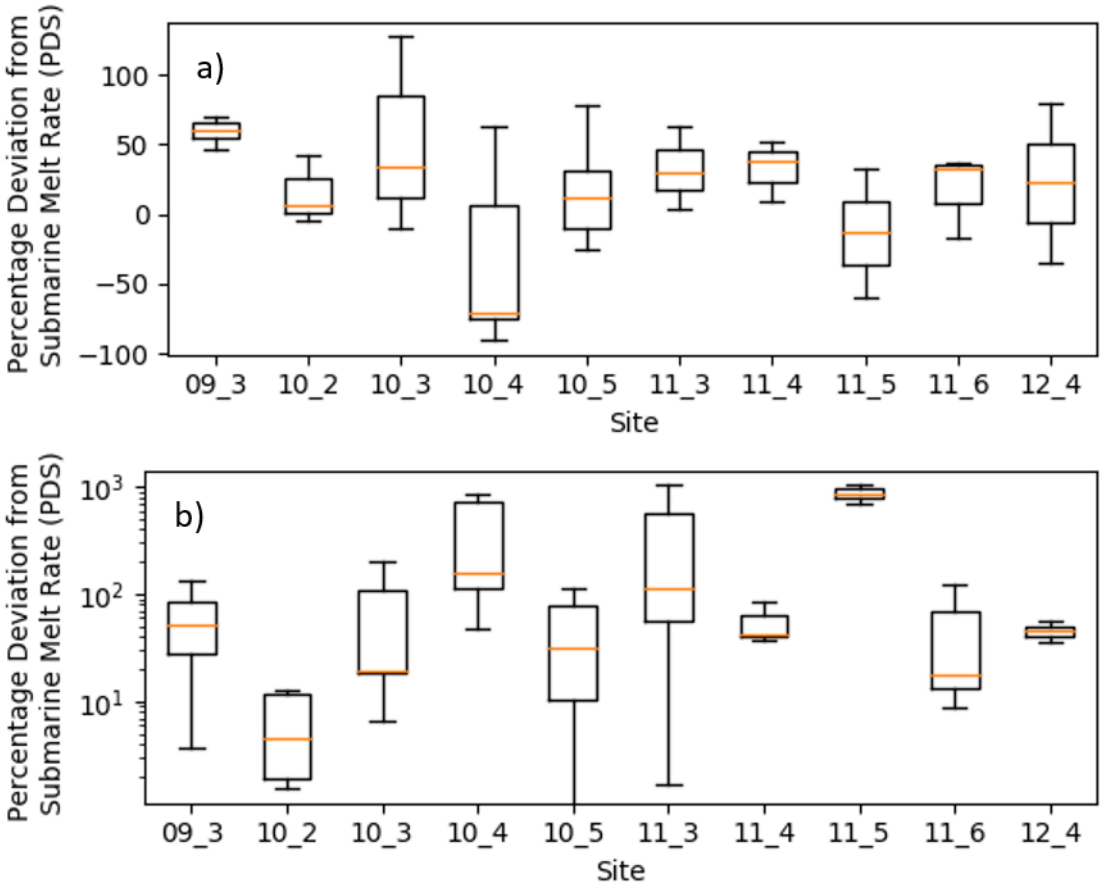

Figure 4.14: Boxplots of Percentage Deviation of Submarine melt rates (PDS) during DWEs across Sermilik fjord between 2009 and 2012: a) PDS calculated from yearly mean at each site; b) PDS calculated from a starting reference point before each DWE. Note the exponential scale on y-axis. See Fig. 3.2 for exact locations.

Comparing the relative strength of the events in 2010 against the PDS divided by the mean of each site showed a strong association (Fig. 4.15). Maximum wind speed was a better predictor of SMR increase than event duration (Fig. 4.15).

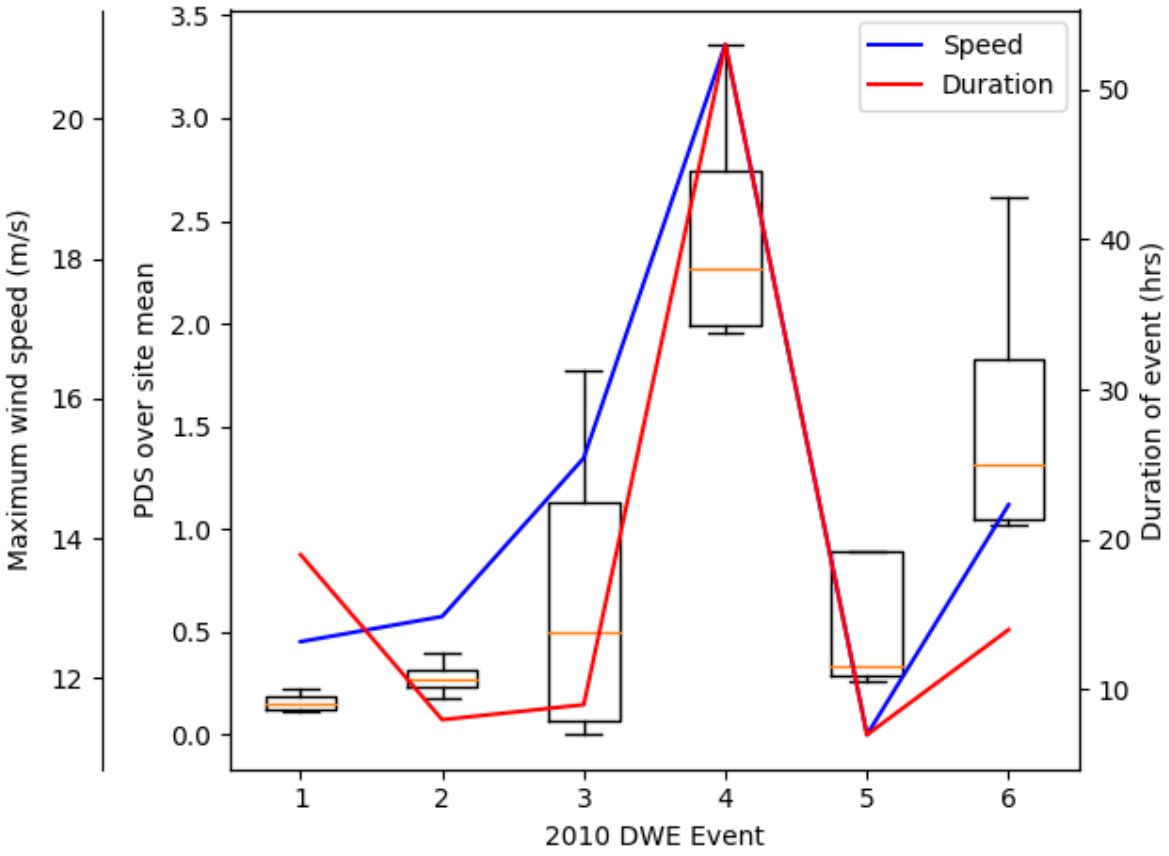

Figure 4.15: Boxplots showing Percentage Deviation of Submarine melt rates (PDS) over the mean submarine melt rate (SMR) increase for DWEs across 2010-2011 for each site, during DWEs across Sermilik Fjord in 2010. In essence, each boxplot shows the variation of submarine melt during a particular event once seasonality and station location has been accounted for. The value derived by PDS over site mean is the multiple increase compared to the mean increase because of DWE in 2010. For example, DWE 1 increased SMRs across the fjord by between 0.15 and 0.3 times of mean DWE induced increase in SMRs. The blue line shows the maximum speed of each DWE and the red its duration.

Sea-ice removal:

Sea ice was removed from both the fjord and the shelf during a DWE (Fig. 4.16). In non-summer months sea-ice persists on shelf waters and covered the majority of the shelf. During a typical event, in terms of maximum speed and duration, during non-summer months sea-ice in removed from the shelf directly away from the shore, while sea ice within the fjord was swept into the shelf predominately from the right-hand side of the fjord (Fig. 4.16). During the event, a clear channel was formed down the right-hand side of the fjord pushing sea ice into the shelf and against the left-hand bank. This ice subsequently broke up and flowed out the fjord too. Ultimately shelf sea-ice was only

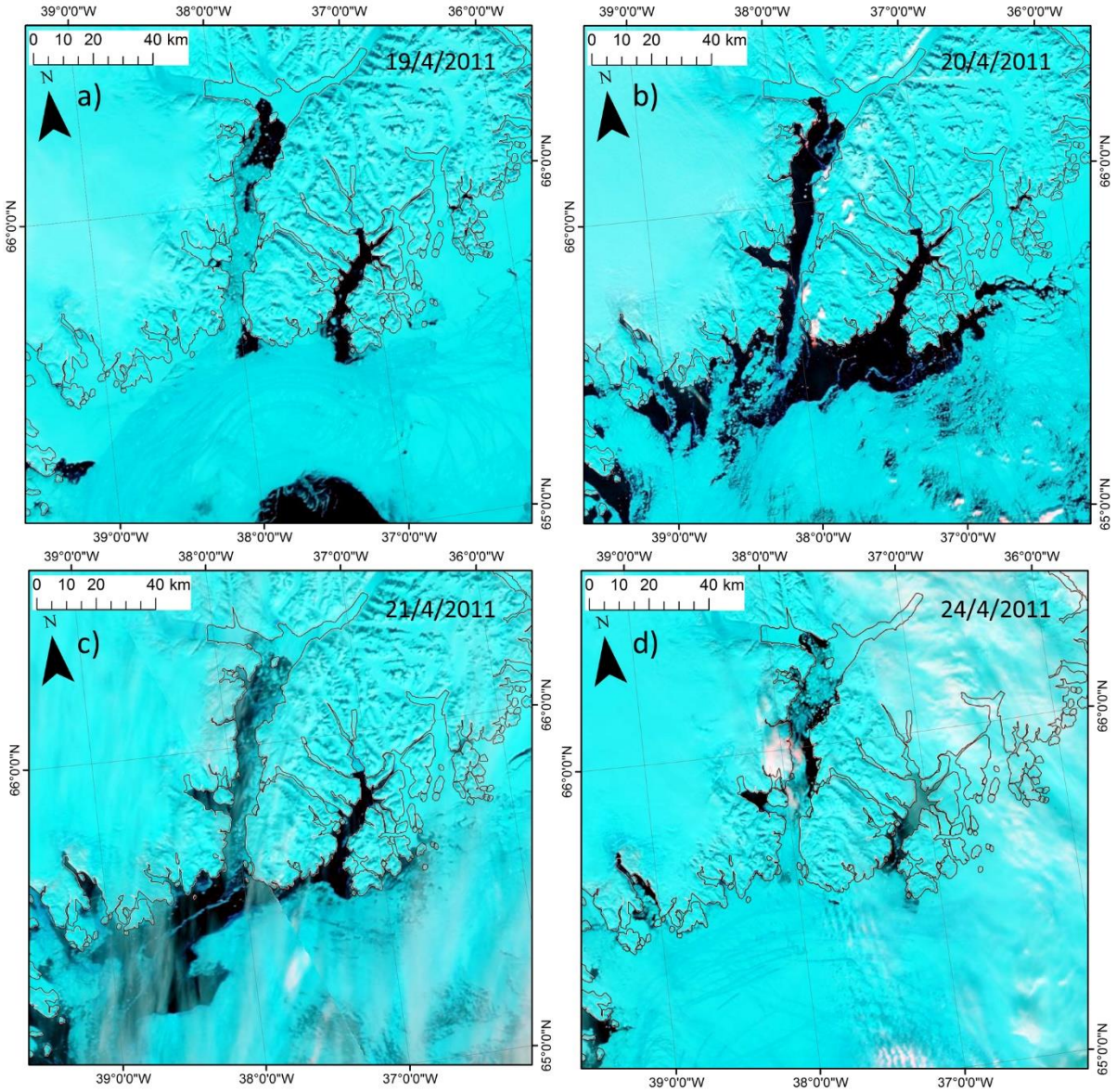

Figure 4.16: MODIS Aqua 721 images of Sermilik Fjord in April 2011 over the course of a katabatic wind event which occurred on 20/4/2011: a) the day before the event; b) day of the event, sea ice has been clear from the fjord and shelf; c) the day after, sea-ice import from EGC; d) fives days after when sea-ice coverage restored.

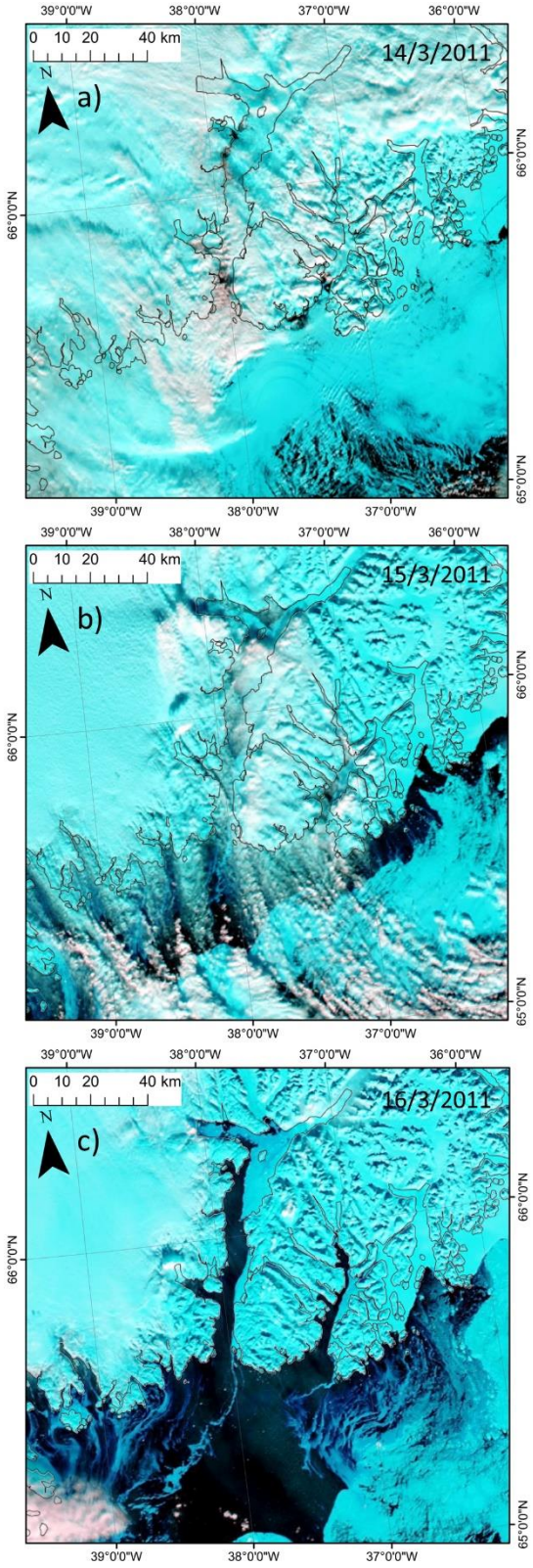

Figure 4.18: MODIS Aqua 721 images of Sermilik Fjord during March 2011 during a katabatic wind event which occurred during 14/03/2011: a) the of the event; b) the after the event, removal of sea-ice from fjord; c) two days after, removal of sea ice from shelf.

pushed 20km offshore and was never completed removed, although a channel through the ice is formed west of the fjord mouth (Fig. 4.16). Within a day of the event, coastal sea ice starts to return, moving in along the EGC.

In stronger events, most of the coastal sea ice was advected offshore, creating a large break in the coastal sea ice coming down the East Coast of Greenland (Figs. 4.17, 4.18). As a result, this ice took longer to return but the shelf was almost entirely covered again within three days (Fig. 4.18). Sea ice within the fjord was again predominately removed from the right-hand side, but in larger quantities. Sea ice only remained at the top of the fjord and down the east, with ice near the glacier terminus thin and fractured by areas of open water (Fig. 4.17).

Sea-ice concentration on the shelf generally decreased as a result of a DWE. Weak events shifted the sea ice off the coast but failed to completely remove it from the shelf (Fig. 4.18). On the other hand, stronger events completely removed the ice from the shelf and created a large break in East Greenland Coast sea-ice flow (Fig. 4.18). Very weak events not only failed to remove the sea ice from the shelf but also showed complementary increase in sea-ice flow from the EGC (Fig. 4.18). As such very weak events can actually increase the sea-ice levels on the shelf. Looking at the period between 2009-2013 events below a maximum wind speed of 12m/s increased the sea-ice on the shelf. Events greater than 12m/s decreased the sea-ice concentration proportionally to maximum wind speed (Fig. 4.19). Maximum wind speed had a significant influence on sea-ice concentrations s

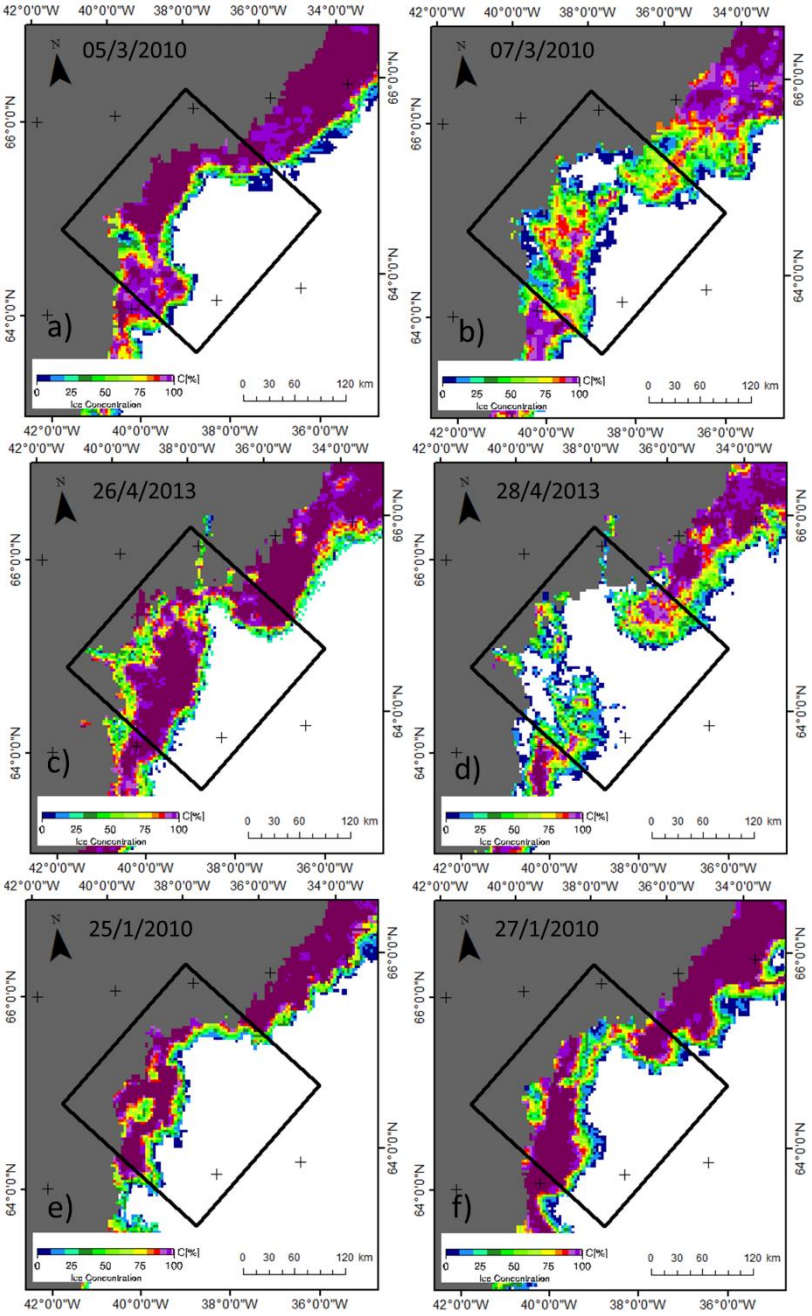

Figure 4.18: Sea-ice concentrations across Sermilik Fjord a day before and after DWEs: a, b) sea-ice concentrations before and after a DWE on 06/3/2010 which had a maximum speed of 17.9m/s and a duration of 30hrs; c, d) sea-ice concentrations before and after a DWE on 27/4/2013 which had a maximum speed of 21.6m/s and duration of 24hrs; e, f) sea-ice concentrations before a katabatic wind on 26/1/2010 which had a maximum speed of 11.4m/s and duration of 3hrs.

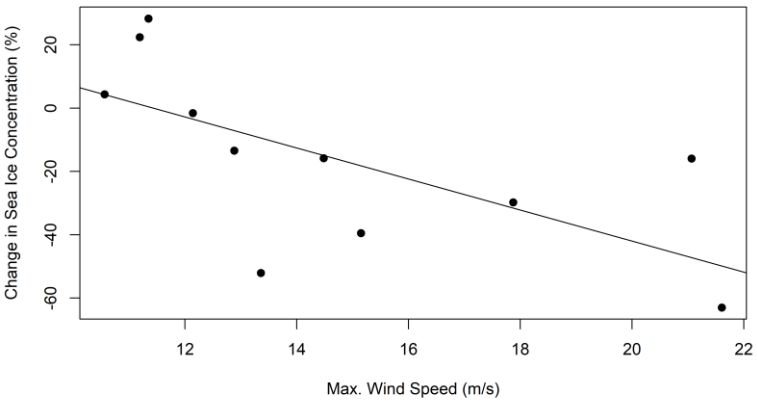

Figure 4.19: Percentage change in sea-ice concentrations on the shelf outside Sermilik Fjord during DWEs between 2009-2013 in non-summer months. Regression line is also plotted. R-squared value of 0.3728 and p = 0.027.

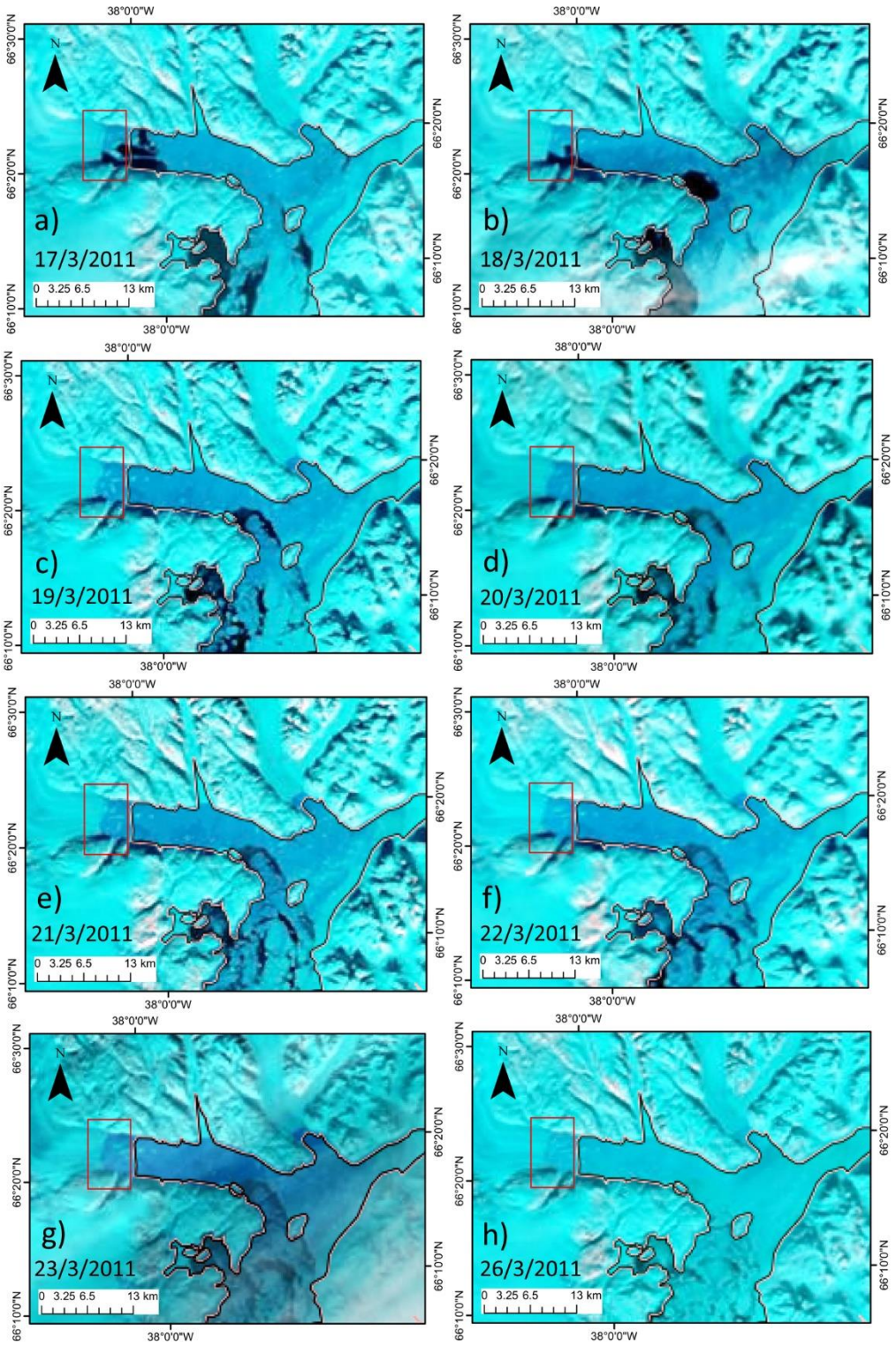

Figure 4.20: MODIS Aqua 721 images of Helheim Glacier and the top of Sermilik Fjord showing the retreat of the glacier terminus after a strong DWE that occurred on 14/03/2011 which had a maximum speed of 21.1m/s and duration of 53hrs. Images are taken from 17/3/2011 until 26/3/2011: a-h) show the retreat of Helheim Glacier terminus; c) shows major calving event; e) shows more extensive calving. Also note the large new icebergs floating away from the terminus.

on the shelf ($p<0.01$) and explained 44% of the variation in sea-ice concentration change (Fig. 4.19). However sea-ice concentration did not vary significantly with DWE duration, $p = 0.164$ (analysis not displayed).

Break up of ice-melange:

Most DWE events removed sea ice from the fjord and shelf along with partially break-up of the ice-melange present in front of the glacier terminus (Fig. 4.16). During the katabatic wind event itself, only small fractions of the melange were broken off. It is the subsequent few days where large

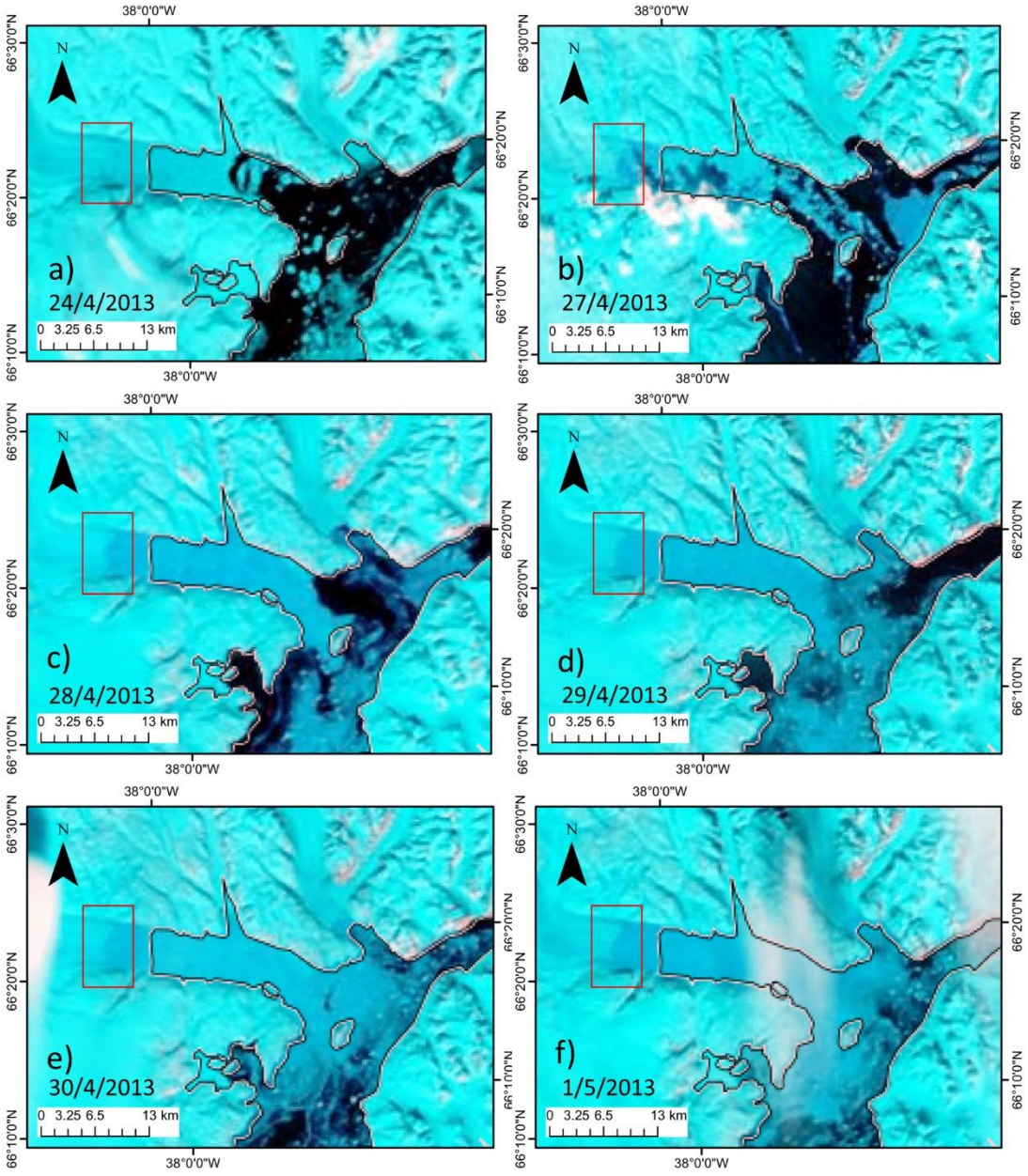

Figure 4.21: MODIS Aqua 721 images of Helheim Glacier and the top of Sermilik Fjord showing the retreat of the glacier terminus after a strong DWE that occurred on 27/04/2013 which had a maximum speed of 21.6m/s and duration of 24hrs. Images are taken from 24/4/2013 until 1/5/2013: a-f) show the retreat of Helheim Glacier terminus.

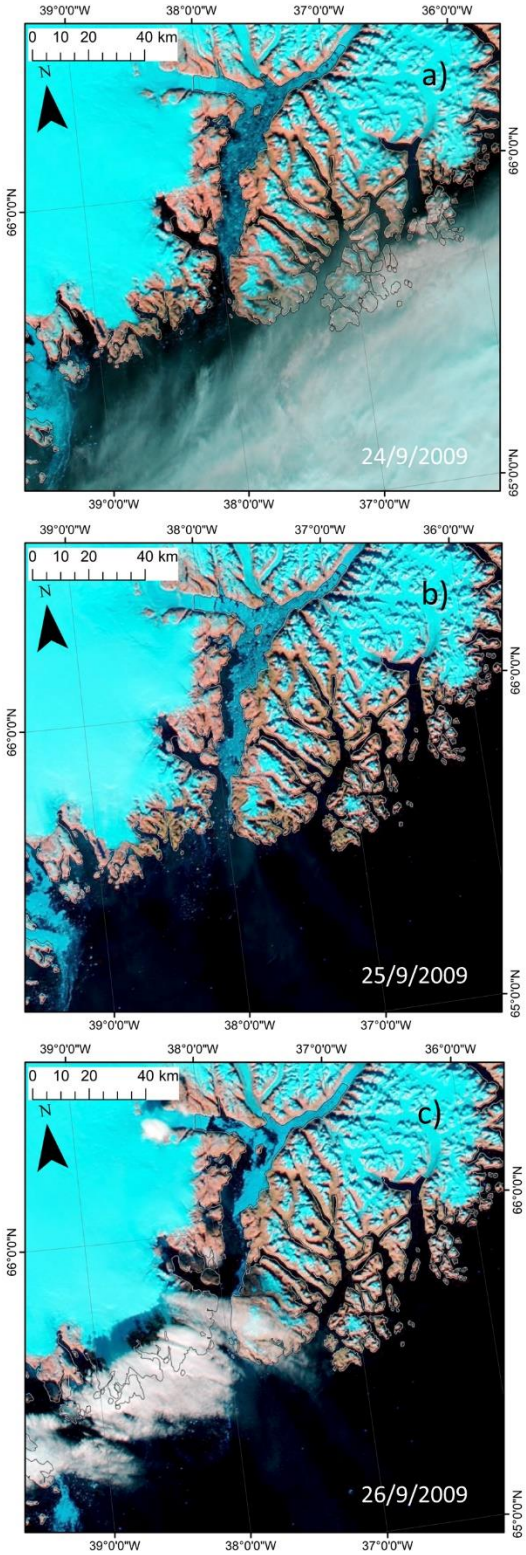

Figure 4.22: MODIS Aqua 721 images of Sermilik Fjord in the summer 2009 during a DWE that occurred 25/9/2009 and had a maximum speed of 14.2m/s of 29hrs: a) the day before the event; b) the day of the event, increased iceberg and sea-ice flow out the glacier; c) the day after, sea ice and icebergs removed from fjord.

sections of ice and icebergs held within it are released down the fjord (Fig. 4.16). Stronger events, where wind speed exceeds 20m/s, do more damage, breaking up the majority of the ice melange leaving just small sections in front of the terminus (Fig. 4.17).

In the days following a strong DWE the glacier terminus is exposed to areas of open water or thin sea ice (Figs. 4.20, 4.21). The results of a series of large calving events can be seen in the week after the strong event in March 2011 (Fig. 4.20). Initially the calving occurred on the south side of the terminus where it was exposed to open water, but subsequent calving took place on the northern side. Along with calving, as shown by the newly created icebergs, the terminus underwent noticeable retreat (Fig. 4.20). A similar pattern was seen in 2013 in the week after a strong event following the break-up of the ice-melange (Fig. 4.21).

In the summer months, little sea ice is present in the fjord although icebergs are seen throughout, and an ice-melange extended from the glacier terminus (Fig. 4.22). During the DWE in September 2009, the thin sea ice in the upper fjord was broken up and channel of open water created on the west of the fjord. Parts of the ice melange were broken up in ripples with the pieces broken off flowing down the fjord. Much more of the ice-melange is removed in comparison to an event of similar magnitude in non-summer months (Figs. 4.16, 4.22).

Overall picture:

Looking at the fjord system as a whole during one katabatic wind event it is clear that increased down-fjord winds have range of effects across the whole

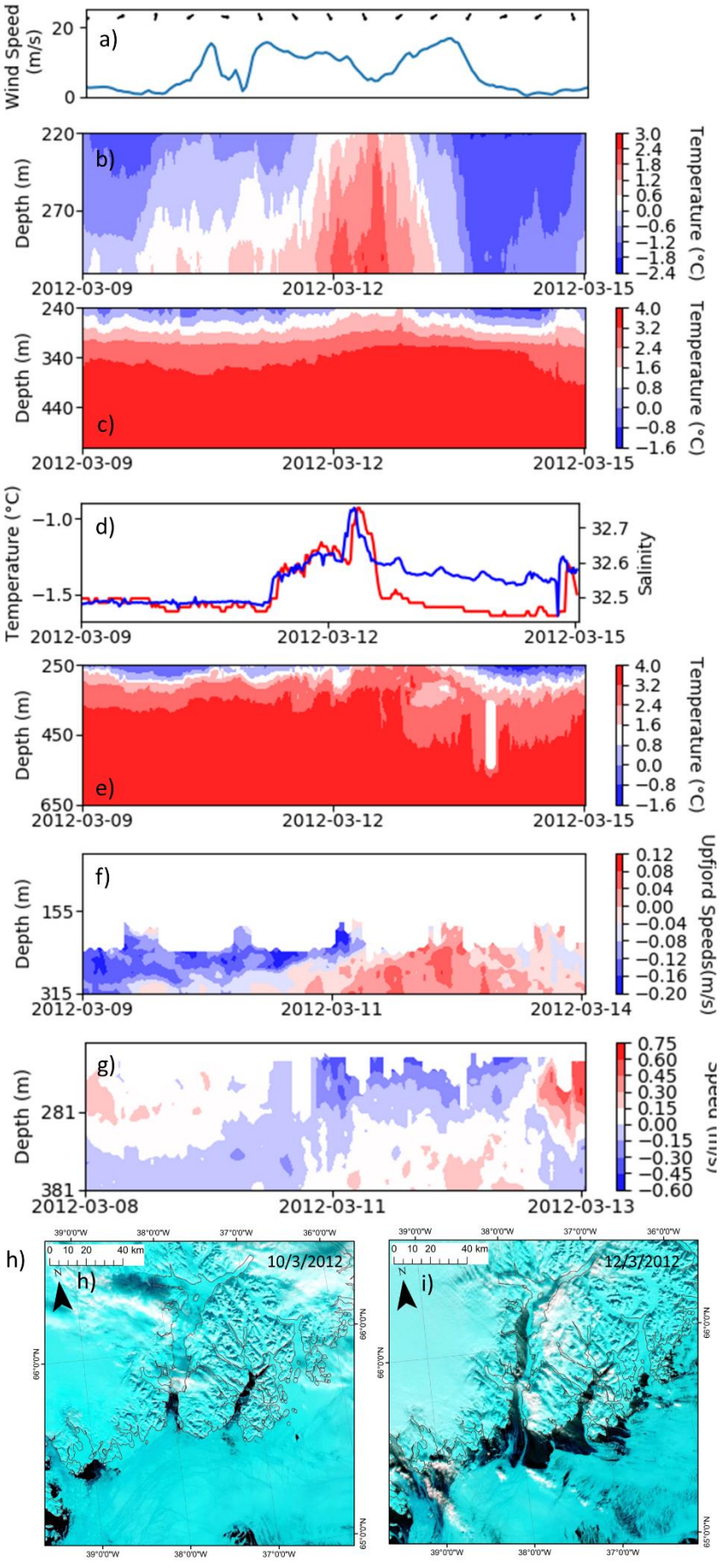

Figure 4.23: Wind speed and direction for a DWE on 11/3/2012 and the corresponding temperature, current profiles along with the satellite imagery: a) wind speed and direction at Sermilik Fjord; b) temperature profile at site 11_2 to the east of the fjord mouth; b) temperature profile at site 11_3 to the west of the fjord mouth; d) temperature and salinity at 13m at site 11_5 at the upper fjord; e) temperature profile at site 11_6 at the mid-fjord; f) current profiles at site 11_A at the upper fjord; g) current profiles at site 11_6 at the mid-fjord; g) MODIS 721 images a day before and after the DWE; h) MODIS 721 imagery the day before the event; i) MODIS 721 imagery the day after the event. See Fig. Site for exact locations of profiles. Note the differing temperature and speed scales between the panels.

system (Fig. 4.23). Shelf waters to the east of the fjord mouth have a large influx of warm water which remains sustained for just the length of the event. On the other hand, the warm water increase is more limited to the west of the fjord. This matches with the sea-ice concentrations where sea ice is fully removed from coastal waters to the east of the fjord mouth but only partially removed to the west. SMR rates here do, however, increase by up to 85% relative to the start of the event (Fig. 4.14).

Within the middle of the fjord, near surface down-fjord currents are intensified during the wind event (Fig. 4.23). Lower down, below the thermocline, warm water moves up-fjord as the thermocline shoals. In the days after the DWE, the waters surrounding the thermocline are less stratified once the thermocline resumes its original position. This thermocline movement coincides with a switch to up-fjord currents in the near surface waters and an opposite switch further down the fjord. The up-fjord near surface current rapidly increases in strength to 0.8m/s. The area around the mid-fjord buoy is cleared of sea-ice but at the east side of the fjord the sea ice remains concentrated (Fig. 4.22).

In the upper fjord there is more of delay before currents below 200m shift to moving up-fjord, reaching peak velocity around 2 days after the start of the DWE (Fig. 4.22). The ADCP profile is limited and does not reveal near surface currents. However, the ice melange remains intact and this probably explains the limits of the ADCP (Fig. 4.22). Surface waters show an increase of 0.6°C during the event and sea-ice is removed from the location of the buoy situated on the west coast of the upper fjord (Fig. 4.22). SMRs increased by up to 1034% from the start of the event (Fig. 4.14).

Chapter 5:

Discussion:

Katabatic wind characteristics:

Individual katabatic wind events varied greatly in their maximum speed and duration. None of the wind events were close to the potential maximum wind speed of 90m/s often referenced in the literature (Born and Böcher 2001). More importantly, the maximum downslope wind speed observed in the ERA5 data, 23.55m/s, was well below the Fjord Station maximum of 36.18m/s - suggesting that ERA5 fails to resolve some component of katabatic wind formation. A similar issue was discovered in ERA-Interim, which failed to resolve mountain wave breaking so it too underestimated downslope air flow speed, suggesting a comparable problem to that noted in ERA5 (Oltmanns *et al.* 2014, 2015). However, further, more detailed investigation of the dynamics of downslope flow formation in ERA5 would need to be undertaken to pinpoint this issue, although the coarse topographical and model resolution may be responsible (Oltmanns *et al.* 2015). Importantly, though, this study has shown that ERA5 underestimates maximum downslope flow allowing the mitigation for this in any future work.

In agreement with previous reports, katabatic winds are shown to predominate in winter months (Fig. 4.3, Oltmanns *et al.* 2014). All three datasets analysed show similar patterns - although summer events are more common at Station Coast, on the banks of Sermilik Fjord. Another noticeable variation is the much lower number of events seen in February in the ERA5 dataset (Fig. 4.3). It is hard to analyse the cause of these variations especially given the differences in timescales of the datasets, although unresolved wave dynamics due to poor resolution are most likely contributors to these variations (Oltmanns *et al.* 2015). DMI and ERA5 datasets show a much better comparison, aiding the hypothesis that poor topographical resolution causes the disparity with ERA5, given the more topographically straightforward location of the DMI station. ERA5 provides a good representation of katabatic wind occurrence throughout the year, but the above findings suggest that users should be mindful of its limitations (Figs. 4.2, 4.3).

Although there is a significant relationship between DWE maximum wind speed and duration, relatively little of the variation, 35%, of the latter is explained by the former (Fig. 4.1). The low R-squared values suggest that these two DWE characteristics - although related - show some degree of independence. It is therefore important to consider both maximum wind speed and duration when establishing katabatic wind strength and influence. Further analysis of katabatic wind characteristics

could create a base equation to define strength translating into wind stress. However, given the variable sea-ice concentrations this would need to be seasonally adaptable.

Fjord circulation:

Generalised flow pattern:

Clear warm water influxes are seen throughout Sermilik Fjord as a result of katabatic winds, and usually last roughly the same time period as the DWE duration. There is seasonal variation, with location in fjord and katabatic wind strength also being factors affecting the influxes (Figs. 4.8-4.12). These warm water influxes correlate with up-fjord currents, and colder water masses correlate with down-fjord currents (Figs. 4.6, 4.7). Warm water must therefore be coming into the fjord from the shelf, with colder glacially modified water generally flowing in the opposite direction (Straneo *et al.* 2010b, 2012, Inall *et al.* 2014, Jackson *et al.* 2014, Sutherland, Straneo, *et al.* 2014). Current profiles in the mid-fjord indicate a pycnocline between two currents of opposite directions at around 200m prior to and during DWEs (Fig. 4.6). This agrees well with previous studies showing the pycnocline at 200m (Straneo *et al.* 2012, Jackson *et al.* 2014). Unfortunately, mid-fjord temperature profiles do not extend to a depth this shallow; however, a thermocline between 200-300 would fit the data (Fig. TP4).

Immediately after down-fjord wind stress is reduced, a sudden alternation in the direction of the currents occurs. Specifically, currents above 200m switch to up-fjord flow and those below 200m switch to down-fjord flow (Fig. 4.6). From the temperature profiles it can be inferred that shoaling of the thermocline is compensating for the increased down-fjord flow above 200m (Figs. 4.6, 4.7). The strong up-fjord flow post-DWE occurs as the thermocline relaxes, but the temperature of this return flow is unclear due to the limitations of the temperature profiles (Fig. 4.11-j). The return flow is likely to be an intermediary return flow, similar to those seen in intermediary circulation, with a temperature of between 1.5-2°C (Fig. 4.11-j), Straneo *et al.* 2010, Jackson *et al.* 2014).

Comparison to intermediary circulation:

Circulatory changes within the fjord seem to be almost immediate, following the general pattern that upper waters down-fjord flow intensifies, while deep waters, below the pycnocline, have a corresponding intensification in the up-fjord direction (Figs. 4.6, 4.7). This trend is also shown in the temperature profiles within the fjord and on the shelf, and response time to the wind forcing seems to be roughly uniform no matter what the location (Figs. 4.8-4.12). These katabatic wind induced circulation changes differ from intermediary circulation, where the flow takes time to penetrate up the fjord (Straneo and Cenedese 2015). Some upper fjord profiles show some delay, (Fig. 4.12-d) but this will be because of ice coverage rather than any time lag in the propagation of the warm water

flow up the fjord. The immediate increase in temperatures and warm inflow throughout the fjord means that this circulation must be highly efficient at transferring heat up the fjord.

Another difference between katabatic wind driven circulation relative to intermediary circulation concerns the increases in temperature of surface waters near to the front of the ice melange (Fig. 4.12). Intermediary circulation has been shown to greatly increase the heat content within the fjord, but it remains unclear how effective such circulation is at heating the upper fjord (Jackson *et al.* 2014). Although modelling studies in Kangerdlussuaq have shown intermediary circulation to be highly efficient (Fraser and Inall 2018), it would not be expected to heat surface waters but rather to increase water column heat content through shoaling of the thermocline (Straneo and Cenedese 2015). It is therefore hard to explain the sudden rapid increase in temperature in the surface waters present near the glacier front (Fig. 4.12). The rapid removal of surface waters could lead to upwelling of bottom waters at the head of the fjord. If this mechanism does occur, the glacier terminus could be exposed to warm waters at all depths, rapidly increasing melting (Jenkins 2011).

Shelf waters:

Warm influxes into the fjord originate from the east of the fjord mouth on the shelf, shown by the large temperature increases in profiles here during DWEs, compared to weak or unresponsive profiles to the west of the fjord mouth (Fig. 4.12). It is unclear if the observed temperature changes are as a result of any influence from the EGC or are a direct result of rotational forcing. Either way, this is hypothesised that this must lead to an across-fjord gradient (Fig. 5.1) which unfortunately

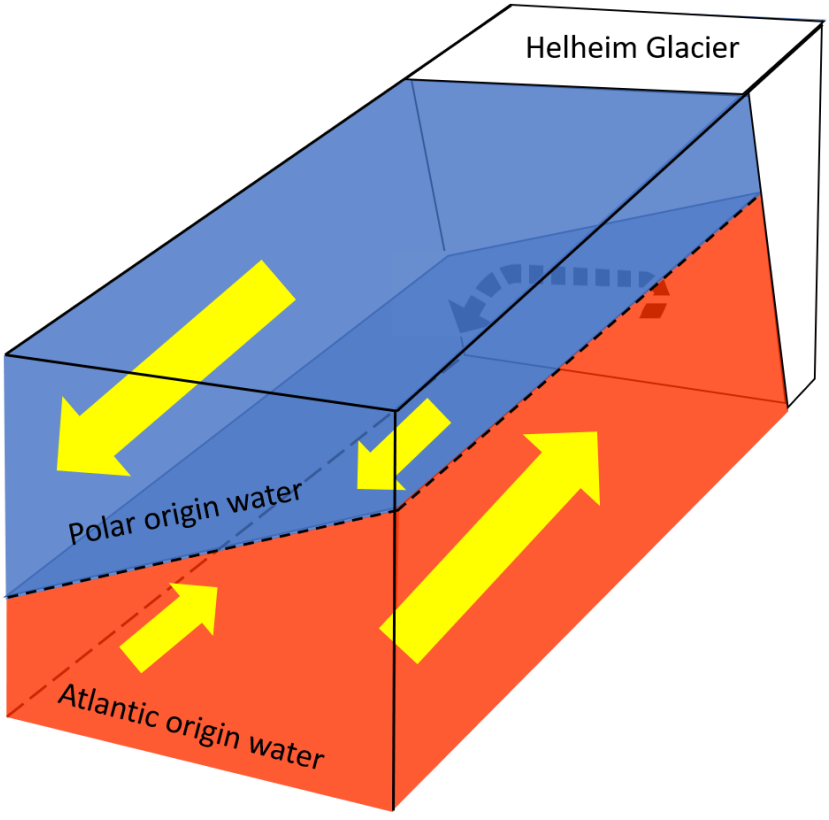

Figure 5.1: Schematic of proposed katabatic wind driven circulation in Sermilik Fjord. Known current directions are shown by yellow arrows with the size of the arrow relative to the magnitude of the flow. The dashed black arrow indicates proposed flow at the top of the fjord. The dotted line between the two water masses shows the thermocline as the Atlantic origin water, red area is warm and saline, while the polar origin water, blue area is cold and fresh.

cannot be seen due to the lack of sufficient data across the fjord (Fig. 3.2). The hypothesis is based on analogy from coastal current movements (Fig. 2.3), where warm water inflow into the fjord would have been expected to come from the west or at least the south due to the northward flow of the Irminger Current (Straneo *et al.* 2016).

Current velocity probes at 224m on the centre of the shelf show an alternating east-west water movement (Fig. 4.4), suggesting the pycnocline sits around this depth and that its height is constantly shifted by water pulses. There is however no clear relationship with katabatic wind speed and current speed in either direction across the fjord mouth. Oddly, temperature profiles across this site, 9_3 (Fig. 3.2), in non-summer months show an influx of warm water across this depth (Fig. 4.8). No significant in-fjord or out-fjord movement was detected at 224m, meaning that the warm water coming off the shelf cannot be heading directly into the fjord. The easterly or westerly current movements detected must be shifts in the height of the coastal currents (Sutherland and Pickart 2008), while the temperature increases in the upper layer must be provided by insurgent waters coming towards the coast at an undetected angle by the data analysis. Further work is required to establish the exact nature of the route of warm water influxes onto the shelf which is largely unknown despite the well-established origin of the warm water (Jackson *et al.* 2014, Sutherland, Straneo, *et al.* 2014, Straneo *et al.* 2016).

In summer months, shelf waters respond differently to down-fjord wind forcing and, unlike non-summer months, there is no clear warm water influx around 200m (Fig. 4.8-b). Instead a very warm water mass, with a temperature around 6°C higher than surrounding water, is seen between 135-185m one day after the DWE. This water mass could be warm, relatively saline, solar heated coastal water downwelling because of increased surface freshwater export from the fjord. This proposal is supported by the downward movement and cooling of this water mass over time (Fig. 4.8-b). Since this is the only profile observed, because of the winter predominance of katabatic winds, little should be concluded from the presence of this profile, other than that there is no warm water influx - possibly because of increased buoyancy driven circulation in summer months (Inall *et al.* 2014, Jackson *et al.* 2014, Sutherland, Straneo, *et al.* 2014, Cowton *et al.* 2016).

Fjord mouth:

Fjord mouth temperature profiles show less pronounced warm water influxes compared to the shelf, although the poor resolution of these profiles should be noted (Fig. 4.10, Data and Methods). Warm water influxes can be seen shoaling the thermocline to around a depth of 250m for the duration of the DWE (Fig. 4.10). The temperature profiles do not provide the whole picture as up-fjord warm water fluxes are shown at 520m during down-fjord wind forcing (Fig. 4.5). Current speeds seem to be a function of down-fjord wind speed, with strong events increasing up-fjord currents to around

0.5m/s. Similarly, the length of these up-fjord pulses seems to correlate to DWE duration (Fig. 4.5). Current profiles are perhaps a better measure of warm water influx at the fjord mouth than temperature profiles as, due to the greater depth and gateway-like nature of the fjord mouth, the thermocline will shoal less here than in other parts of the fjord or shelf.

Mid-fjord:

Current velocities in both upper and lower water layers peak in the mid-fjord before reducing towards the upper-fjord and shelf, following a similar pattern as seen in intermediary circulation (Jackson *et al.* 2014, Sutherland, Roth, *et al.* 2014).

The best comparison of across-fjord temperature gradients is displayed between site 10_2 situated near the east bank of the mid-fjord, compared to sites 11_6 and 12_4 which are located near the centre channel on the mid-fjord (Fig. 3.2). Towards the east bank, the variation is much more pronounced, suggesting an across-fjord thermocline shoaling from west to east (Fig. 5.1).

Upper fjord:

Surface water temperatures immediately increase in the upper fjord during katabatic wind events (Fig. 4.12) which, as previously discussed, could lead to possible upwelling near the ice melange or terminus. Warm water fluxes here are much shorter-lived than elsewhere in the fjord or on the shelf, usually only lasting for between 4-6hrs. Secondary pulses of increased temperature occur around 12hrs after the initial spike (Fig. 4.12). Subsequent pulses reduce in magnitude and duration. This suggests that it is the same flow returning and the gap in-between the pulses could be the resonance time of the fjord (Jackson *et al.* 2018).

During the increased temperature spikes, salinity also increases supporting the suggestion that some form of upwelling is occurring. When the temperature drops off, however, salinity remains high or decreases only slowly, suggesting some form of ice melting occurring (Jenkins 2011), removing the heat content from the water and producing freshwater which then fails to mix with the saline water.

Deeper waters in the fjord show a switch from down-fjord flow to up-fjord flow during katabatic wind events (Fig. 4.11). This is opposite to flows at equivalent depths seen at the mid-fjord and the boundary layer between the two flows seems to lie further down at around 250-300m. Without the complete profile it is hard to interpret or understand the circulatory pattern in the upper fjord, however it would be unexpected for the flows seen at the mid-fjord to not also occur at the upper-fjord. Rather, their relative position in the water column may have moved along with the layer boundaries (Figs. 4.6, 4.7).

Summary of circulatory changes:

Katabatic wind stress induced fjord circulatory changes in non-summer months are very similar to the final stage of intermediary circulation (Fig. 1.3, Straneo *et al.* 2010, Jackson *et al.* 2014, Sutherland, Straneo, *et al.* 2014, Spall *et al.* 2017), but without the major time delay following the wind forcing (Harden, Straneo, *et al.* 2014). Increased wind stress removes surface waters out of the fjord resulting in a compensatory return flow at depth, which is composed of warm saline Atlantic origin water (Figs. 4.6, 4.7, 4.11). During the DWE, the polar origin water shrinks and the thermocline shoals (Figs. 4.8-4.11). There is then a return flow when the pycnocline is depressed and the bottom Atlantic origin water layer is depressed, once the down-fjord wind forcing ceases (Fig. 4.6, 4.7). The circulation in summer months remains unclear, but changes can be predicted to be weaker because of the dominance of buoyancy driven circulation (Inall *et al.* 2014, Sutherland, Straneo, *et al.* 2014, Cowton *et al.* 2016). Also, the infrequency of katabatic wind event during summer reduces its importance (Oltmanns *et al.* 2014).

During the first stage of katabatic wind driven circulation changes, heat increases are immediately seen throughout the fjord, marking a major difference compared to intermediary circulation (Jackson *et al.* 2014). This is because changes from DWEs are driven by surface water export within the fjord rather than density changes on the shelf (Straneo *et al.* 2011, Jackson *et al.* 2014, Straneo and Cenedese 2015). As such, katabatic wind driven circulation provides warm water directly to the glacier front highly efficiently and is guaranteed to increase submarine melt rates, even though the temperature increases are short lived.

Submarine melt rates:

Calculated submarine melt rates (SMR) vary with the position across the fjord, along with the strength of DWE (Figs. 4.14, 4.15). Even in locations relatively removed from the glacier, the melt rates can provide a good indication of the heat content within the water column around the area of expected warm water inflows (Jackson *et al.* 2014). Sites towards the top of the fjord displayed the highest increases in submarine melt rates, up to 1000% relative to rates prior to the DWE, again suggesting that katabatic wind driven circulation is very efficient at moving warm water to the glacier terminus. However, these sites were at the shallowest depth and SMR increases also seem to associate inversely with depth; the site with the lowest increase, site 10_2, was also the deepest (Fig. 4.14). This is to be expected, as warm bottom waters are not likely to increase in temperature, rather the thermocline shoals and so increases heat content in the intermediary and upper waters (Straneo *et al.* 2010b, Jackson *et al.* 2014, Sutherland, Straneo, *et al.* 2014). Depth was accounted for as far as possible given the limitations of the extent of the profiles (Data and Methods), although clearly some variation from depth remains.

Beyond the depth induced variation, the heat content measured for the central shelf (site 10_3), western shelf (site 11_4), fjord mouth (site 10_5) and central mid-fjord (sites 11_6 and 12_4) was very similar, showing the transfer of heat from shelf to the middle of the fjord (Figs. 3.2, 4.14). Together with the temperature profiles this gives a clear picture of efficient heat transfer at a depth of around 250m from the shelf to mid-fjord (Figs. 4.8-4.11). Understanding of changes further up the fjord remains unclear due to the issues sampling at these locations (Straneo *et al.* 2012). However, despite the uncertainty in the method of heat delivery to the glacier front, submarine melt rates do increase dramatically there due to katabatic wind events (Fig. 4.14).

Towards the east of the fjord mouth, estimations of increases in submarine melt rate caused by DWEs are highly variable (Fig. SMR). This could be because of high sea-ice concentrations observed coming southwards down the EGC (Fig. 4.18, Sutherland and Pickart 2008). Sea-ice removal is heavily dependent on the strength of the katabatic wind (Fig. 4.19). As such, the variability in this area could be much more dependent on sea-ice coverage or DWE strength than the fjord, which is rarely fully covered by sea ice (Andres *et al.* 2015).

Removing the seasonality and variation with location, increased SMRs are associated with stronger DWEs (Fig. 4.19). Maximum katabatic wind speed is a much better predictor of increased heat content of the water column or SMR than the duration of the DWE, suggesting a dominant effect of wind speed over duration in how wind stress is transferred to the water column (Fig. 4.19). The strongest event in 2010, maximum wind speed of 21.61m/s, increased SMRs by a factor of between 8-12 times relative to the weakest event that year, maximum wind speed of 12.52m/s, suggesting a non-linear response between down-fjord wind stress and SMRs (Fig. 4.19). This is expected since wind stress is a quadratic function of wind speed (Large and Pond 1981, Spall and Pedlosky 2018). Currently modelling studies looking at katabatic wind influences do not account for the large variations in wind speed (Spall *et al.* 2017, Spall and Pedlosky 2018). Based on this result any variation unaccounted for in wind strength is likely to be magnified in any SMR or water column heat content estimations.

Sea-ice removal:

In agreement with previous work, sea-ice was removed from the shelf and fjord during DWEs (Figs. 4.16-4.22, Oltmanns *et al.* 2014). Removal from the fjord itself was not quantified because of the lack of passive microwave sea-ice concentration data, due to close proximity of the surrounding ice-covered land (Spreen *et al.* 2008). In non-summer months, when sea-ice predominates in the fjord, weak and strong DWEs successfully remove the majority of sea-ice (Figs. 4.16, 4.17). Clear water formation on the west side of the fjord highlights the clear rotational influence on the surface water

when down-fjord wind stress is applied (Figs. Sat1, Sat2). This supports the notion that currents within the Sermilik Fjord are affected by the Coriolis effect, and that across-fjord gradients should be considered, especially when modelling (Sutherland, Roth, *et al.* 2014, Jackson *et al.* 2018). Tying this together with the noticeable across-fjord and shelf temperature differences, advocates at least a basic fjord model where the thermocline shoals from west to east (Fig. 5.1). These observations also raise the possibility that large unobserved across-fjord gradients are created during katabatic wind events driven by the increased outflow down the west side. Given that the majority of the moored buoys reside on the east of the fjord, unobserved warm water influxes down the west of the fjord could occur. However, this is unlikely as warm water influxes on the shelf are higher on the eastern side (Fig. 4.9). There must be some form of wind set up towards the west, overturning current or across terminus circulation to compensate for the differing total volume fluxes between the east and west (Fig. 5.1). Any compensatory processes in the upper fjord will be short lived, spanning a similar time to the DWE-induced warm water inflow, but could significantly increase submarine melting. Similar processes, such as free convection, have been proposed from models but never observed in the field (Cowton *et al.* 2015, Schild *et al.* 2018).

DWE-induced removal of sea ice from the shelf has previously been observed to reduce sea-ice concentrations by 26% (Oltmanns *et al.* 2014). However, removal is dependent on the magnitude of the katabatic wind (Figs. 4.18, 4.19). The nominal threshold of 12m/s was observed, below which sea-ice concentrations on the shelf actually increase because of compensatory flow from the EGC (Fig. 4.18). The existence of this wind speed threshold highlights the need to account for katabatic wind strength when measuring offshore sea-ice or freshwater flux, as weak events will not induce offshore export. Incorporation of this analysis, where an increase of a unit wind speed causes a reduction in sea-ice concentrations of 4.9% (Fig. 4.19), in offshore flux models would increase accuracy (Spall and Pedlosky 2018). This would account for the potentially dominant effect that infrequent strong DWEs could have on the annual freshwater export budget. If a yearly DWE strength pattern could be established, coupling this together with its relationship to offshore sea-ice removal, could provide a mechanism for long-term predictions. The prevalence of katabatic winds across the east Greenland coast suggest similar relationships occur at fjords such as Kangerdlussuaq Fjord (Doyle *et al.* 2005). The gradient of sea-ice concentration against DWE maximum wind speed is probably a function of local coastal oceanography, meaning variation will exist between different east coast fjords systems. However the basic trend is predicted to remain similar, especially below 69°N where the presence of the Irminger Current allows rapid melt post offshore advection (Seale *et al.* 2011, Sutherland *et al.* 2013), with weak speeds increasing sea-ice concentration and a linear increase in sea-ice removal in wind speeds above this.

In contrast to DWE maximum wind speed, sea-ice concentration on the shelf did not significantly vary with DWE duration. This observation, along with the better correlation of maximum wind speed with submarine melt rates (Fig. 4.15), shows maximum wind speed to be a better proxy for DWE strength and forcing on the environment. The quadratic nature of wind speed to wind stress (Large and Pond 1981), is probably the main reason that wind speed is a much better predictor of katabatic increased SMR and sea-ice export than DWE duration.

Since sea-ice removal from the shelf occurs almost immediately and lasts for several days post DWE, large-scale sea-ice removal due to strong DWEs could promptly affect AMOC and local freshening in the Irminger Sea (Weijer *et al.* 2012, Sutherland *et al.* 2013). Over annual timescales, sea-export from katabatic winds is unlikely to be displayed compared to the far greater freshwater import from the EGC (Holfort *et al.* 2008, Spall and Pedlosky 2018). However, given the intensity and localisation of these freshwater fluxes it could play an important role in short-term changes in AMOC and the Irminger Sea freshwater budget.

Sea-ice effect on fjord circulation:

Since sea ice is so successfully removed from the fjord, along with persistent open water areas within the fjord (Andres *et al.* 2015), it has little influence in restricting down-fjord wind induced warm water inflow within the fjord itself. There is some suggestion that the area to the east of the fjord mouth, where sea-ice is readily supplied by the EGC (Fig. 4.18), is affected by its high sea-ice concentrations (Fig. TP2). Concerns raised about the uncertainty of wind stress transfer to the water column because of sea-ice concentrations do not seem to be significant, increasing the accuracy of katabatic wind driven fjord and shelf models (Spall *et al.* 2017, Spall and Pedlosky 2018).

One potential effect of sea-ice within the fjord, is the pattern of removal increasing across-fjord gradient (Figs. 4.16, 4.17, 5.1). Previous modelling studies have assumed across-fjord gradients exhibit only rotational effects (Cowton *et al.* 2016, Spall *et al.* 2017), but sea-ice removal from the west side of the fjord (Fig. 4.16, 4.17) may lead to much greater across-fjord gradients. This highlights the need to 3D model fjord circulation dynamics (Jackson *et al.* 2018), especially with regards to katabatic wind driven circulation.

Ice melange removal:

The majority of DWEs analysed and observed between 2009-2013 did not successfully break up the ice melange in front of the terminus of Helheim Glacier (Figs. 4.16, 4.17, 4.22). A typical event created an area of open water in the upper fjord, and in the following days the sea-ice in front of the glacier was eroded (Fig. 4.16). Surface water temperature increases in the upper fjord during the same event were short-lived, only spiking for around 8hrs, although the rapid increase in

temperature and steady decline in salinity suggest melting of sea-ice had occurred (Fig. 4.12-f). The short-term spike in temperature means submarine melting is not responsible for the continued retreat of sea-ice observed in the upper fjord days after the DWE. Instead, katabatic wind stress it is likely to have caused fracturing of the sea-ice which only drifts apart in the subsequent days. Although the typical reduction of sea-ice and ice melange from a DWE did not leave the terminus exposed to open water, future reductions from rising *in situ* air and water temperatures could facilitate this. This leads to the very realistic possibility that in the near future typical katabatic winds will lead to open water formation at the glacier terminus inducing calving and subsequent retreat (Christoffersen *et al.* 2012).

Currently only strong events, those above the 20m/s threshold, completely remove the ice melange (Fig. 4.20, 4.21). Interestingly, the melange is not removed during the DWE but over the course of a few days post-DWE, suggesting again that wind induced fracturing is behind the continual break-up. There is a delay before surface waters increase in a series of warm pulses, raising *in situ* water temperatures by up to 0.6°C (Fig. 4.12-d). Raised water upper fjord water temperatures last for over a day and it is therefore unclear if submarine melting is behind the break-up of the ice melange.

Terminus stability:

Following the disintegration of the ice melange from strong katabatic wind events, the terminus undergoes significant retreat and calving (Fig. 4.20, 4.21). The retreat and calving of the glacier front for the first of the two strong katabatic wind events, occurred between 3-12 days after the initial DWE (Fig. 4.20). The second retreat was less sustained, only lasting for around five days after the DWE, although high cloud coverage on some days makes this difficult to pinpoint (Fig. 4.21). Increased surface water temperatures in the upper fjord for the first event only lasted a day, suggesting melt rates may not have been the cause of the calving (Fig. 4.12-f). The deep submarine melt rates remain unclear, given the limited profile of the water temperature, although based on the analysis of the warm water influxes into the fjord from katabatic winds, increased submarine melt rates are unlikely to be sustained for more than a couple of days.

The sustained calving of the glacier in the ten days after the wind event could mean a shift in the internal dynamics (Benn *et al.* 2007, Bassis and Jacobs 2013) caused by katabatic winds, either indirectly through increased submarine melt rates or directly through the removal of the sea-ice melange (Figs. 4.12-f, 4.20, 4.21). Although submarine melt rates were dramatically increased throughout the fjord during a strong DWE (Fig. 4.15), these increases were short-lived, especially in the upper fjord (Fig. 4.12-f). So, contrary to previous research (O'Leary and Christoffersen 2013, Benn *et al.* 2017, Slater *et al.* 2017), it seems improbable that submarine melt rates are the main

driver of the calving . It should be noted that the assumption that high calving rates are caused by undercutting from submarine melting is based on observation made in the summer environment (Benn *et al.* 2017). Instead, the removal of the ice melange seems to be the main driver of increased calving and so terminus retreat (Figs. 4.20, 4.21, Christoffersen *et al.* 2012). Removal of the ice melange is known to provide important buttressing to the terminus, but studies have mainly focused on spring or summer months (Amundson *et al.* 2010, Christoffersen *et al.* 2012). The subsequent retreat of the terminus following the loss of buttressing suggests that ice melange plays a dominant role in non-summer terminus dynamics. Speculation of its importance in driving winter readvancement has been shown by modelling studies (Todd and Christoffersen 2014).

The sustained retreat and series of calving events over the following week (Fig. 4.20) suggests that amplification through weakness propagation up the glacier occurred (O'Leary and Christoffersen 2013). Amplification of calving, increasing retreat, has previously been attributed to undercutting by submarine melting (O'Leary and Christoffersen 2013, Benn *et al.* 2017) although the process of amplification is poorly understood (Schild *et al.* 2018). The loss of buttressing from the ice melange is centred on the upper section of the glacier (Todd and Christoffersen 2014). Its loss could result in instability with a similar effect to undercutting, resulting in the observed calving amplification.

The removal of the ice-melange results in the formation of an area of open water in front of the terminus (Figs. 4.20, 4.21). Previous work has linked open water formation to the retreat of Kangerdlussuaq Glacier through increased exposure to fjord waters (Christoffersen *et al.* 2012). So although heat content provided by katabatic winds may be lower than from barrier winds (Spall *et al.* 2017), melting of the terminus could be on the same magnitude or greater.

Another key piece of evidence that non-summer glacier retreat is controlled by buttressing from the ice melange is the threshold maximum of wind speed, of around 20m/s, required to cause retreat. No retreat was observed as a result of any of the DWEs below this threshold analysed between 2009-2013. In contrast, as discussed above, DWEs with a wind speed greater than 20m/s cause a significant break up of the ice melange (Figs. 4.20, 4.21). The coupling of ice melange break-up with glacier retreat highlights its dominant control on terminus dynamics and calving rates in non-summer months (Reeh *et al.* 2001, Christoffersen *et al.* 2012, Todd and Christoffersen 2014).

Decadal change:

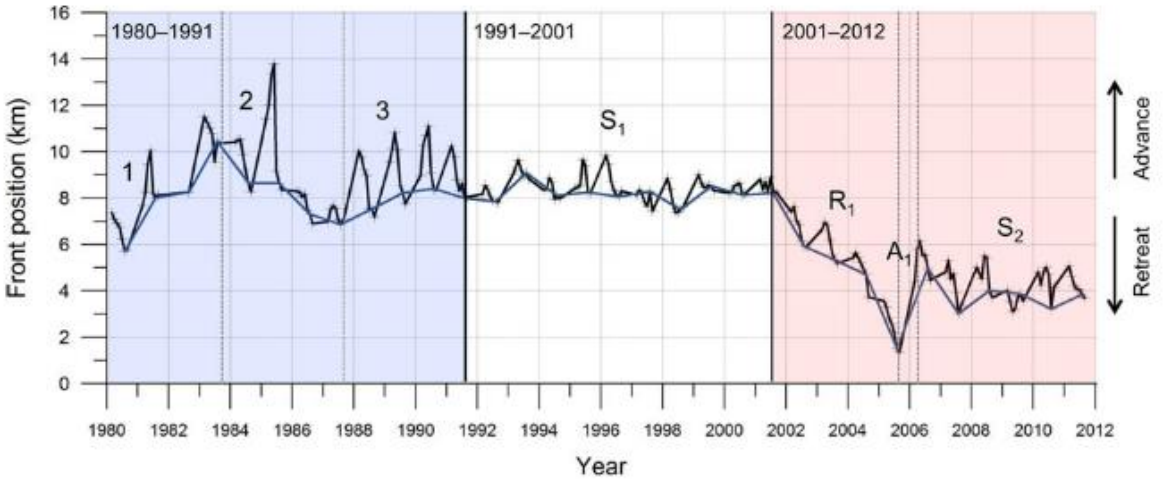

Figure 5.2: Extent of Helheim Glacier terminus based of satellite imagery. The black line shows sub-annual terminus extent, based on the calculation from Miles *et al*., (2016), while the blueline shows the end of summer terminus extent. Note the large retreat from 2001-2005.

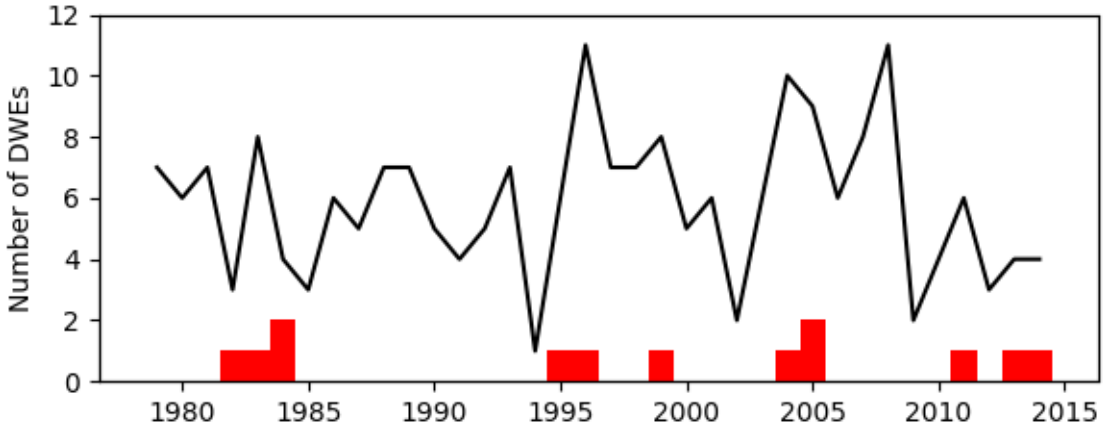

Figure 5.3: Number of DWEs and strong DWEs based on ERA5 reanalysis data for Sermilik Fjord. The black line shows the number of DWEs per year, while the red bars show the number of DWEs with a maximum speed above 20m/s annually. Note the association of these strong events with periods of retreat of Helheim Glacier (Fig. 5.2).

Nick et al., (2009) showed that Helheim Glacier retreat between 2000-2005 was caused by a shift in the calving dynamics, and this study has shown that katabatic winds could be an important driver in calving rates changes. This raises questions on the importance of katabatic winds over longer time scales. There is no clear trend in the number of katabatic wind events since 1958 (Fig. 4.2, Oltmanns *et al.* 2014), showing no connection with Helheim Glacier retreat (Fig. 5.2). However, looking only at events over the observed threshold of 20m/s to induce glacier retreat rather than purely the number of events per year, periods of sustained retreat coincide with strong DWEs (Figs. 5.2, 5.3). It is proposed that a series of strong katabatic winds between 2004-2005 played a significant role in

the retreat of Helheim Glacier, removing the ice-melange and so causing an increase in the calving rate, leading to a sustained period of retreat (Figs. 4.20, 5.3, Nick *et al.* 2009). Other periods of strong katabatic wind events are not so clearly related to terminus retreat, suggesting either that the ice-melange was not fully removed, or that the glacier was less sensitive to the loss of buttressing. Since wind stress is not the only cause of ice-melange removal, increases in air temperature and submarine melting could make the melange more susceptible to removal to katabatic winds (Christoffersen *et al.* 2012). Increased ocean temperatures also lead to increased sensitivity of the glacier to other forcing, such as the loss of buttressing from katabatic wind removal (Cowton *et al.* 2018). As ocean temperatures increase, it is therefore possible that retreat distance because of ice melange removal will increase. As a result, the direct influence of strong DWEs on Helheim Glacier retreat could also increase. Additionally, an increase in air temperature could reduce the DWE maximum wind speed threshold to remove the ice melange, potentially raising the number of katabatic wind induced melange removal events.

Katabatic wind events below this threshold of 20m/s will not have a significant effect on glacier retreat. Such weak DWEs provide important circulatory changes on a short term scale but in the variability at Sermilik Fjord their influence is only small (Jackson *et al.* 2014). These weak DWEs will increase non-summer submarine melting, but these are only small changes in comparison to barrier wind driven intermediary circulation (Spall *et al.* 2017). Although these DWEs induce fjord renewal and warm water influxes on decadal scales, glacier retreat will remain a function of ocean heat content as the numbers of such weak DWEs show no long-term trend (Fig. 4.2, 5.3, Cowton *et al.* 2018). However, the high inter-annual variability of the number of DWEs, along with similar patterns of barrier wind events (Harden *et al.* 2011), could cause some inter-annual variation in submarine melting and so terminus retreat. Any model predicting future retreat of south eastern Greenlandic glacier on timescales of less than 10 years should therefore include a katabatic and barrier wind induced submarine melting component.

Unlike weaker events, those above the ice melange removal threshold could have implications on longer-term timescales. Significant retreat from the removal of the ice-melange can cause a retreat noticeable on yearly terminus position trends (Christoffersen *et al.* 2011).

Wider implications of study:

The largely unexplored effects of katabatic winds on fjord circulation, sea-ice export and terminus stability leaves a number of important areas requiring further research. This study has highlighted the wide ranging and potentially large-scale impacts of katabatic winds on Sermilik Fjord. Future

research requirements can be broken down into four wider implications: location, direct effects on terminus stability, fjord circulation changes and sea-ice export.

Location:

This study has shown the importance of researching katabatic winds in Sermilik Fjord and how they cause warm water influxes and can directly cause the retreat of Helheim Glacier. Katabatic wind events are known to occur throughout Greenland, especially across the east coast (Heinemann 1999, Heinemann and Klein 2002). They have been predicted to cause significant retreat at Kangerdlussuaq Glacier (Christoffersen *et al.* 2012). Future research should focus on establishing katabatic wind driven effects and variations across Greenland, primarily down the east coast. Since tidewater glaciers account for the majority of the mass loss in Greenland (Shepherd *et al.* 2012), direct katabatic wind influence could be a factor in retreat in a large number of glaciers. The west coast of Greenland has weaker katabatic winds and reduced fjord circulation due to shallower sills (Klein *et al.* 2001, Schumann *et al.* 2012, Bendtsen *et al.* 2014, Gladish, Holland, Rosing-Asvid, *et al.* 2015), although the ice-melange removal can lead to retreat (Todd and Christoffersen 2014). It is therefore important to investigate direct katabatic wind influences at least at one west coast tidewater glacier.

Direct effects on terminus stability:

Direct katabatic wind induced retreat has been shown by this study on two strong wind events, suggesting a trend rather than anomalous observations. Therefore, further investigation into quantifying, understanding and determining the threshold at which down-fjord wind stress causes ice melange breaks up is required. Quantifying the mass loss suffered by the glacier, dependent on *in situ* conditions, would be an important step in establishing the overall importance of direct katabatic wind stress compared to the well known drivers of mass loss, such as plume driven melt (Slater *et al.* 2017). Understanding the impact of the other factors, such as increased air temperature that can aid ice melange break up caused by down-fjord wind stress driven, is required. The threshold, of 20m/s, established in this study needs to be verified over a much larger data than just between 2009-2013, and could be expanded across the MODIS imagery. This is particularly accessible given the establishment of a long-term time series of katabatic winds provided by this study along with previous studies (Oltmanns *et al.* 2014). Also, as it known that ERA reanalysis can underestimate maximum katabatic wind speeds, it is unclear how this ERA5 20m/s threshold transfers into true wind speed, so further investigation of ERA5 representation of downslope flows is also needed.

Looking at the wider importance of the ice melange to terminus stability, highlighted by the effect of its katabatic wind driven removal, suggests its presence is more important in non-summer months than intermediary circulation driven SMRs. Calving amplification due to the loss of the ice melange is

another area in which is under investigated (Todd and Christoffersen 2014, Benn *et al.* 2017), as currently most research into calving dynamics is trying to link to SMRs (Benn *et al.* 2017, How *et al.* 2017, Schild *et al.* 2018).

Fjord circulation changes:

The establishment of the route of warm water influxes from the shelf to the fjord mouth would be a step forward, since this study and others have shown the importance of across-fjord gradients especially towards the fjord mouth (Fig. 5.1, Jackson *et al.* 2018). Determination of such routes would give a better understanding of fjord-shelf interaction, particularly with regard to coastal currents.

Development of quantification of DWE strength or effect, based on maximum wind speed and duration, is a possible advancement in order to predict SMRs at the glacier. This study has shown a non-linear relationship between SMR and maximum wind speed, and a similar weaker relationship with duration. If these two observations could be quantified by wind strength, such quantification would allow the calculation and addition of katabatic wind induced submarine melting based purely off metadata. This would be a useful simple addition to fjord-glacier models within the southeast of Greenland.

Sea-ice export:

The linear relationship of sea-ice removal from the shelf with maximum katabatic wind speed could be expanded across the MODIS imagery timeseries from 2001. This would provide a more conclusive relationship based off a far greater number of DWEs. If expanded to include other fjords on the east coast synonymous with katabatic winds, such as Kangerdlussuaq (Christoffersen *et al.* 2012), it could be factored into the freshwater budget of AMOC and the Irminger Sea.

Conclusions:

Katabatic flows are sufficiently modelled by ERA5 to allow the use of this reanalysis data to track DWEs across Sermilik Fjord (Fig. 4.2), if the user was aware of certain caveats. ERA5 underestimates the katabatic wind speed, and this is assumed to be due to unresolved wave dynamics caused by poor topographical and model resolution (Oltmanns *et al.* 2014).

Katabatic wind events lead to large changes in fjord circulation, terminus stability and sea-ice export across the Sermilik Fjord area. Fjord circulatory changes take the form of warm water influxes into the fjord which can raise SMRs by up to 1000% in the upper fjord (Fig. 4.14). Despite overall inflow of warm water being substantially lower than barrier wind driven intermediary circulation (Spall *et al.* 2017), heat transfer across the fjord seems to be more efficient with immediate increases in temperature seen throughout (Figs. 4.8-4.12). The strength of the DWE event has a controlling

influence on increasing SMRs and intermediary heat content in fjord, as increases of 65% of maximum wind speed can increase SMRs by up to 12-fold (Fig. 4.15). Direct influences on the glacier terminus stability have been shown to be more important than increased SMRs (Christoffersen *et al.* 2012). As a result, this study has demonstrated the importance of ice melange buttressing removal in increasing calving, especially in non-summer months (Amundson *et al.* 2010, Todd and Christoffersen 2014). Katabatic wind driven melange removal can also be a potential cause of the change in calving dynamics that led to the rapid retreat of Helheim Glacier (Fig. 5.2, 5.3, Nick *et al.* 2009).

Clearly katabatic winds cannot be held solely responsible for Helheim Glacier retreat; instead this study points to the need to consider their influence when discussing glacier retreat. Rather than focusing solely on ocean warming induced melting, research should also focus on causes of glacier sensitivity to ocean induced retreat and the mechanisms by which ocean heat is passed to the glacier. In order to answer this question fjord circulation processes have been widely studied (Straneo *et al.* 2010b, Inall *et al.* 2014, Jackson *et al.* 2014, Straneo and Cenedese 2015). This study suggests, at least in terms of katabatic winds, that circulatory processes play a secondary role to the direct effect of the break-up of the ice melange. Maintenance of terminus stability by the ice melange has widely been discussed, but few studies have concluded its removal as the cause of terminus retreat (Christoffersen *et al.* 2012).

Sea-ice export from the shelf is shown to be a function of DWE strength, an important observation for the inclusion of these results into modelling on the freshwater budgets AMOC and the Irminger Sea, and so global thermohaline circulation (Bamber *et al.* 2012, Weijer *et al.* 2012). Sea-ice removal from the fjord is insignificant in preventing katabatic wind driven circulation but its removal pattern aids the development of across-fjord gradients (Fig. 5.1), which should be accounted for in fjord circulatory models (Cowton *et al.* 2016, Jackson *et al.* 2018). Preliminary katabatic wind speed thresholds have been established for sea-ice removal from the shelf of 12m/s (Fig. 4.19) and for ice melange removal of 20m/s (Figs. 4.20, 4.21).

Whilst katabatic winds have previously been assumed to play a minor role in fjord dynamics (Sutherland, Roth, *et al.* 2014, Spall *et al.* 2017), the direct effect of katabatic wind driven retreat at Helheim Glacier highlights their significance. The importance of the ice melange in the retreat of the glacier during non-summer months has also been observed, suggesting perhaps that both strong katabatic winds and ice-melange removal are more important to terminus stability than shelf forced submarine melting events.

References:

Amundson, J.M., Fahnestock, M., Truffer, M., Brown, J., Lüthi, M.P., and Motyka, R.J., 2010. Ice mélange dynamics and implications for terminus stability, Jakobshavn Isbræ, Greenland. *Journal of Geophysical Research*, 115 (F1), F01005.

Andres, M., Silvano, A., Straneo, F., and Watts, D.R., 2015. Icebergs and sea ice detected with inverted echo sounders. *Journal of Atmospheric and Oceanic Technology*, 32 (5), 1042–1057.

van Angelen, J.H., van den Broeke, M.R., and van de Berg, W.J., 2011. Momentum budget of the atmospheric boundary layer over the Greenland ice sheet and its surrounding seas. *Journal of Geophysical Research*, 116 (D10), D10101.

Bacon, S., Marshall, A., Holliday, N.P., Aksenov, Y., and Dye, S.R., 2014. Seasonal variability of the East Greenland Coastal Current. *Journal of Geophysical Research: Oceans*, 119 (6), 3967–3987.

Bamber, J., Van Den Broeke, M., Ettema, J., Lenaerts, J., and Rignot, E., 2012. Recent large increases in freshwater fluxes from Greenland into the North Atlantic. *Geophysical Research Letters*, 39 (19), L19501.

Bartholomaus, T.C., Larsen, C.F., and O'neel, S., 2013. Does calving matter? Evidence for significant submarine melt. *Earth and Planetary Science Letters*, 380, 21–30.

Bassis, J.N. and Jacobs, S., 2013. Diverse calving patterns linked to glacier geometry. *Nature Geoscience*, 6 (10), 833–836.

Beaird, N.L., Straneo, F., and Jenkins, W., 2018. Export of Strongly Diluted Greenland Meltwater From a Major Glacial Fjord. *Geophysical Research Letters*, 45 (9), 4163–4170.

Bendtsen, J., Mortensen, J., and Rysgaard, S., 2014. Seasonal surface layer dynamics and sensitivity to runoff in a high Arctic fjord (Young Sound/Tyrolerfjord, 74°N). *Journal of Geophysical Research: Oceans*, 119 (9), 6461–6478.

Benn, D.I., Aström, J., Zwinger, T., Todd, J., Nick, F.M., Cook, S., Hulton, N.R.J., and Luckman, A., 2017. Melt-under-cutting and buoyancy-driven calving from tidewater glaciers: New insights from discrete element and continuum model simulations. *Journal of Glaciology*, 63 (240), 691–702.

Benn, D.I., Warren, C.R., and Mottram, R.H., 2007. Calving processes and the dynamics of calving glaciers. *Earth-Science Reviews*, 82 (3–4), 143–179.

Born, E.W. and Böcher, J., 2001. *The ecology of Greenland*. Ministry of Environment and Natural

Resources.

Brandi's Buzzar Blog: Chinook, Santa Ana and Katabatic Winds [online], 2016. Available from: http://buzzar-brandi.blogspot.com/2016/05/chinook-santa-ana-and-katabatic-winds.html [Accessed 2 Jun 2019].

Van Den Broeke, M., Bamber, J., Ettema, J., Rignot, E., Schrama, E., Van Berg, W.J. De, Van Meijgaard, E., Velicogna, I., and Wouters, B., 2009. Partitioning recent Greenland mass loss. *Science*, 326 (5955), 984–986.

Bromwich, D.H., Cassano, J.J., Klein, T., Heinemann, G., Hines, K.M., Steffen, K., and Box, J.E., 2002. Mesoscale Modeling of Katabatic Winds over Greenland with the Polar MM5*. *Monthly Weather Review*, 129 (9), 2290–2309.

Bromwich, D.H., Du, Y., Hines, K.M., Bromwich, D.H., Du, Y., and Hines, K.M., 1996. Wintertime Surface Winds over the Greenland Ice Sheet. *Monthly Weather Review*, 124 (9), 1941–1947.

Cappelen, J., 2019. *Weather observations from Tórshavn, The Faroe Islands 1953-2018-Observation data with description*.

Carroll, D., Sutherland, D.A., Hudson, B., Moon, T., Catania, G.A., Shroyer, E.L., Nash, J.D., Bartholomaus, T.C., Felikson, D., Stearns, L.A., Noël, B.P.Y., and van den Broeke, M.R., 2016. The impact of glacier geometry on meltwater plume structure and submarine melt in Greenland fjords. *Geophysical Research Letters*, 43 (18), 9739–9748.

Carroll, D., Sutherland, D.A., Shroyer, E.L., Nash, J.D., Catania, G.A., and Stearns, L.A., 2015. Modeling Turbulent Subglacial Meltwater Plumes: Implications for Fjord-Scale Buoyancy-Driven Circulation. *Journal of Physical Oceanography*, 45 (8), 2169–2185.

Cenedese, C. and Linden, P.F., 2014. Entrainment in two coalescing axisymmetric turbulent plumes. *Journal of Fluid Mechanics*, 752, R2.

Chauché, N., Hubbard, A., Gascard, J.-C., Box, J.E., Bates, R., Koppes, M., Sole, A., Christoffersen, P., and Patton, H., 2014. Ice-ocean interaction and calving front morphology at two west Greenland tidewater outlet glaciers. *The Cryosphere*, 8, 1457–1468.

Christoffersen, P., Mugford, R.I., Heywood, K.J., Joughin, I., Dowdeswell, J.A., Syvitski, J.P.M., Luckman, A., and Benham, T.J., 2011. Warming of waters in an East Greenland fjord prior to glacier retreat: mechanisms and connection to large-scale atmospheric conditions. *The Cryosphere*, 5, 701–714.

Christoffersen, P., O'Leary, M., Van Angelen, J.H., and Van Den Broeke, M., 2012. Partitioning effects from ocean and atmosphere on the calving stability of kangerdlugssuaq glacier, east greenland. *Annals of Glaciology*, 53 (60), 249–256.

Close, S., Herbaut, C., Houssais, M.-N., and Blaizot, A.-C., 2018. Mechanisms of interannual- to decadal-scale winter Labrador Sea ice variability. *Climate Dynamics*, 51 (7–8), 2485–2508.

Cohen, J., Screen, J.A., Furtado, J.C., Barlow, M., Whittleston, D., Coumou, D., Francis, J., Dethloff, K., Entekhabi, D., Overland, J., and Jones, J., 2014. Recent Arctic amplification and extreme mid-latitude weather. *Nature Geoscience*, 7 (9), 627–637.

Cottier, F.R., Nilsen, F., Skogseth, R., Tverberg, V., Skarðhamar, J., and Svendsen, H., 2010. Arctic fjords: a review of the oceanographic environment and dominant physical processes. *Geological Society, London, Special Publications*, 344 (1), 35–50.

Cowton, T., Slater, D., Sole, A., Goldberg, D., and Nienow, P., 2015. Modeling the impact of glacial runoff on fjord circulation and submarine melt rate using a new subgrid-scale parameterization for glacial plumes. *Journal of Geophysical Research: Oceans*, 120 (2), 796–812.

Cowton, T., Sole, A., Nienow, P., Slater, D., Wilton, D., and Hanna, E., 2016. Controls on the transport of oceanic heat to Kangerdlugssuaq Glacier, East Greenland. *Journal of Glaciology*, 62 (236), 1167–1180.

Cowton, T.R., Sole, A.J., Nienow, P.W., Slater, D.A., and Christoffersen, P., 2018. Linear response of east Greenland's tidewater glaciers to ocean/atmosphere warming. *Proceedings of the National Academy of Sciences*, 115 (31), 7907–7912.

Doyle, J.D., Shapiro, M.A., Jiang, Q., Bartels, D.L., Doyle, J.D., Shapiro, M.A., Jiang, Q., and Bartels, D.L., 2005. Large-Amplitude Mountain Wave Breaking over Greenland. *Journal of the Atmospheric Sciences*, 62 (9), 3106–3126.

El-Tahan, M., Venkatesh, S., and El-Tahan, H., 1987. Validation and Quantitative Assessment of the Deterioration Mechanisms of Arctic Icebergs. *Journal of Offshore Mechanics and Arctic Engineering*, 109 (1), 102.

Enderlin, E.M. and Howat, I.M., 2013. Submarine melt rate estimates for floating termini of Greenland outlet glaciers (2000–2010). *Journal of Glaciology*, 59 (213), 67–75.

Enderlin, E.M., Howat, I.M., Jeong, S., Noh, M.J., Van Angelen, J.H., and Van Den Broeke, M.R., 2014. An improved mass budget for the Greenland ice sheet. *Geophysical Research Letters*, 41 (3), 866–872.

Ettema, J., Van Den Broeke, M.R., Van Meijgaard, E., Van De Berg, W.J., Box, J.E., and Steffen, K., 2010. Climate of the Greenland ice sheet using a high-resolution climate model-Part 1: Evaluation. *The Cryosphere*, 4, 511–527.

Foga, S., Stearns, L.A., and van der Veen, C.J., 2014. Application of Satellite Remote Sensing Techniques to Quantify Terminus and Ice Mélange Behavior at Helheim Glacier, East Greenland. *Marine Technology Society Journal*, 48 (5), 81–91.

Fraser, N.J. and Inall, M.E., 2018. Influence of Barrier Wind Forcing on Heat Delivery Toward the Greenland Ice Sheet. *Journal of Geophysical Research: Oceans*, 123 (4), 2513–2538.

Fried, M.J., Catania, G.A., Bartholomaus, T.C., Duncan, D., Davis, M., Stearns, L.A., Nash, J., Shroyer, E., and Sutherland, D., 2015. Distributed subglacial discharge drives significant submarine melt at a Greenland tidewater glacier. *Geophysical Research Letters*, 42 (21), 9328–9336.

Geyer, W.R. and MacCready, P., 2014. The Estuarine Circulation. *Annual Review of Fluid Mechanics*, 46 (1), 175–197.

Gillard, L.C., Hu, X., Myers, P.G., and Bamber, J.L., 2016. Meltwater pathways from marine terminating glaciers of the Greenland ice sheet. *Geophysical Research Letters*, 43 (20), 10873–10882.

Gladish, C. V., Holland, D.M., Lee, C.M., Gladish, C. V., Holland, D.M., and Lee, C.M., 2015. Oceanic Boundary Conditions for Jakobshavn Glacier. Part II: Provenance and Sources of Variability of Disko Bay and Ilulissat Icefjord Waters, 1990–2011*. *Journal of Physical Oceanography*, 45 (1), 33–63.

Gladish, C. V., Holland, D.M., Rosing-Asvid, A., Behrens, J.W., Boje, J., Gladish, C. V., Holland, D.M., Rosing-Asvid, A., Behrens, J.W., and Boje, J., 2015. Oceanic Boundary Conditions for Jakobshavn Glacier. Part I: Variability and Renewal of Ilulissat Icefjord Waters, 2001–14*. *Journal of Physical Oceanography*, 45 (1), 3–32.

Hanna, E., Cappelen, J., Fettweis, X., Huybrechts, P., Luckman, A., and Ribergaard, M.H., 2009. Hydrologic response of the Greenland ice sheet: the role of oceanographic warming. *Hydrological Processes*, 23 (1), 7–30.

Harden, B.E., Pickart, R.S., and Renfrew, I.A., 2014. Offshore Transport of Dense Water from the East Greenland Shelf. *Journal of Physical Oceanography*, 44 (1), 229–245.

Harden, B.E., Renfrew, I.A., and Petersen, G.N., 2011. A Climatology of wintertime barrier winds off southeast Greenland. *Journal of Climate*, 24 (17), 4701–4717.

Harden, B.E., Straneo, F., and Sutherland, D.A., 2014. Moored observations of synoptic and seasonal variability in the East Greenland Coastal Current. *Journal of Geophysical Research: Oceans*, 119 (12), 8838–8857.

Heinemann, G., 1999. The KABEG'97 field experiment: An aircraft-based study of katabatic wind dynamics over the Greenland ice sheet. *Boundary-Layer Meteorology*, 93 (1), 75–116.

Heinemann, G. and Klein, T., 2002. Modelling and observations of the katabatic flow dynamics over Greenland. *Tellus, Series A: Dynamic Meteorology and Oceanography*, 54 (5), 542–554.

Holfort, J., Hansen, E., Østerhus, S., Dye, S., Jónsson, S., Meincke, J., Mortensen, J., and Meredith, M., 2008. Freshwater Fluxes East of Greenland. *In*: *Arctic–Subarctic Ocean Fluxes*. Dordrecht: Springer Netherlands, 263–287.

Holland, D.M., Thomas, R.H., De Young, B., Ribergaard, M.H., and Lyberth, B., 2008. Acceleration of Jakobshavn Isbr triggered by warm subsurface ocean waters. *Nature Geoscience*, 1 (10), 659–664.

How, P., Benn, D.I., Hulton, N.R.J., Hubbard, B., Luckman, A., Sevestre, H., Pelt, W.J.J.V., Lindbäck, K., Kohler, J., and Boot, W., 2017. Rapidly changing subglacial hydrological pathways at a tidewater glacier revealed through simultaneous observations of water pressure, supraglacial lakes, meltwater plumes and surface velocities. *Cryosphere*, 11 (6), 2691–2710.

Howat, I.M., Box, J.E., Ahn, Y., Herrington, A., and McFadden, E.M., 2010. Seasonal variability in the dynamics of marine-terminating outlet glaciers in Greenland. *Journal of Glaciology*, 56 (198), 601–613.

Howat, I.M., Joughin, I., Tulaczyk, S., and Gogineni, S., 2005. Rapid retreat and acceleration of Helheim Glacier, east Greenland. *Geophysical Research Letters*, 32 (22), 1–4.

Inall, M.E., Murray, T., Cottier, F.R., Scharrer, K., Boyd, T.J., Heywood, K.J., and Bevan, S.L., 2004. Oceanic heat delivery via Kangerdlugssuaq Fjord to the south-east Greenland ice sheet.

Inall, M.E., Murray, T., Cottier, F.R., Scharrer, K., Boyd, T.J., Heywood, K.J., and Bevan, S.L., 2014. Oceanic heat delivery via Kangerdlugssuaq Fjord to the south-east Greenland ice sheet. *Journal of Geophysical Research: Oceans*, 119 (2), 631–645.

Inall, M.E., Nilsen, F., Cottier, F.R., and Daae, R., 2015. Shelf/fjord exchange driven by coastal-trapped waves in the Arctic. *Journal of Geophysical Research: Oceans*, 120 (12), 8283–8303.

Jackson, R.H., Lentz, S.J., and Straneo, F., 2018. The Dynamics of Shelf Forcing in Greenlandic Fjords.

Journal of Physical Oceanography, 48 (11), 2799–2827.

Jackson, R.H. and Straneo, F., 2016. Heat, Salt, and Freshwater Budgets for a Glacial Fjord in Greenland. *Journal of Physical Oceanography*, 46 (9), 2735–2768.

Jackson, R.H., Straneo, F., and Sutherland, D.A., 2014. Externally forced fluctuations in ocean temperature at Greenland glaciers in non-summer months. *Nature Geoscience*, 7 (7), 503–508.

Jenkins, A., 2011. Convection-Driven Melting near the Grounding Lines of Ice Shelves and Tidewater Glaciers. *Journal of Physical Oceanography*, 41 (12), 2279–2294.

Johnson, H.L., Münchow, A., Falkner, K.K., and Melling, H., 2011. Ocean circulation and properties in Petermann Fjord, Greenland. *Journal of Geophysical Research*, 116 (C1), C01003.

Joughin, I., Alley, R.B., and Holland, D.M., 2012. Ice-Sheet Response to Oceanic Forcing. *Science*, 338 (6111), 1172–1176.

Joughin, I., Howat, I., Alley, R.B., Ekstrom, G., Fahnestock, M., Moon, T., Nettles, M., Truffer, M., and Tsai, V.C., 2008. Ice-front variation and tidewater behavior on Helheim and Kangerdlugssuaq Glaciers. *J. Geophys. Res*, 113, 1004.

Joughin, I., Howat, I.M., Fahnestock, M., Smith, B., Krabill, W., Alley, R.B., Stern, H., and Truffer, M., 2008. Continued evolution of Jakobshavn Isbrae following its rapid speedup. *Journal of Geophysical Research*, 113 (F4), F04006.

Joughin, I.M., Tulaczyk, I., Howat, I.M., Joughin, I., Tulaczyk, S., and Gogineni, S., 2005. Rapid retreat and acceleration of Helheim Glacier, east Greenland. *Geophys. Res. Lett*, 32, 22502.

Jungclaus, J.H., Haak, H., Latif, M., and Mikolajewicz, U., 2005. Arctic-North Atlantic interactions and multidecadal variability of the meridional overturning circulation. *Journal of Climate*, 18 (19), 4013–4031.

Khan, S.A., Kjeldsen, K.K., Kjær, K.H., Bevan, S., Luckman, A., Aschwanden, A., Bjørk, A.A., Korsgaard, N.J., Box, J.E., van den Broeke, M., van Dam, T.M., and Fitzner, A., 2014. Glacier dynamics at Helheim and Kangerdlugssuaq glaciers, southeast Greenland, since the Little Ice Age. *The Cryosphere*, 8 (4), 1497–1507.

Klein, T. and Heinemann, G., 2002. Interaction of katabatic winds and mesocyclones near the eastern coast of Greenland. *Meteorological Applications*, 9 (4), 407–422.

Klein, T., Heinemann, G., Bromwich, D.H., Cassano, J.J., and Hines, K.M., 2001. Mesoscale modeling of katabatic winds over Greenland and comparisons with AWS and aircraft data. *Meteorology*

and Atmospheric Physics, 78 (1–2), 115–132.

Klinck, J.M., O'Brien, J.J., Svendsen, H., Klinck, J.M., O'Brien, J.J., and Svendsen, H., 1981. A Simple Model of Fjord and Coastal Circulation Interaction. *Journal of Physical Oceanography*, 11 (12), 1612–1626.

Large, W.G. and Pond, S., 1981. Open Ocean Momentum Flux Measurements in Moderate to Strong Winds. *Journal of Physical Oceanography*, 11 (3), 324–336.

Luckman, A., Benn, D.I., Cottier, F., Bevan, S., Nilsen, F., and Inall, M., 2015. Calving rates at tidewater glaciers vary strongly with ocean temperature. *Nature Communications*, 6 (1), 8566.

Luckman, A., Murray, T., de Lange, R., and Hanna, E., 2006. Rapid and synchronous ice-dynamic changes in East Greenland. *Geophysical Research Letters*, 33 (3), L03503.

Ma, Y. and Bassis, J.N., 2019. The Effect of Submarine Melting on Calving From Marine Terminating Glaciers. *Journal of Geophysical Research: Earth Surface*, 124 (2), 334–346.

Magorrian, S.J. and Wells, A.J., 2016. Turbulent plumes from a glacier terminus melting in a stratified ocean. *Journal of Geophysical Research: Oceans*, 121 (7), 4670–4696.

Mankoff, K.D., Straneo, F., Cenedese, C., Das, S.B., Richards, C.G., and Singh, H., 2016. Structure and dynamics of a subglacial discharge plume in a Greenlandic fjord. *Journal of Geophysical Research: Oceans*, 121 (12), 8670–8688.

McDougall, T.J. and Wotherspoon, S.J., 2014. A simple modification of Newton's method to achieve convergence of order 1+2. *Applied Mathematics Letters*, 29, 20–25.

Mernild, S.H., Hansen, B.U., Jakobsen, B.H., and Hasholt, B., 2008. Climatic conditions at the Mittivakkat Glacier catchment (1994–2006), Ammassalik Island, SE Greenland, and in a 109-year perspective (1898–2006). *Geografisk Tidsskrift-Danish Journal of Geography*, 108 (1), 51–72.

Mernild, S.H., Howat, I.M., Ahn, Y., Liston, G.E., Steffen, K., Jakobsen, B.H., Hasholt, B., Fog, B., and Van As, D., 2010. The Cryosphere Freshwater flux to Sermilik Fjord, SE Greenland. *The Cryosphere*, 4, 453–465.

Miles, V. V., Miles, M.W., and Johannessen, O.M., 2016. Satellite archives reveal abrupt changes in behavior of Helheim Glacier, southeast Greenland. *Journal of Glaciology*, 62 (231), 137–146.

Moffat, C., 2014. Wind-driven modulation of warm water supply to a proglacial fjord, Jorge Montt Glacier, Patagonia. *Geophysical Research Letters*, 41 (11), 3943–3950.

Moon, T., Joughin, I., Smith, B., and Howat, I., 2012. 21st-century evolution of Greenland outlet glacier velocities. *Science*, 336 (6081), 576–578.

Moore, G.W.K. and Moore, G.W.K., 2014. Mesoscale Structure of Cape Farewell Tip Jets. *Journal of Climate*, 27 (23), 8956–8965.

Moore, G.W.K., Renfrew, I.A., and Cassano, J.J., 2013. Greenland plateau jets. *Tellus, Series A: Dynamic Meteorology and Oceanography*, 65, 1–16.

Moore, G.W.K., Renfrew, I.A., Moore, G.W.K., and Renfrew, I.A., 2005. Tip Jets and Barrier Winds: A QuikSCAT Climatology of High Wind Speed Events around Greenland. *Journal of Climate*, 18 (18), 3713–3725.

Mortensen, J., Lennert, K., Bendtsen, J., and Rysgaard, S., 2011. Heat sources for glacial melt in a sub-Arctic fjord (Godthåbsfjord) in contact with the Greenland Ice Sheet. *Journal of Geophysical Research*, 116 (C1), C01013.

Motyka, R.J., Truffer, M., Fahnestock, M., Mortensen, J., Rysgaard, S., and Howat, I., 2011. Submarine melting of the 1985 Jakobshavn Isbræ floating tongue and the triggering of the current retreat. *Journal of Geophysical Research: Earth Surface*, 116 (1), F01007.

Mouginot, J., Rignot, E., Bjørk, A.A., Broeke, M. van den, Millan, R., Morlighem, M., Noël, B., Scheuchl, B., and Wood, M., 2019. Forty-six years of Greenland Ice Sheet mass balance from 1972 to 2018. *Proceedings of the National Academy of Sciences*, 116 (19), 9239–9244.

Nettles, M., Larsen, T.B., Elósegui, P., Hamilton, G.S., Stearns, L.A., Ahlstrøm, A.P., Davis, J.L., Andersen, M.L., De Juan, J., Khan, S.A., Stenseng, L., Ekström, G., and Forsberg, R., 2008. Step-wise changes in glacier flow speed coincide with calving and glacial earthquakes at Helheim Glacier, Greenland. *Geophysical Research Letters*, 35 (24).

Nick, F.M., Vieli, A., Andersen, M.L., Joughin, I., Payne, A., Edwards, T.L., Pattyn, F., and van de Wal, R.S.W., 2013. Future sea-level rise from Greenland's main outlet glaciers in a warming climate. *Nature*, 497 (7448), 235–238.

Nick, F.M., Vieli, A., Howat, I.M., and Joughin, I., 2009. Large-scale changes in Greenland outlet glacier dynamics triggered at the terminus. *Nature Geoscience*, 2 (2), 110–114.

O'Leary, M. and Christoffersen, P., 2013. Calving on tidewater glaciers amplified by submarine frontal melting. *Cryosphere*, 7 (1), 119–128.

Olauson, J., 2018. ERA5: The new champion of wind power modelling? *Renewable Energy*, 126, 322–

331.

Oltmanns, M., Straneo, F., Moore, G.W.K., Mernild, S.H., Oltmanns, M., Straneo, F., Moore, G.W.K., and Mernild, S.H., 2014. Strong Downslope Wind Events in Ammassalik, Southeast Greenland. *Journal of Climate*, 27 (3), 977–993.

Oltmanns, M., Straneo, F., Seo, H., and Moore, G.W.K., 2015. The Role of Wave Dynamics and Small-Scale Topography for Downslope Wind Events in Southeast Greenland. *Journal of the Atmospheric Sciences*, 72 (7), 2786–2805.

Overland, J., Francis, J.A., Hall, R., Hanna, E., Kim, S.-J., Vihma, T., Overland, J., Francis, J.A., Hall, R., Hanna, E., Kim, S.-J., and Vihma, T., 2015. The Melting Arctic and Midlatitude Weather Patterns: Are They Connected?*. *Journal of Climate*, 28 (20), 7917–7932.

Parish, T.R. and Bromwich, D.H., 1987. The surface windfield over the Antarctic ice sheets. *Nature*, 328 (6125), 51–54.

Parish, T.R., Cassano, J.J., Parish, T.R., and Cassano, J.J., 2001. Forcing of the Wintertime Antarctic Boundary Layer Winds from the NCEP–NCAR Global Reanalysis. *Journal of Applied Meteorology*, 40 (4), 810–821.

Pickart, R.S., Spall, M.A., Ribergaard, M.H., Moore, G.W.K., and Milliff, R.F., 2003. Deep convection in the Irminger Sea forced by the Greenland tip jet. *Nature*, 424 (6945), 152–156.

Reeh, N., Thomsen, H.H., Higgins, A.K., and Weidick, A., 2001. Sea ice and the stability of north and northeast Greenland floating glaciers. *Annals of Glaciology*, 33, 474–480.

Renfrew, I.A., Outten, S.D., and Moore, G.W.K., 2009. An easterly tip jet off Cape Farewell, Greenland. I: Aircraft observations. *Quarterly Journal of the Royal Meteorological Society*, 135 (645), 1919–1933.

Rignot, E. and Kanagaratnam, P., 2006. Changes in the Velocity Structure of the Greenland Ice Sheet. *Science*, 311, 986–990.

Rignot, E., Velicogna, I., van den Broeke, M.R., Monaghan, A., and Lenaerts, J.T.M., 2011. Acceleration of the contribution of the Greenland and Antarctic ice sheets to sea level rise. *Geophysical Research Letters*, 38 (5), L05503.

Rignot, E., Xu, Y., Menemenlis, D., Mouginot, J., Scheuchl, B., Li, X., Morlighem, M., Seroussi, H., van den Broeke, M., Fenty, I., Cai, C., An, L., and de Fleurian, B., 2016. Modeling of ocean-induced ice melt rates of five west Greenland glaciers over the past two decades. *Geophysical Research*

Letters, 43 (12), 6374–6382.

Sabine Christopher, L., Feely Richard, A., Gruber, N., Key Robert, M., Lee, K., Bullister John, L., Wanninkhof, R., Wong, C.S., Wallace Douglas, W.R., Tilbrook, B., Millero Frank, J., Peng Tsung, H., Kozyr, A., Ono, T., and Rios Aida, F., 2004. The oceanic sink for anthropogenic CO (sub 2). *Science*, 305 (5682), 367–371.

Schild, K.M. and Hamilton, G.S., 2013. Seasonal variations of outlet glacier terminus position in Greenland. *Journal of Glaciology*, 59 (216), 759–770.

Schild, K.M., Renshaw, C.E., Benn, D.I., Luckman, A., Hawley, R.L., How, P., Trusel, L., Cottier, F.R., Pramanik, A., and Hulton, N.R.J.J., 2018. Glacier Calving Rates Due to Subglacial Discharge, Fjord Circulation, and Free Convection. *Journal of Geophysical Research: Earth Surface*, 1–16.

Schjøth, F., Andresenb, C.S., Straneo, F., Murray, T., Scharrer, K., and Korablev, A., 2012. Campaign to map the bathymetry of a major Greenland fjord. *Eos, Transactions American Geophysical Union*, 93 (14), 141–142.

Schumann, K., Völker, D., and Weinrebe, W.R., 2012. Acoustic mapping of the Ilulissat Ice Fjord mouth, West Greenland. *Quaternary Science Reviews*, 40, 78–88.

Sciascia, R., Straneo, F., Cenedese, C., and Heimbach, P., 2013. Seasonal variability of submarine melt rate and circulation in an East Greenland fjord. *Journal of Geophysical Research: Oceans*, 118 (5), 2492–2506.

Seale, A., Christoffersen, P., Mugford, R.I., and O'Leary, M., 2011. Ocean forcing of the Greenland Ice Sheet: Calving fronts and patterns of retreat identified by automatic satellite monitoring of eastern outlet glaciers. *Journal of Geophysical Research*, 116 (F3), F03013.

Shepherd, A., Ivins, E.R., A, G., Barletta, V.R., Bentley, M.J., Bettadpur, S., Briggs, K.H., Bromwich, D.H., Forsberg, R., Galin, N., Horwath, M., Jacobs, S., Joughin, I., King, M.A., Lenaerts, J.T.M., Li, J., Ligtenberg, S.R.M., Luckman, A., Luthcke, S.B., McMillan, M., Meister, R., Milne, G., Mouginot, J., Muir, A., Nicolas, J.P., Paden, J., Payne, A.J., Pritchard, H., Rignot, E., Rott, H., Sorensen, L.S., Scambos, T.A., Scheuchl, B., Schrama, E.J.O., Smith, B., Sundal, A. V., van Angelen, J.H., van de Berg, W.J., van den Broeke, M.R., Vaughan, D.G., Velicogna, I., Wahr, J., Whitehouse, P.L., Wingham, D.J., Yi, D., Young, D., and Zwally, H.J., 2012. A Reconciled Estimate of Ice-Sheet Mass Balance. *Science*, 338 (6111), 1183–1189.

Slater, D.A., Nienow, P.W., Cowton, T.R., Goldberg, D.N., and Sole, A.J., 2015. Effect of near-terminus subglacial hydrology on tidewater glacier submarine melt rates. *Geophysical Research Letters*,

42 (8), 2861–2868.

Slater, D.A., Nienow, P.W., Goldberg, D.N., Cowton, T.R., and Sole, A.J., 2017. A model for tidewater glacier undercutting by submarine melting. *Geophysical Research Letters*, 44 (5), 2360–2368.

Spall, M.A., Jackson, R.H., and Straneo, F., 2017. Katabatic Wind-Driven Exchange in Fjords. *Journal of Geophysical Research: Oceans*, 122 (10), 8246–8262.

Spall, M.A. and Pedlosky, J., 2018. Shelf–Open Ocean Exchange Forced by Wind Jets. *Journal of Physical Oceanography*, 48 (1), 163–174.

Spreen, G., Kaleschke, L., and Heygster, G., 2008. Sea ice remote sensing using AMSR-E 89-GHz channels. *Journal of Geophysical Research*, 113 (C2), C02S03.

Stearns, L.A. and Hamilton, G.S., 2007. Rapid volume loss from two East Greenland outlet glaciers quantified using repeat stereo satellite imagery. *Geophysical Research Letters*, 34 (5).

Stouffer, R.J., Yin, J., Gregory, J.M., Dixon, K.W., Spelman, M.J., Hurlin, W., Weaver, A.J., Eby, M., Flato, G.M., Hasumi, H., Hu, A., Jungclaus, J.H., Kamenkovich, I. V., Levermann, A., Montoya, M., Murakami, S., Nawrath, S., Oka, A., Peltier, W.R., Robitaille, D.Y., Sokolov, A., Vettoretti, G., Weber, S.L., Stouffer, R.J., Yin, J., Gregory, J.M., Dixon, K.W., Spelman, M.J., Hurlin, W., Weaver, A.J., Eby, M., Flato, G.M., Hasumi, H., Hu, A., Jungclaus, J.H., Kamenkovich, I. V., Levermann, A., Montoya, M., Murakami, S., Nawrath, S., Oka, A., Peltier, W.R., Robitaille, D.Y., Sokolov, A., Vettoretti, G., and Weber, S.L., 2006. Investigating the Causes of the Response of the Thermohaline Circulation to Past and Future Climate Changes. *Journal of Climate*, 19 (8), 1365–1387.

Straneo, F., 2015a. Water temperature, conductivity, and currents data collected by CTDs and current meters on moored buoys in the Sermilik Fjord and Kangerdlugssuaq Glacier, in East Greenland from 2009-08 to 2012-09 (NCEI Accession [online]. *NOAA National Centers for Environmental Information*. Available from: https://accession.nodc.noaa.gov/0127320 [Accessed 1 Feb 2019].

Straneo, F., 2015b. Temperature and conductivity, and water currents data collected by CTDs and current meters on moored buoys in the Sermilik Fjord, Greenland from 2010-08 to 2011-08 (NCEI Accession 0123282) [online]. *NOAA National Centers for Environmental Information*. Available from: https://accession.nodc.noaa.gov/0123282 [Accessed 1 Feb 2019].

Straneo, F. and Cenedese, C., 2015. The Dynamics of Greenland's Glacial Fjords and Their Role in Climate. *Annual Review of Marine Science*, 7 (1), 89–112.

Straneo, F., Curry, R.G., Sutherland, D.A., Hamilton, G.S., Cenedese, C., Våge, K., and Stearns, L.A., 2011. Impact of fjord dynamics and glacial runoff on the circulation near Helheim Glacier. *Nature Geoscience*, 4 (5), 322–327.

Straneo, F., Hamilton, G., Stearns, L., and Sutherland, D., 2016. Connecting the Greenland Ice Sheet and the Ocean: A Case Study of Helheim Glacier and Sermilik Fjord. *Oceanography*, 29 (4), 34–45.

Straneo, F., Hamilton, G.S., Sutherland, D.A., Stearns, L.A., Davidson, F., Hammill, M.O., Stenson, G.B., and Rosing-Asvid, A., 2010a. Rapid circulation of warm subtropical waters in a major glacial fjord in East Greenland. *Nature Geoscience*, 3 (3), 182–186.

Straneo, F., Hamilton, G.S., Sutherland, D.A., Stearns, L.A., Davidson, F., Hammill, M.O., Stenson, G.B., and Rosing-Asvid, A., 2010b. Rapid circulation of warm subtropical waters in a major glacial fjord in East Greenland. *Nature Geoscience*, 3 (3), 182–186.

Straneo, F. and Heimbach, P., 2013. North Atlantic warming and the retreat of Greenland's outlet glaciers. *Nature*, 504 (7478), 36–43.

Straneo, F., Sutherland, D., and Harden, B., 2015. Water Temperature, conductivity, and currents data collected by CTDs and current meters on moored buoys in the Sermilik Fjord, Greenland from 2012-09-18 to 2013-08-20 (NCEI Accession 0127325). [online]. *NOAA National Centers for Environmental Information*. Available from: https://accession.nodc.noaa.gov/0127325 [Accessed 1 Feb 2019].

Straneo, F., Sutherland, D., Harden, B., and Jackson, R., 2015. Temperature, conductivity, and water currents data collected by CTDs and current meters on moored buoys in the Sermilik Fjord, Greenland from 2011-08-20 to 2012-09-16 (NCEI Accession 0126772). [online]. *NOAA National Centers for Environmental Information*. Available from: https://accession.nodc.noaa.gov/0126772 [Accessed 1 Feb 2019].

Straneo, F., Sutherland, D.A., Holland, D., Gladish, C., Hamilton, G.S., Johnson, H.L., Rignot, E., Xu, Y., and Koppes, M., 2012. Characteristics of ocean waters reaching Greenland's glaciers. *Annals of Glaciology*, 53 (60), 202–210.

Sutherland, D.A. and Pickart, R.S., 2008. The East Greenland Coastal Current: Structure, variability, and forcing. *Progress in Oceanography*, 78 (1), 58–77.

Sutherland, D.A., Roth, G.E., Hamilton, G.S., Mernild, S.H., Stearns, L.A., and Straneo, F., 2014. Quantifying flow regimes in a Greenland glacial fjord using iceberg drifters. *Geophysical*

Research Letters, 41 (23), 8411–8420.

Sutherland, D.A. and Straneo, F., 2012. Estimating ocean heat transports and submarine melt rates in sermilik fjord, greenland, using lowered acoustic doppler current profiler (LADCP) velocity profiles. *Annals of Glaciology*, 53 (60), 50–58.

Sutherland, D.A., Straneo, F., and Pickart, R.S., 2014. Characteristics and dynamics of two major Greenland glacial fjords. *Journal of Geophysical Research: Oceans*, 119 (6), 3767–3791.

Sutherland, D.A., Straneo, F., Stenson, G.B., Davidson, F.J.M., Hammill, M.O., and Rosing-Asvid, A., 2013. Atlantic water variability on the SE Greenland continental shelf and its relationship to SST and bathymetry. *Journal of Geophysical Research: Oceans*, 118 (2), 847–855.

Todd, J. and Christoffersen, P., 2014. Are seasonal calving dynamics forced by buttressing from ice mélange or undercutting by melting? Outcomes from full-Stokes simulations of Store Glacier, West Greenland. *The Cryosphere*, 8, 2353–2365.

Våge, K., Spengler, T., Davies, H.C., and Pickart, R.S., 2009. Multi-event analysis of the westerly Greenland tip jet based upon 45 winters in ERA-40. *Quarterly Journal of the Royal Meteorological Society*, 135 (645), 1999–2011.

Vieli, A. and Nick, F.M., 2011. Understanding and Modelling Rapid Dynamic Changes of Tidewater Outlet Glaciers: Issues and Implications. *Surveys in Geophysics*, 32 (4–5), 437–458.

Walsh, K.M., Howat, I.M., Ahn, Y., and Enderlin, E.M., 2012. Changes in the marine-terminating glaciers of central east Greenland, 2000-2010. *The Cryosphere*, 6, 211–220.

Walter, J.I., Box, J.E., Tulaczyk, S., Brodsky, E.E., Howat, I.M., Ahn, Y., and Brown, A., 2012. Oceanic mechanical forcing of a marine-terminating Greenland glacier. *Annals of Glaciology*, 53 (60), 181–192.

Weijer, W., Maltrud, M.E., Hecht, M.W., Dijkstra, H.A., and Kliphuis, M.A., 2012. Response of the Atlantic Ocean circulation to Greenland Ice Sheet melting in a strongly-eddying ocean model. *Geophysical Research Letters*, 39 (9), n/a-n/a.

Xu, Y., Rignot, E., Menemenlis, D., and Koppes, M., 2012. Numerical experiments on subaqueous melting of Greenland tidewater glaciers in response to ocean warming and enhanced subglacial discharge. *Annals of Glaciology*, 53 (60), 229–234.